

DISSERTATION ZUR ERLANGUNG DES DOKTORGRADES
DER FAKULTÄT FÜR CHEMIE UND PHARMAZIE
DER LUDWIG-MAXIMILIANS-UNIVERSITÄT MÜNCHEN

**Studying the mitochondrial Hsp70,
Ssc1, *in vitro* and *in organello* using
single-molecule Förster Resonance
Energy Transfer**

Vanessa Trauschke

aus
Appenweier, Deutschland

2021

ERKLÄRUNG

Diese Dissertation wurde im Sinne von §7 der Promotionsordnung vom 28. November 2011 von Herrn Prof. Don C. Lamb, Ph.D., betreut.

EIDESSTATTLICHE VERSICHERUNG

Diese Dissertation wurde eigenständig und ohne unerlaubte Hilfe erarbeitet.

München, 05.07.2021

Vanessa Trauschke

Dissertation eingereicht am	09.06.2021
1. Gutachter:	Prof. Don C. Lamb, Ph.D.
2. Gutachterin:	PD Dr. Dejana Mokranjac
Mündliche Prüfung am	25.06.2021

Celebrate your personal victories
because no one else understands
what it took to achieve them.

- Nitya Prakash

Abstract

Hsp70 proteins are molecular chaperones that stabilize unfolded proteins and are important for preventing protein aggregation. The mitochondrial Hsp70 of yeast, Ssc1, is additionally involved in translocation of proteins into the mitochondrial matrix. The functions of proteins are to a significant extent determined by their conformational dynamics and interactions with other biomolecules. Single-molecule Förster Resonance Energy Transfer (smFRET) is a widely applied and powerful method to study the conformational dynamics of proteins.

We performed smFRET measurements of Ssc1 *in vitro*, which revealed conformational dynamics on the sub-millisecond and second timescale. Our investigations further gave new insights into the influence of nucleotides, substrate and the cochaperones Mdj1 and Mge1 on the structure and dynamic behavior of Ssc1.

While *in vitro* experiments allow for precise control of the buffer and available interaction partners, the obtained conformational changes and kinetics might not be the same as *in vivo*. However, smFRET experiments in living cells remain challenging because of high background, need of low labeled sample concentrations and the challenge of getting the labeled proteins into living cells. Here, we perform *in organello* smFRET measurements on Ssc1 inside isolated mitochondria to get an idea about the conformation and dynamics in its natural environment while containing low background and high signal intensities.

Our *in organello* experiments showed that most Ssc1 inside mitochondria is substrate-bound. This observation implies substantial consequences for the role of Ssc1 as a chaperone and in protein translocation into the matrix. Tracking of single Ssc1 proteins inside mitochondria further allowed us to put mobility and conformation of Ssc1 into context and assign a small fraction of substrate-free but translocase-bound Ssc1.

Contents

1. Introduction	1
2. Biophysical Background	4
2.1. Fluorescence	4
2.1.1. Labeling with organic fluorophores	6
2.2. Förster Resonance Energy Transfer (FRET)	6
2.3. The power of single-molecule measurements	8
2.4. Single-molecule fluorescence microscopy	9
2.4.1. Total internal reflection fluorescence (TIRF) microscopy	9
2.4.1.1. Highly inclined and laminated optical sheet (HILO) microscopy and variable-angle epifluorescence microscopy (VAEM)	11
2.4.1.2. Data and information gained with TIRF-like microscopy	11
2.4.2. Alternating laser excitation (ALEX) and pulsed interleaved excitation (PIE)	12
2.4.3. Confocal fluorescence microscopy	12
2.4.4. Multi-parameter fluorescence detection (MFD)	13
2.4.4.1. FRET efficiency vs. donor lifetime (E- τ -plots)	13
2.4.4.2. Dynamic photon distribution analysis (PDA)	14
2.4.5. FRET calculations and correction factors	16
2.4.5.1. Determination of the γ -factor from experimental data	18
2.5. From <i>in vitro</i> to <i>in vivo</i>	19
3. Biochemical Background	21
3.1. Heat shock proteins	21
3.2. Heat shock proteins of 70 kDa	23
3.2.1. The diverse functions of Hsp70s	23
3.2.2. Secondary and tertiary structure of Hsp70s	25
3.2.3. The substrates of Hsp70s	28
3.2.4. Allosteric regulation of Hsp70s	29
3.3. Ssc1, the mitochondrial Hsp70 of <i>Saccharomyces cerevisiae</i>	32
3.3.1. Stabilization of Ssc1 by Hep1	33
3.3.2. Ssc1 interaction with substrates	33

3.3.3.	Regulation of Ssc1 in protein folding	35
3.3.3.1.	The nucleotide exchange factor Mge1	36
3.3.3.2.	The J protein involved in protein folding, Mdj1	36
3.3.4.	Regulation of Ssc1 in Protein Translocation	37
3.3.4.1.	The peripheral membrane protein Tim44	39
3.3.4.2.	The J protein Tim14 and J-like protein Tim16	39
3.3.4.3.	The nucleotide exchange factor Mge1 in protein translocation	40
3.3.4.4.	Role of Ssc1 in protein translocation	40
3.3.5.	Other interacting proteins	41
3.3.5.1.	Hsp10 and Hsp60	42
3.3.5.2.	Hsp78, a member of the Hsp100 group	42
3.3.5.3.	The role of Ssc1 in the assembly of the cytochrome c oxidase	43
3.4.	Previous FRET experiments of Ssc1	43
4.	<i>In vitro</i> characterization of Ssc1	46
4.1.	The influence of nucleotides and substrate on the conformation of Ssc1	48
4.1.1.	Ssc1 in the presence of ATP	48
4.1.2.	Ssc1 in the presence of ADP	50
4.1.2.1.	The high FRET populations of the domain sensor for ATP- and ADP-bound Ssc1	51
4.1.3.	The influence of substrate on the conformation of Ssc1	51
4.2.	The influence of Mdj1 and Mge1 on the conformation of Ssc1	53
4.2.1.	Ssc1 in the presence of J protein Mdj1	54
4.2.2.	Ssc1 in the presence of nucleotide exchange factor Mge1	56
4.2.3.	Ssc1 in the presence of ATP, substrate, Mdj1 and Mge1	59
4.3.	Dynamic photon distribution analysis of the sub-millisecond dynamics of Ssc1	60
4.3.1.	Kinetics of the domain dynamics	63
4.4.	Slow domain separation in the presence of substrate	63
4.5.	Proposed model of the chaperoning cycle of Ssc1	64
4.6.	Variations of labeling positions of Ssc1	67
4.6.1.	No clear difference in high FRET species of SD-B	68
4.6.2.	SD-C does not show a high FRET species	69
4.6.3.	The function of SD-D is impaired	70
4.6.4.	Defective expression and folding of SD-E	70
4.6.5.	SD-F is a possible candidate to observe the full cycle of Ssc1	70
4.6.6.	Summary	71

5. <i>In organello</i> smFRET measurements of Ssc1	72
5.1. Stepwise realization of <i>in organello</i> smFRET measurements	72
5.1.1. Import of fluorescently labeled Ssc1 into isolated mitochondria	72
5.1.2. Specific immobilization of mitochondria	73
5.1.3. The influence of dyes	75
5.1.4. Single-molecule trace quality <i>in organello</i>	77
5.2. Conformational state of Ssc1 <i>in organello</i>	77
5.2.1. Conformation of Ssc1 <i>in organello</i> with ATP excess	78
5.2.2. Functionality studies of imported Ssc1	79
5.2.3. Ssc1 is mostly substrate-bound <i>in organello</i>	79
5.2.4. The high FRET population under ATP depletion conditions	80
5.2.5. The intermediate FRET population in the presence of ATP	81
5.3. Conformation of the lid sensor of Ssc1 <i>in organello</i>	82
5.4. Tracking of Ssc1 paths inside mitochondria	83
6. Conclusion and Outlook	87
7. Materials and Methods	89
7.1. Molecular biology and biochemistry	89
7.1.1. Materials	89
7.1.1.1. Buffers and solutions	89
7.1.1.2. Plasmids and primers for site-directed mutagenesis	91
7.1.2. Site-directed mutagenesis	91
7.1.2.1. Agarose gel electrophoresis	92
7.1.3. Preparation of chemically competent bacteria	93
7.1.4. Transformation in <i>E. coli</i>	93
7.1.5. Plasmid isolation	93
7.1.6. Next generation sequencing	94
7.1.7. Protein expression	94
7.1.8. Protein purification	94
7.1.8.1. Purification of Mge1	95
7.1.8.2. Purification of Ssc1	95
7.1.9. SDS gel electrophoresis	96
7.1.10. Labeling of proteins with organic fluorophores	96
7.1.11. Import of labeled Ssc1 into isolated mitochondria	97
7.1.11.1. Purification and labeling of presequence-containing Ssc1	97
7.1.11.2. Import of presequence-containing Ssc1 into isolated mitochondria	97

7.2. Biophysical and analysis methods	98
7.2.1. MFD-PIE measurements	98
7.2.1.1. 2-color MFD-PIE microscope	98
7.2.1.2. Calibration, preparation of the sample chamber, and sample dilution	99
7.2.2. Burst selection and data analysis	99
7.2.2.1. Dynamic photon distribution analysis (PDA)	100
7.2.3. HILO measurements	101
7.2.3.1. Single-molecule objective-type TIRF/HILO microscope	101
7.2.3.2. Cleaning and surface passivation of glass coverslides for TIRF microscopy	103
7.2.3.3. Assembly and preparation of probe chambers for <i>in organello</i> smTIRF microscopy	103
7.2.3.4. Single-molecule <i>in organello</i> HILO measurements	103
7.2.4. Trace analysis	104
7.2.4.1. Tracking analysis	105
A. Supplementary Figures and Tables	107
B. List of Figures	112
C. Literature	114
D. Acknowledgments	126

1. Introduction

Proteins are involved in almost all cellular processes. Their function is highly dependent on their amino acid sequence, three-dimensional structure, conformational dynamics, and interactions with small molecules (such as nucleotides), DNA or RNA and other proteins. The amino acid sequence of a protein can be determined by e.g. Edman degradation or mass spectrometry. Interactions with other molecules are reliably observed by cross-linking or pull-down assays. There are powerful techniques to study protein structure like small-angle x-ray scattering (SAXS), x-ray crystallography, cryo-electron microscopy (cryoEM), solution and solid-state NMR, and single-molecule Förster resonance energy transfer (smFRET). Each of these techniques has their own advantages. SAXS is an easy to apply technique which gives information about the overall size and shape of a protein. Many protein structures have been solved by x-ray crystallography which makes use of the diffraction properties of the different atoms of a protein. The drawback of this method is that the protein of interest needs to be crystallized. This sometimes takes several months of screening of reaction conditions or is not possible at all. The evolving field of time-resolved x-ray crystallography is also able to monitor the conformational changes accompanying reaction progress (e.g. substrate binding, nucleotide exchange) over time. While x-ray crystallography is applicable to proteins of all sizes, cryoEM can only resolve structure of proteins larger than 50 kDa. Nonetheless, CryoEM has gained a lot of attention in the last years demonstrated by the awarding of the Nobel prize to Jacques Dubochet, Joachim Frank and Richard Henderson in 2017 "for developing cryo-electron microscopy for the high-resolution structure determination of biomolecules in solution". Proteins do not need to be crystallized and with the recent automatization of the analysis of the extremely large datasets cryoEM produces, it is now possible to resolve structures faster than by x-ray crystallography. Proteins too small for cryoEM can be resolved in their native state by solution NMR, which is applicable to proteins smaller than 100 kDa. Even though the solving of new structures still takes a lot of time, NMR is a powerful and versatile method for studying protein structure, the interactions within a protein, and detecting dynamic areas of the protein.

A valuable technique to qualitatively and quantitatively resolve the conformational dynamics of proteins smFRET. Dynamics can be observed in real-time and on freely diffusing proteins. The fluorophores available have improved drastically in their photostability, allowing for longer

measurement times without the need of photostabilizers, and in regards to their biocompatibility. When the labeling positions are chosen wisely, the fluorophores do not interfere with the structure and function of the protein.^[1] Since fluorescence spectroscopy and microscopy are minimally invasive, smFRET is not limited to *in vitro* measurements. Thus, the structural changes of the protein of interest can be studied in its natural environment with all of its interaction partners present. SmFRET inside living cells still poses some challenges, like the transfer of the labeled protein into the cell without disturbing its structure or the influence of background fluorescence of the cell on the data quality. One way to circumvent these problems is to measure *in organello*, meaning inside isolated cell organelles like mitochondria, and making use of the inherent import machinery. The protein then gets folded inside the organelle with the help of chaperones and can be measured in its native structure.

Nonetheless, none of these great structural methods are able to unravel all aspects of the working mechanism of a protein on their own. If we want to know the complete mechanism of protein function in maximal detail, data collected from different methods needs to be combined, making use of the strengths of each method.

As already mentioned, the function of proteins is influenced by their three-dimensional structure. Thus, correct folding and the maintenance of the protein structure are essential for cellular homeostasis. The family of chaperone proteins (or heat shock proteins) assists proteins in *de novo* folding and ensures the integrity of protein structure. A central component of the chaperone machinery is the family of heat shock proteins of 70 kDa (Hsp70). Hsp70s are highly conserved across species and present in all cell compartments. They are not only involved in protein folding and stabilization, but also in degradation. When they are located in the endoplasmic reticulum, chloroplasts or mitochondria, they also have a central function in protein translocation. Hsp70s have two major domains, a nucleotide binding domain with ATPase activity, and a substrate binding domain with a substrate binding groove and a lid able to close upon substrate. The two domains are connected with a flexible linker. The function of Hsp70 involves large structural changes as could be detected by crystallography, NMR and smFRET.^[2-6] Even though Hsp70s have been extensively studied, central questions remain, including how and when these conformational changes are induced and how the information is transmitted between the two domains. For Ssc1, the mitochondrial Hsp70 of yeast, uncorrelated conformational transitions of the lid and the two domains have been reported, which raises questions about allosteric communication.^[5,6] Because of the variety of functions of Hsp70s, and especially Ssc1, it is also very interesting to understand how Ssc1 is regulated. Many cochaperones interact with Ssc1, such as the nucleotide exchange factor Mge1 and various J proteins. J proteins are associated with different functions of Ssc1. For example, Mdj1 is the J protein involved in protein folding. Here, *in vitro* smFRET is a valuable tool to study the influence of different factors on the structure and conformational transitions of Ssc1, including transition rates. In Chapter 2, the biophysical

concepts relevant to this work are described. In Chapter 3, an overview the structure and function of Hsp70s is given and Ssc1 and its interaction partners are described in more detail. In Chapter 4, Ssc1 was studied in the presence of nucleotides, substrate and the two cochaperones Mge1 and Mdj1. Changes in the dynamic behavior based on the components added could be observed. *In vitro* studies are necessary to understand the influence of each component on Ssc1. Because of its complexity, the whole system cannot be reconstituted *in vitro*. To better understand the functions and regulation of Ssc1, it is necessary to study Ssc1 in its physiological environment in the presence of all components involved. SmFRET measurements inside isolated mitochondria can be a great tool for this. In Chapter 5, we establish an assay to study the conformation of Ssc1 *in organello*. It becomes apparent that most Ssc1 inside mitochondria is substrate-bound, limiting the availability of free Ssc1 for protein translocation. Tracking of single Ssc1 proteins inside mitochondria further allowed us to put the mobility and conformation of Ssc1 into context.

2. Biophysical Background

In order to understand biological systems and their functions, it is important to study the involved biomolecules. The first steps usually involve biochemical assays to gain understanding of the composition of the system and then structural studies to unravel the structure of the core proteins individually or within the whole complex. For all processes in cells, which are involving proteins, compositional and/or conformational changes occur. To understand the functional mechanisms, real-time studies of the system can help. Fluorescence is a powerful tool to study biological mechanisms *in vitro* and *in vivo*. Fluorescence measurements are minimally invasive and can be applied to living cells. In most cases, when positioned correctly, fluorescent labels do not disturb the system.^[1] Besides the localization of biomolecules can be localized in certain parts of the cell with e.g. super resolution microscopy,^[7-9] interactions of two or more biomolecules can be studied by fluorescence correlation spectroscopy.^[10] By using not only one, but two fluorophores, it is not only possible to study multiple proteins simultaneously, but specific interactions between them can be studied and even exact inter- and intramolecular distances can be determined by single-molecule Förster Resonance Energy Transfer (smFRET).

2.1. Fluorescence

Fluorescence is the emission of light by a fluorophore within nanoseconds upon exposure to radiation. A molecule is excited from the ground state S_0 to a higher excited singlet state, e.g. the first excited state S_1 , by absorption of a photon (Figure 2.1 purple). Once excited, the molecule typically relaxes to the lowest vibrational sublevel of S_1 via internal conversion and vibrational relaxation (Figure 2.1 gray). There are several ways for the molecule to return back to the ground state. When this happens via emission of a photon, it is called fluorescence (Figure 2.1 blue). Alternative ways are non-radiative decay (Figure 2.1 gray and dashed line), e.g. by internal conversion, or intersystem crossing (ISC) to the triplet state T_1 and slow relaxation to the ground state from there via phosphorescence (Figure 2.1 yellow). While relaxation via fluorescence commonly occurs on the timescale of nanoseconds, relaxation via the triplet state can take up to seconds because of its spin-forbidden nature. The lifetime τ of a fluorophore is defined as the

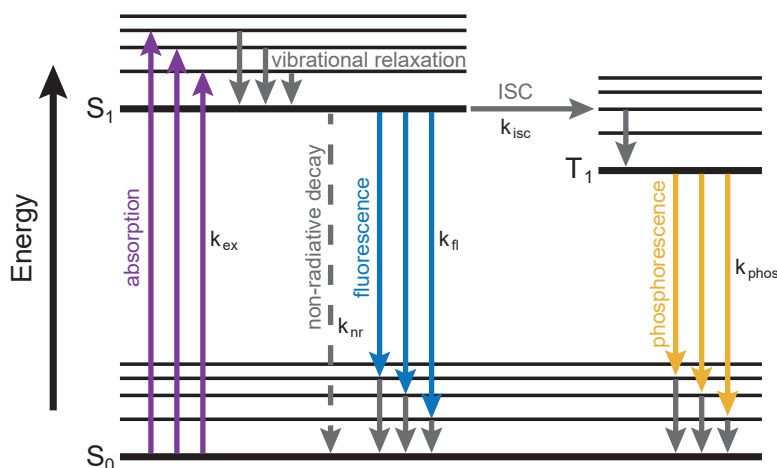


Figure 2.1.: Jablonski diagram showing the basic processes involved in fluorescence. Excitation of a fluorophore by absorption (purple, rate k_{ex}) from the ground state, S_0 , to the a vibrational sublevel of the first excited state, S_1 , followed by vibrational relaxation (gray). The fluorophore returns to the ground state via non-radiative decay (dashed gray line, rate k_{nr}), fluorescence (blue, rate k_{fl}) or, less frequently, via inter system crossing (ISC, rate k_{isc}) to the triplet state, T_1 , followed by phosphorescence (yellow, rate k_{phos}).

time it spends in the excited state before returning to the ground state. It is the inverse of the sum of the rate constants of the relaxation pathways by fluorescence (k_{fl}) and non-radiative decay (k_{nr}).

$$\tau = \frac{1}{k_{fl} + k_{nr}} \quad (2.1)$$

The fluorescent lifetime of a fluorophore is heavily influenced by its surroundings. The solvent, ions, quenchers or other fluorophores can alter the lifetime. Also the proximity to a protein or glass surface can have an influence. Cyanine dyes are particularly well-known for their environmental sensitivity due to the internal *cis-trans* isomerization. Spatial limitations, caused by the proximity of a protein or the coverslide surface, or by increases in the viscosity of the medium, reduces the probability of conversion into the dim *cis*-isomer.^[11,12] This causes a fluorescence enhancement because the cyanine dye is now more often in the highly fluorescent *trans*-conformation.

2.1.1. Labeling with organic fluorophores

To study a sample using fluorescence, the sample needs to be labeled with one or more fluorophores. The most common choice of dyes for fluorescence microscopy are organic fluorophores. They convince with their excellent photophysical properties such as high brightness and photostability. Especially for quantitative single-molecule FRET, these properties as well as their small size are desirable and fluorescent proteins are significantly inferior. Besides their photophysical properties, the charge of the fluorophores is another important factor. Depending on the sample, labeling position, and application, charged and hydrophilic or more hydrophobic fluorophores can be of interest. There are multiple fluorophores available across the whole spectrum (IR, visible and UV) and they should be chosen individually based on the desired properties for each experiment.^[13]

In many cases, it is desirable to label the biomolecule at a specific location. Especially if the biomolecule is a protein, selection of the labeling sites should take the orientation of the residue of choice as well as the surrounding secondary structure into account.^[1] For smFRET studies of dynamically behaving proteins, the labeling positions are chosen so that the difference between the conformations can be well resolved with FRET. Ideally, the distances between the labeling positions differ to degree that leads to high FRET versus low FRET. Labeling can be easily achieved with fluorophore derivatives containing a functional group e.g. maleimide or NHS-ester for cysteine or N-terminal labeling, respectively. Another popular labeling strategy makes use of the so called click chemistry.^[14] These selective and bio-orthogonal reactions have the advantage of quick reaction times and high yields and can be applied to biomolecules such as proteins by incorporation of unnatural amino acids.^[15,16] Unnatural amino acids are also the method of choice for proteins with inherent cysteines which might interfere with labeling via cysteines. This is the case when the inherent cysteine is in a location which is not of interest for labeling but can not be mutated to a different amino acid. However, protein expression with unnatural amino acids often yields less product. Hence, whenever possible, cysteines are still the most commonly used residue for fluorophore stochastic labeling of proteins.

2.2. Förster Resonance Energy Transfer (FRET)

First correctly described by Theodor Förster, Förster resonance energy transfer (FRET) is a non-radiative energy transfer (Figure 2.2) between the excited state of a donor molecule and the ground state of an acceptor molecule.^[17] During this process, mediated by long-range dipole-dipole interactions the acceptor molecule ends up in the excited state and the donor molecule returns to its ground state. The transfer efficiency depends on the extend of spectral overlap

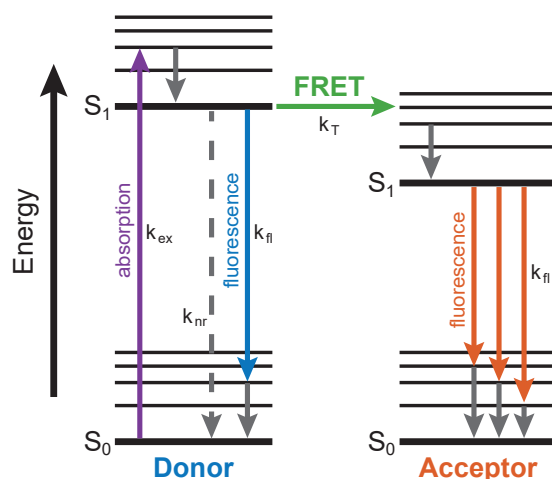


Figure 2.2.: Jablonski diagram of FRET between a donor and an acceptor fluorophore. Excitation of a fluorophore by absorption (purple, rate k_{ex}) from the ground state, S_0 , to the a vibrational sublevel of the first excited state, S_1 , followed by vibrational relaxation (gray). Besides non-radiative decay (dashed gray line, rate k_{nr}) and fluorescence (blue, rate k_{fl}) FRET (green, rate k_T) to the acceptor fluorophore can occur. This excites the acceptor to its first excited state, S_1 , and it can relax to its the ground state, S_0 , via fluorescence (orange, rate k_{fl}) or non-radiative decay (not shown).

between the emission spectrum of the donor and the absorption spectrum of the acceptor, the quantum yield of the donor, the relative orientation of the transition dipole moments of the two molecules and the distance between them. The FRET efficiency E is given by the fraction of excitations that result in energy transfer and can be calculated from the rate of energy transfer k_T and the total of the relaxation rates of the donor, including fluorescence of the donor k_{fl} and non-radiative decay k_{nr} .

$$E = \frac{k_T}{k_T + k_{fl} + k_{nr}} = \frac{k_T}{k_T + \tau_D^{-1}} \quad (2.2)$$

The rate of transfer k_T depends on τ_D (the lifetime of the donor fluorophore), R_0 (the Förster radius) and R (the distance between the donor and the acceptor dye).

$$k_T = \frac{1}{\tau_D} \left(\frac{R_0}{R} \right)^6 \quad (2.3)$$

From Equation 2.2 and 2.3, the strong distance dependence of E becomes apparent:

$$E = \frac{R_0^6}{R_0^6 + R^6} \quad (2.4)$$

The Förster radius R_0 is defined as the distance between the donor and the acceptor molecule where the transfer efficiency is 50 %. R_0 combines the extent of spectral overlap between the emission spectrum of the donor and the absorption spectrum of the acceptor J , the quantum yield of the donor Q_D and the relative orientation of the transition dipole moments of the two molecules κ^2 :

$$R_0^6 = \frac{9000(\ln 10)}{128\pi^5 N_A n^4} J \kappa^2 Q_D \quad (2.5)$$

In practice, depending on the choice of organic dye pairs used, FRET is an excellent tool to measure distances between about 35 and 80 nm. Since a lot of proteins and nucleic acids, like DNA or RNA, have these dimensions, FRET is well suited to study distances within biomolecules.

2.3. The power of single-molecule measurements

Fluorescence has the advantage that it can be detected with high sensitivity, and even a single molecule can be detected. The strength of looking at a single molecule instead of the complete entity at once is well accepted in the field of structural biology. Biological systems exhibit a high degree of heterogeneity and biological processes are rarely synchronized. This leads to the fact that observations on the bulk scale are averaged and often hide the true state of the system. In contrast to ensemble measurements, single-molecule measurements allow us to see each molecule on its own and divide them into subclasses, if they behave differently. The data is thus non-averaged and heterogeneities are clearly visible. Each subpopulation can be looked at in further detail. This also means that rare events can be detected, which would otherwise go unnoticed and disappear behind the predominant population. Furthermore, reaction rates can be determined individually by making time-resolved measurements without the necessity of synchronizing the system. The challenge for single-molecule fluorescence measurements is to detect single molecules in the presence of many more molecules in the solution.

2.4. Single-molecule fluorescence microscopy

In order to detect single fluorescent molecules, the concentration of fluorophores needs to be low enough to detect them individually. Due to the diffraction limit of light, single molecules immobilized on a surface can only be distinguished when they are around 250-300 nm apart. Besides the need for low concentrations, the background needs to be kept to a minimum. A good way to achieve this is the reduction of the observation volume. Two approaches have proven to be successful: inserting a pinhole to achieve a limited observation volume (confocal volume), or using total internal reflection and the resulting evanescent field to only excite a limited volume. In this thesis, both approaches are used and described in more detail below.

2.4.1. Total internal reflection fluorescence (TIRF) microscopy

In a typical epi-fluorescence microscope with widefield illumination the laser light penetrates most of the sample in the probe chamber (Figure 2.3a). Total internal reflection fluorescence (TIRF) microscopy reduces the background detected by spatially limiting the excitation volume. It makes use of the fact that total internal reflection can be achieved when light hits an interface between a medium with high refractive index (n_2) and a medium with lower refractive index (n_1) at an angle exceeding the critical angle, which is given by:

$$\theta_C = \sin^{-1} \left(\frac{n_1}{n_2} \right) \quad (2.6)$$

The interface between glass and aqueous solution is such an interface. At the interface, an evanescent field is generated, reaching up to 200 nm into the solution, limiting the excitation volume to molecules in close proximity to the glass surface. The intensity $I(z)$ of the evanescent field depends on the polarization and decays exponentially from the intensity at the interface $I(0)$ with the distance z the interface.

$$I(z) = I(0) \exp \left(\frac{-z}{d} \right) \quad (2.7)$$

When λ_0 is the wavelength of the reflected light in vacuum, the decay constant d is given by:

$$d = \frac{\lambda_0}{4\pi} (n_2^2 \sin^2 \theta_C - n_1^2)^{-1/2} \quad (2.8)$$

TIRF microscopy can be applied to molecules immobilized on a glass surface, which can then be observed over longer time-scales than in diffusion limited solution experiments. There are two approaches to TIRF microscopy commonly applied. Prism-type TIRF uses a prism to generate the evanescent field. The sample is excited through the prism and the emission is collected on the opposite site by the objective. The probability to detect background from the reflected laser light is low. In objective-type TIRF microscopy, the laser light is lead through the objective using the lens to exceed the critical angle (Figure 2.3b). Since excitation and emission pathways both go through the objective, the reflected laser light needs to be carefully filtered out. However, since the sample is illuminated from the bottom instead of the top, and no prism is needed, sample preparation is less demanding and the sample more accessible for manipulation during the measurement. Typically, the strong biotin-streptavidin interaction is used for immobilization of fluorescently-labeled biomolecules to a passivated surface (Figure 2.4a).

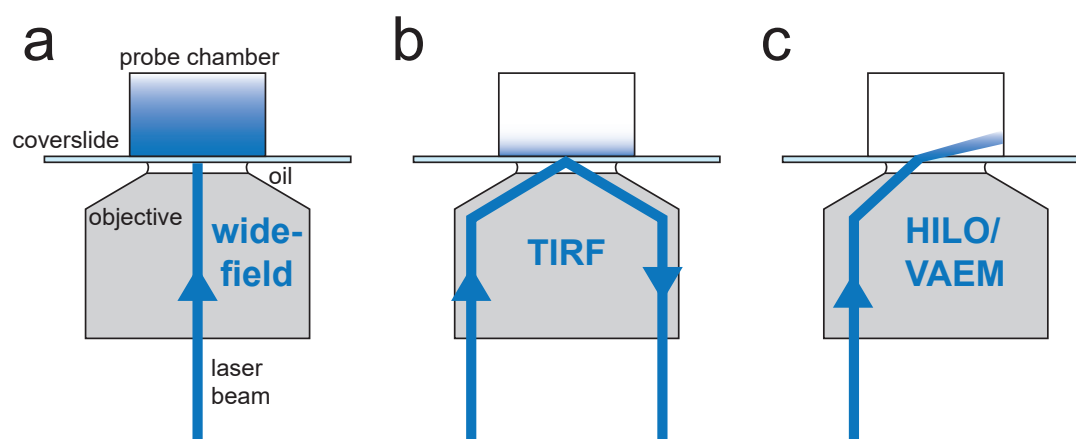


Figure 2.3.: Widefield illumination, TIRF and HILO/VAEM. a) Widefield illumination. The laser beam is guided through the center of the objective and resulting in a high depth of illumination. b) Total internal reflection fluorescence. The laser beam reaches the glass-water interface at a super-critical angle, leading to total internal reflection and the creation of an evanescent field of 100–200 nm into the probe chamber. c) Highly inclined and laminated optical sheet or variable-angle epifluorescence microscopy. The use of subcritical angles gives rise to illumination with an optical sheet and variable depths of illumination.

2.4.1.1. Highly inclined and laminated optical sheet (HILO) microscopy and variable-angle epifluorescence microscopy (VAEM)

When the sample of interest, together with its immobilization chain extends over more than 200 nm, or when measuring inside of cells, TIRF is not well suited for excitation on a fluorescence microscope. An alternative is to use highly inclined and laminated optical sheet (HILO) microscopy^[18] or variable-angle epifluorescence microscopy (VAEM).^[19] The two techniques were developed simultaneously and only vary slightly. In both cases, highly inclined subcritical incident angles are used in an objective-type fluorescence microscope (Figure 2.3c). Light is thus not reflected at the surface, but refracted at a very high angle:

$$n_1 \sin\theta_1 = n_2 \sin\theta_2 \quad (2.9)$$

The advantage of these methods is a high signal-to-noise ratio due to reduced background combined with a higher illumination depth than achieved by TIRF microscopy. The higher the incident angle, the narrower the optical shield for illumination and the higher the signal-to-noise ratio.

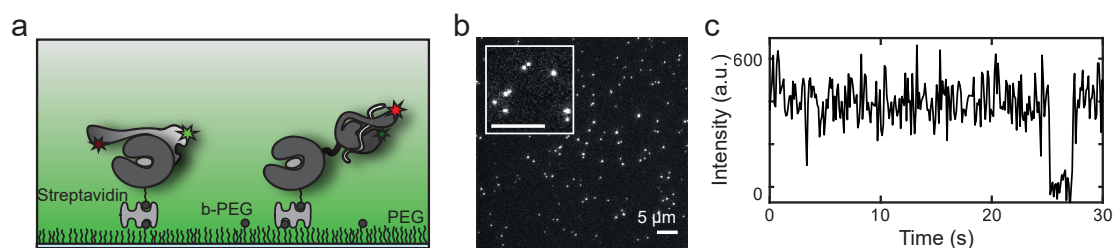


Figure 2.4.: An overview of a typical TIRF experiment. a) Immobilization scheme. The surface is passivated with PEG. A low percentage of PEG molecules carry a biotin-moiety. Biotinylated biomolecules can be immobilized with streptavidin as an adaptor. The evanescent field exciting the fluorophores is illustrated in green. b) Typical field of view (512x512 px) with each white dot representing a single-molecule. The inset is a zoom-in and the scale bar is also 5 μm. c) Exemplary time trace extracted from a movie acquired with TIRF microscopy. The trace includes a blinking event of the fluorophore.

2.4.1.2. Data and information gained with TIRF-like microscopy

One main advantage of TIRF microscopy is the collection of hundreds of fluorescence trajectories at the same time (Figure 2.4b), because it is a camera-based approach. Further, because of the

detection close to the surface, immobilized molecules are used and they can be monitored over longer time-scales until photobleaching (Figure 2.4c). Depending on the fluorophores used and if photostabilization reagents are added, molecules can be observed for up to several minutes. In this way, conformational dynamics on the time-scale of seconds can be detected.

2.4.2. Alternating laser excitation (ALEX) and pulsed interleaved excitation (PIE)

Photophysically induced dark states of the acceptor can be mistaken as 0 % FRET. Also, the labeling efficiency is never 100 % and it is possible that this molecule does not carry an acceptor dye. In order to distinguish these possibilities, it is necessary to determine the presence of a photoactive acceptor. This can be achieved by excitation of the acceptor directly with a separate laser line. This concept was developed by *Kapanidis et al.* with alternating laser excitation (ALEX)^[20] and further advanced by *Müller et al.* with pulsed interleaved excitation (PIE).^[21] Here, two or more pulsed laser sources are used alternatively with sufficient delay to avoid timely overlap of the resulting photons emitted from the excited fluorophores. Besides ensuring activity of the acceptor dye, the second (or third) laser line can also be used to determine the stoichiometry of the labels on a biomolecule and simplify the calculation of correction factors. Pulsed interleaved excitation, in combination with multi-parameter fluorescence detection (MFD),^[22,23] can also yield other helpful information about the system, like fluorescence lifetime of the fluorophores and anisotropies. For further details, see *Hendrix, Lamb (2013)*.^[24]

2.4.3. Confocal fluorescence microscopy

Another way of reducing the observation volume is realized in confocal microscopy. Here, the observation volume is reduced by implementation of a pinhole at the focal point in the image plane of the detection path. Light coming from above or below the focal plane is not focused on the pinhole and does thus not reach the detector. Commonly, the fluorescent signal is detected with avalanche photodiodes (APDs). When the sample concentration is diluted down to the range of 10–100 pM, single molecules can be detected individually. A fluorescent molecule diffusing through the confocal volume is detected as a burst of photons on an avalanche photo diode (APD). For this reason, this measurement method is often called burst measurement. Bursts can be identified by defining the minimum number of photons per burst and per defined time window. The threshold resulting from the selection criteria is represented in Figure 2.5b with a dashed horizontal line. Identified bursts above this threshold are marked with circles in the upper graph and shown in red in the lower graph. During analysis, bursts are further refined by the stoichiometry of the dyes. The observation time of freely diffusing molecules is limited,

but if dynamics occur during this time (typically <3 ms for proteins), they can be detected and evaluated. This is further discussed in Section 2.4.4.1.

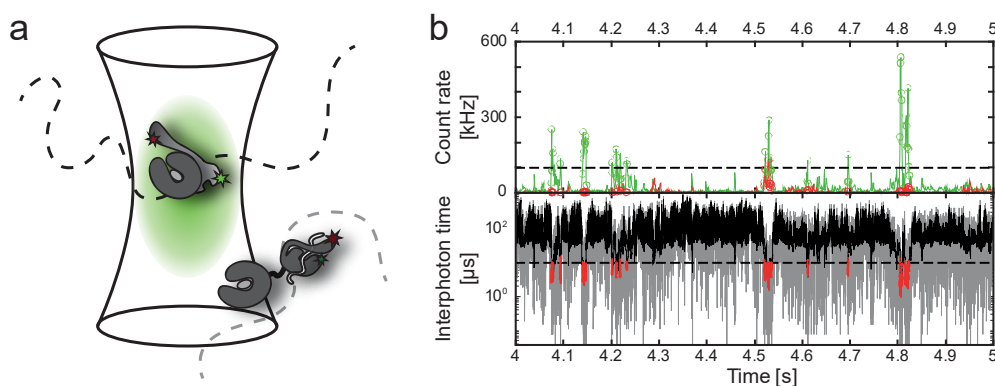


Figure 2.5.: An overview of a burst measurement. a) Scheme of a confocal volume and freely diffusing molecules. Bursts of photons are detected by molecules diffusing through the confocal volume. b) Resulting time trace of these bursts of photons. Horizontal lines demonstrate the selection criteria (minimum of 50 photons per time window of $500 \mu\text{s}$) for the definition of a burst. Bursts are represented with circles in the upper graph and in red in the lower graph.

2.4.4. Multi-parameter fluorescence detection (MFD)

Multi-parameter fluorescence detection (MFD) separates photons with respect to their polarization, wavelength and arrival time. This is achieved by splitting the fluorescence signal into detection channels by using both, polarizing, as well as dichroic beamsplitters. Further, because of the use of pulsed lasers, time-correlated single-photon counting (TCSPC) gives access to the fluorescent lifetimes of the fluorophores. Besides intensity and lifetime, the spectral range and anisotropy of each fluorophore are available. In combination with pulsed interleaved excitation (PIE), a single smFRET measurement is sufficient for an accurate FRET analysis, since this measurement itself provides all the information required for calibration and determination of the correction factors.^[21–23] Possible artifacts caused by donor or acceptor quenching, photobleaching or blinking can be identified and eliminated.^[23]

2.4.4.1. FRET efficiency vs. donor lifetime (E- τ -plots)

Conformational dynamics on the sub-millisecond to millisecond timescale can be detected in MFD-PIE measurements. A valuable plot to identify conformational dynamics in a burst

measurement is by plotting the FRET efficiency versus the donor lifetime (E- τ -plot, Figure 2.6). For a static molecule, the two parameters are related:

$$E_{static} = 1 - \frac{\tau_{D(A)}}{\tau_{D(0)}} \quad (2.10)$$

with $\tau_{D(A)}$ and $\tau_{D(0)}$ being the donor lifetime in the presence and absence of the acceptor, respectively. FRET efficiency and donor lifetime show a linear relationship, which is represented in the static FRET line (Figure 2.6). Taking into consideration the flexibility introduced by the linkers used for attachment of the fluorophores results in a slight bend of the static FRET lines at high FRET efficiencies. In the case of conformational dynamics, the resulting FRET efficiency is averaged depending on the kinetics of the dynamics. While the intensity-based FRET efficiency is species-averaged, the lifetime is a donor-photon-weighted average. Since the lifetime depends only on the donor signal, less photons are detected for a high FRET state. Thus, the low FRET state has a higher contribution to the burst-wise lifetime decay and longer lifetimes are observed, which leads to a shift to the right from the static FRET line.^[25,26] This shift can be described by the dynamic FRET line, which is defined as:

$$E_{dynamic} = 1 - \frac{\tau_{1(A)}\tau_{2(A)}}{\tau_{D(0)}(\tau_{1(A)} + \tau_{2(A)} - \tau_{D(A)})} \quad (2.11)$$

with $\tau_{1(A)}$ and $\tau_{2(A)}$ as the lifetimes of the FRET states between which the dynamics occur. The two lifetimes can be determined by lifetime fits. Their respective locations on the static FRET line describe the endpoints of the dynamic FRET line (Figure 2.6).

2.4.4.2. Dynamic photon distribution analysis (PDA)

The histograms obtained from the FRET measurements can be further analyzed with photon distribution analysis (PDA) to gain information about the underlying distances and also about the heterogeneity of the system. PDA is applied to the proximity ratio distributions and has a higher accuracy than a direct analysis of the FRET efficiency because also statistical parameters are accounted for. Distances of fluorophores are proposed and the theoretical proximity ratio distribution, based on shot-noise limited signal distribution, is calculated based on them. The resulting histogram is then compared with the experimentally obtained histogram. The process is repeated and refined to optimize the parameters. The linear least squares method was used to optimize the fit. The theoretical histograms take shot noise, variations due to linker mobility of

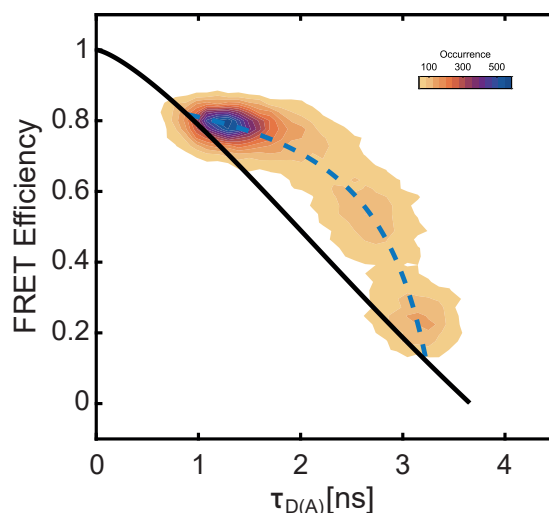


Figure 2.6.: Exemplary E- τ -plot. The FRET efficiency E is plotted versus the donor lifetime in presence of the acceptor ($\tau_{D(A)}$). The solid black line represents the static FRET line and the dashed blue line represents a dynamic FRET line. Populations located on the dynamic FRET line behave dynamically.

the dyes, crosstalk, direct excitation and background into account.^[27] The parameter $\chi_{Red.}^2$ reports on how well the theoretical histogram is in agreement with the experimental data and is ideally 1.

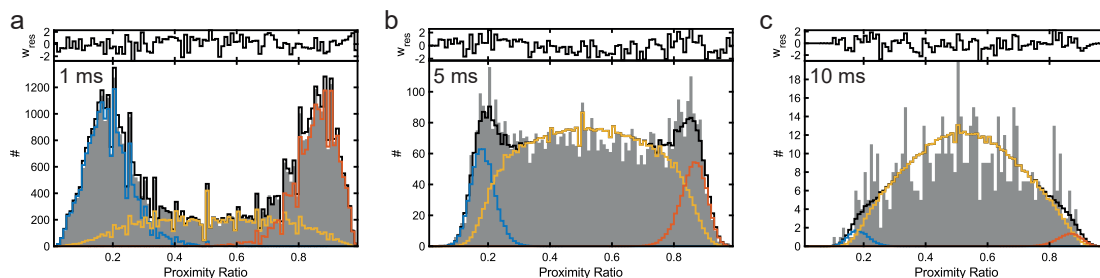


Figure 2.7.: Dynamic PDA fit of a series of proximity ratio histograms generated at different time bins. Simulated data between a high (orange) and a low (blue) FRET state with dynamic interconversion (yellow) with rates of $k = 0.3 \text{ ms}^{-1}$ in both directions. With increasing size of the time bins from 1 ms (a), to 5 ms (b) and to 10 ms (c), more averaging due to dynamic interconversion occurs.

Dynamic PDA fit is a valuable tool to quantify the kinetics of dynamic samples. When conformational dynamics between two distinct states exist in a sample, different histogram representations of the proximity ratios are possible due to dynamic mixing (Figure 2.7). The shape of the histogram depends on the kinetics of the dynamics and the binning. For dynamics much slower than the binning time, two distinct populations are visible, since the dynamics are rarely detected within the time bin. The histogram looks like a static histogram with two populations. For faster

dynamics, the probability of detecting them increases and a bridge in the averaged proximity ratio appears between the two populations. The faster the dynamics get, the more pronounced the bridge becomes. When the dynamics are much faster than the binning time, they occur multiple times during a bin and only one averaged population is observed.^[28] For larger bin times, more averaging occurs than for shorter bin times. This can be exploited for determination of the conversion rates in dynamic PDA. By comparing histograms from the same measurement, but with different bin sizes, conclusions can be drawn about the conversion rates. With a global fit using different bin sizes, dynamic mixing can be differentiated from statistical noise. It is also possible to determine the kinetic rates in the presence of further, static, populations.

2.4.5. FRET calculations and correction factors

The FRET efficiency can be calculated by the decrease in donor lifetime or donor intensity.

$$E = 1 - \frac{\tau_{DA}}{\tau_D} = 1 - \frac{F_{DA}}{F_D} \quad (2.12)$$

where τ_{DA} and F_{DA} are the fluorescence lifetime and intensity of the donor in the presence of the acceptor, and τ_D and F_D in the absence of the acceptor. It is also valuable to have the information from the acceptor signal and confirm that the donor intensity changes are anticorrelated with the acceptor intensity changes, and thereby exclude photophysics of the donor. In this case, the proximity ratio can be calculated from donor and acceptor fluorescence intensities (F_D, F_A):

$$\varepsilon = \frac{F_A}{F_A + F_D} \quad (2.13)$$

To quantitatively calculate the FRET efficiency, there are several factors that need to be corrected for. It is possible that a fraction of the donor emission is detected in the acceptor channel, which would add to the acceptor emission. This happens because of the broad fluorescence spectra that overlap to some extent. Optical filters in the detection path are chosen such that as much acceptor signal as possible reaches the detector or the camera. For this reason, some crosstalk of the donor dye is always detected in the acceptor channel. The crosstalk, α , can be determined out of the calculated proximity ratio in measurements of only the donor dye.

$$\alpha = \frac{F_{DA}^{D_{only}}}{F_{DD}^{D_{only}}} = \frac{E_{PR}^{D_{only}}}{1 - E_{PR}^{D_{only}}} \quad (2.14)$$

It is further possible that the acceptor dye gets directly excited by the laser beam used for donor excitation rather than by FRET. This effect occurs because the absorption spectra of the dyes also overlap to some extent and the acceptor dye also slightly absorbs at the optimized excitation wavelength of the donor dye. The direct excitation δ can be calculated in acceptor only measurements by comparison of the fluorescence signal after excitation with both lasers.

$$\delta = \frac{F_{DA}^{A_{only}}}{F_{AA}^{A_{only}}} = \frac{S_{raw}^{A_{only}}}{1 - S_{raw}^{A_{only}}} \quad (2.15)$$

Another important correction factor is the γ -factor. It corrects for the differences in the detection efficiencies (η_A, η_D) between the two dyes and the different quantum yields (Φ_D, Φ_A) of the acceptor and donor fluorophores.

$$\gamma = \frac{\Phi_A \eta_A}{\Phi_D \eta_D} \quad (2.16)$$

The final formula for absolute FRET efficiency is given by including all three correction factors: crosstalk α , direct excitation δ and the γ -factor.

$$E = \frac{F_{DA} - \alpha F_{DD} - \delta F_{AA}}{F_{DA} - \alpha F_{DD} - \delta F_{AA} + \gamma F_{DD}} \quad (2.17)$$

In a similar fashion, the stoichiometry S can be calculated, if ALEX or PIE are implemented for the measurement setup. The stoichiometry is a measure of the labeling ratio of the molecule of interest.

$$S_{DA} = \frac{F_{DA} + F_{DD}}{F_{DA} + F_{DD} + F_{AA}} \quad (2.18)$$

But also the stoichiometry is influenced by crosstalk α , direct excitation δ , the γ -factor and the additional correction factor β , which accounts for different excitation efficiencies. It takes into account the extinction coefficients ϵ and incident laser power I at the excitation wavelengths

λ_{exc} .^[29]

$$\beta = \frac{\varepsilon_A^{\lambda_{exc}^A} I_A}{\varepsilon_D^{\lambda_{exc}^D} I_D} \quad (2.19)$$

For molecules only labeled with a donor fluorophore, the stoichiometry is close to 1. For molecules only labeled with an acceptor fluorophore, it is close to 0. The corrected stoichiometry can then be calculated by including all four correction factors.

$$S_{DA} = \frac{F_{DA} - \alpha F_{DD} - \delta F_{AA} + \gamma F_{DD}}{F_{DA} - \alpha F_{DD} - \delta F_{AA} + \gamma F_{DD} + \beta F_{AA}} \quad (2.20)$$

Ideally, double-labeled molecules with a ratio of 1:1 for donor and acceptor dyes, should have a stoichiometry of 0.5, after applying all correction factors.

2.4.5.1. Determination of the γ -factor from experimental data

Depending on the method used, the data available and the dynamic behavior of the system, there are multiple methods to determine the γ -factor.

In TIRF microscopy, the correction factors can be determined molecule-by-molecule. If the acceptor bleaches before the donor, the increase in fluorescence in intensity can be directly compared to the decrease in intensity in the acceptor channel.

$$\gamma = \frac{\Delta F_{DA}^{corr}}{\Delta F_{DD}} \quad (2.21)$$

Here, the crosstalk and direct excitation corrected fluorescence intensity of the acceptor (F_{DA}^{corr}) is used. However, often the acceptor fluorophores are more stable than the donor fluorophores and traces for this kind of γ correction are rare. For dynamic FRET traces, the γ -factor can be determined from the difference in intensity change between the donor and the acceptor channel, every time the FRET efficiency changes. This leads to higher statistics per trace and a more robust correction factor.

A more robust method for γ correction, which can be applied for both burst data on a PIE-MFD

setup and traces collected on a TIRF microscope, is using the dependency of stoichiometry and FRET efficiency. The γ -factor can be determined by a linear fit of the relation between the inverse of the crosstalk and direct excitation corrected stoichiometry and the FRET efficiency. The slope Σ and the intercept Ω from the best linear fit $\frac{1}{S} = \Omega + \Sigma E$ are related to β and γ .^[29]

$$\beta = \Omega + \Sigma - 1 \quad (2.22)$$

$$\gamma = \frac{\Omega - 1}{\Omega + \Sigma - 1} \quad (2.23)$$

For completeness, the γ factor can also be determined by using the fluorescence lifetime information of the donor fluorophore, if available (e.g. for MFD-PIE data). In the case of a static system, the relation between the donor lifetime and the FRET efficiency is linear, as discussed in Section 2.4.4.1.

2.5. From *in vitro* to *in vivo*

In vitro smFRET measurements are valuable to establish protein conformations under well-defined conditions. Nevertheless, the conditions used usually differ strongly from *in vivo* conditions. Oftentimes, components like nucleotides are added in large excess *in vitro* to fully saturate the nucleotide binding pockets. But even if the concentrations used are derived from common concentrations within the cell, concentrations also vary within one single cell. Local concentrations of the components influencing the protein behavior are different depending on their location in the cell (e.g. at the membrane, in the cytosol, in organelles, in the nucleus). Many expression patterns or ionic concentrations also depend on the cell cycle and on possible stress situations. Furthermore more interaction partners are often present within a cell than under reconstituted *in vitro* conditions. The interacting partners can strongly influence kinetics and equilibria. It is thus a logical next step to study conformational cycles of proteins also in their natural environment *in vivo*.

There are several challenges to quantitative *in vivo* smFRET. First, a suitable fluorophore combination needs to be selected. It seems straightforward to choose fluorescent proteins, since recombinant proteins can be easily expressed within a cell. This however, has several drawbacks. One drawback is their poor photophysical properties, especially the low molecular brightness. A second drawback is their size. Because of their size short distances can not be probed. Further, the size can limit free rotation, in which case the relative dipole orientation factor κ^2 cannot be assumed to be $2/3$ and needs to be determined in order to calculate quantitative FRET efficiencies.

The size of the fluorescent proteins can also influence the dynamic behavior of the studied proteins. Also, expression usually does not lead to single-molecule concentrations but rather to a high amount of fluorescently tagged proteins. However, qualitative smFRET with fluorescent proteins has been successfully applied to study the interaction of proteins within cells using fluorescence lifetime imaging microscopy (FLIM).^[30]

For quantitative *in vitro* FRET measurements organic fluorophores are preferred. To use the brighter and more stable organic fluorophores for *in vivo* smFRET measurements, they need to be internalized by the cell. Two possible methods are electroporation and microinjection. In electroporation, the labeled proteins or DNA can enter the cell during transient pores generated by applied voltage.^[31] The advantage is that many cells can be treated at the same time, but proteins can only reach the cytosol and not organelles. With microinjection the location can be chosen precisely, but only one cell can be treated at a time. So far, *in vivo* smFRET has been applied to folding studies and disordered proteins.^[31–34] Both kinds of measurements do not require the tertiary structure of proteins to stay intact during internalization. SmFRET has also been performed at the membrane of living cells with the fluorescent dyes on the outside of the membrane for easier access.^[35] Measurements can be carried out on a confocal microscope or on a widefield microscope. However, on a widefield microscope, in order to see single-molecules, TIRF needs to be applied and thus measurements need to be carried out close to the surface. Related to this is the high fluorescent background of the cells, resulting in a low signal-to-background ratio. Brighter dyes are needed to increase the signal intensity. Addition of photostabilizing agents to the cell is not straight-forward since many photostabilizers are toxic. This problem is being approached with the development and application of novel intramolecular photostabilizers.^[35]

An alternative for studying proteins in organelles is *in organello* measurements. Here, measurements are carried out inside isolated organelles, limiting the fluorescent background. Isolating mitochondria from yeast cells is a well-established process and they survive for several hours after extraction from the host cells and can even be frozen and re-thawed. Like the endoplasmic reticulum (ER) or the nucleus, mitochondria are equipped with their own protein translocation system, which can be high-jacked by addition of a targeting presequence to the protein sequence. *Rupa Banerjee* succeeded in importing fluorescently labeled proteins into isolated mitochondria. The proteins are subsequently folded inside the mitochondrial matrix and fully functional. SmFRET measurements inside isolated mitochondria (*in organello*) are thus a good alternative to *in vivo* measurements. They are more gentle to the protein of interest, allow external manipulation and also have improved signal-to-noise ratios, because of the absence of the high fluorescent background of the cell. This makes it possible to measure the conformation of mitochondrial proteins in a natural environment using smFRET and also look on the changes based on the energetic state of the mitochondria.

3. Biochemical Background

3.1. Heat shock proteins

Correct protein structure is crucial for the functioning of living cells. Protein folding and maintenance of their three-dimensional structure, even under stress conditions, are thus important processes in all cellular compartments. An imbalance in these processes leads to protein aggregation can be lethal. An important family of proteins, which ensures the proper folding of proteins, is heat shock proteins (Hsp). The name of this protein family originates from their discovery because of the upregulation of their expression after the exposure of cells to heat stress. Later, it was discovered, that other stressors, such as cold shock or oxidative stress, also lead to overexpression of heat shock proteins. Furthermore, this class of proteins is not only involved in stress response, to prevent aggregation or induce disaggregation, but also in general house-keeping activities. These involve cellular processes like *de novo* protein folding, assembly or disassembly of protein complexes, regulation of protein activity, protein translocation and protein degradation.^[36] Because they supervise the correct folding of proteins, many Hsps are commonly also known as chaperones. Typically, Hsps are divided into six subclasses based on their size and molecular weight (small Hsps, Hsp40s, Hsp60s, Hsp70s, Hsp90s, and Hsp100s). Small Hsps are of different molecular weight and form oligomeric structures of 9–40 subunits (Figure 3.1a). They perform chaperoning activities by transitioning between different complexes.^[37] Hsp40s have the J domain (Figure 3.1b, J domain in blue) as a common feature and hold many regulatory functions. Besides the J domain, the proline rich region and the GF domain (glycine-phenylalanine rich domain) are characteristic, while the C-terminal domain varies between species and functions.^[38] Hsp60s assemble into homo-oligomeric rings (Figure 3.1c). Two of these rings can form a complex with a cavity in which proteins can be enclosed for folding. The cavity can be closed by a homo-oligomeric complexes of Hsp10 on both sides.^[39] Hsp60-Hsp10 complexes are often called chaperonins. Hsp70s consist of a nucleotide binding domain, a substrate binding domain and a lid^[3] (Figure 3.1d) and have diverse functions, they will be discussed in further detail below. Hsp90s form dimers which have an open and a closed state (Figure 3.1e) depending on the nucleotide state.^[40,41] They promote folding by transitioning between these states. Hsp100s form oligomeric rings and unfold and disaggregate proteins by threading of the amino acid chain

through the center of the ring.^[42] Many of these Hsp classes also interact and work together.^[36] For example, Hsp40s are known to regulate the function of Hsp70.^[43] Another process is the handover of substrates from the Hsp70 to Hsp90^[44,45] or Hsp60^[46] for further folding. But also the cooperation of Hsp70 and Hsp100 in protein disaggregation.^[47] Especially Hsp70s play a central role in the folding and maintenance of protein structures.

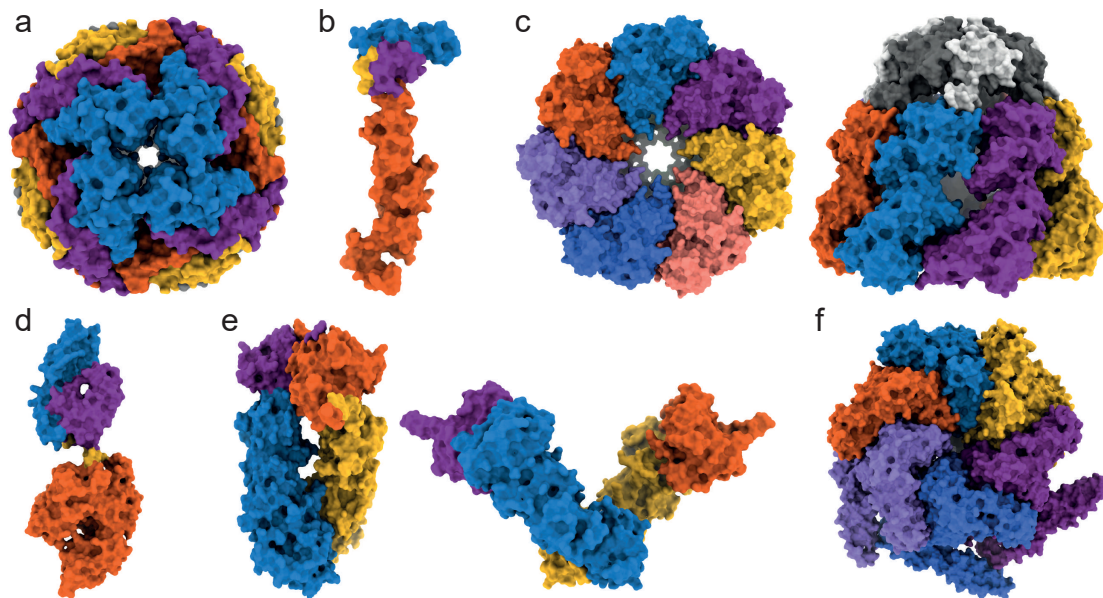


Figure 3.1.: Exemplary structures of the different classes of heat shock proteins. a) 24-mer of Hsp14 (PDB: 3VQK). Small Hsps commonly form oligomeric structures. The top view of the ball-like structure is shown. b) The Hsp40 DnaJ of *T. thermophilus* (PDB: 4J80). The J domain (blue), proline rich region (yellow) and GF domain (purple) are highly conserved. c) The human mitochondrial Hsp60-Hsp10 complex (PDB: 6MRD). Each Hsp60 is colored differently. Two of these complexes can form a larger complex. In the bottom view (left) the cavity can be seen. The side view (right) shows the interaction of the Hsp10 7-mer with the Hsp60 7-mer. d) The Hsp70 DnaK of *E. coli* (PDB: 2KHO). Hsp70 consists of a nucleotide binding domain (orange), a substrate binding domain (purple) and a lid (blue). e) The closed form of the Hsp90 dimer of *S. cerevisiae* (left, PDB: 2CG9) and the open form of the Hsp90 dimer of *E. coli* (right, PDB: 2IOQ). One protein is colored in blue with the N-terminal ATP-binding domain in purple and the other protein is colored in yellow with the N-terminal domain in orange. f) The hexameric complex of Hsp100 ClpB of *E. coli* (PDB: 5OG1). Each Hsp100 is in a different color and a small channel remains in the center.

3.2. Heat shock proteins of 70 kDa

The heat shock proteins of 70 kDa molecular weight are ATP-regulated molecular chaperones. Hsp70s consist of two main domains, the substrate-binding domain (SBD) and the nucleotide-binding domain (NBD). The domains are connected with a flexible linker. The SBD can be further divided into a base, which contains the substrate-binding groove, and a lid, which can enclose the substrate. Hsp70s are involved in all of the above stated house-keeping and stress-related activities. Many Hsp70s are abundantly expressed under normal growth conditions. They are conserved across all species and major cell compartments, e.g. cytosol, nucleus, endoplasmic reticulum (ER), mitochondria and chloroplasts. However, some specialization depending on their environment exists. If multiple Hsp70s exist within one compartment, they are usually involved in different functions. Examples are DnaK and HscA in *E. coli* where DnaK is mainly involved in protein folding and HscA is responsible for iron-sulfur cluster synthesis.^[48] The multiple functions of one single Hsp70 are regulated by a variety of Hsp40 cochaperones, also known as J proteins, and nucleotide exchange factors (NEF).^[43,49]

3.2.1. The diverse functions of Hsp70s

The role of Hsp70 in protein folding

The main function of Hsp70s is folding of nascent protein chains emerging from the ribosome. They are also involved in folding after translocation into e.g. mitochondria or the ER. To this end, Ssc1 binds hydrophobic sequences in its substrate binding pocket. Proteins are translated amino acid by amino acid and some need to be prevented from premature folding until the whole sequence of the protein is complete. The same also applies for translocation. In many cases, the native structure cannot be formed, when only a part of the protein chain is available. Without intervention of Hsp70s, non-native interactions within the beginning of the amino acid sequence can lead to misfolded proteins. By binding to multiple sequences within the protein, Hsp70s prevent this premature folding. Many proteins can fold independently after stabilization by Hsp70s. Proteins needing further assistance in maturation are handed over to Hsp90s or the chaperonins Hsp60 and Hsp10.^[44,50,51]

The role of Hsp70 in protein translocation across membranes

Another essential role of some Hsp70s is the translocation of proteins across membranes. Most proteins found in mitochondria and chloroplasts and all proteins in the ER are synthesized in the cytosol.^[52] Thus, they need to be translocated into the organelles. To this end, they contain specific sequences targeting them to the corresponding organelle. In the cytosol, Hsp70s bind to the precursor protein to keep it in an unfolded state until translocation. Inside the organelle, Hsp70s are associated with the translocation channel and bind to the incoming polypeptide chain. As the only ATP-driven part of the import motor, Hsp70s provide the driving force for precursor proteins to be translocated. The force is generated by entropic pulling.^[53,54] In the ER, BiP is the Hsp70 responsible for this task; in mitochondria it is Ssc1 in yeast or mortalin in higher eukaryotes.^[55–57]

Hsp70 preventing and solubilizing aggregates

Hsp70s prevent aggregation by binding to exposed hydrophobic stretches in proteins. In this way, intermolecular contacts and thus the formation of large aggregates is prevented. Possible substrates are partially unfolded proteins or proteins, which have been disaggregated and need to be refolded. Whereas Hsp70s show some ability to solubilize aggregates, they are not able to dissolve all aggregates completely. To this end, they need to work together with small Hsps and Hsp100s. The protein family of Hsp100s, like bacterial ClpB or Hsp104 in yeast, forms ring structures and is able to thread peptide chains through the central pore. This leads to disentanglement of the aggregates. Hsp70s can activate this mechanism and also alter the surface of the aggregates to facilitate the threading mechanism.^[36,58]

The role of Hsp70 in iron-sulfur cluster synthesis

The prokaryotic HscA or the eukaryotic mitochondrial Hsp70 of yeast, Ssq1 are both involved in iron-sulfur cluster synthesis.^[48,59,60] Both proteins are essential, and their depletion leads to accumulation of iron, a lack of Fe/S containing enzymes and the cells are hypersensitive to oxidative agents.^[61] Deletion of Ssq1 can be rescued by overexpression of Ssc1.^[61] In higher eukaryotes this specialization is lost and there is only one mitochondrial Hsp70, mortalin.^[59] Together with the J protein Hsc20 (HscB in *E. coli*, Jac1 in *S. cerevisiae*), the Hsp70s bind the Isu scaffold.^[48,62] Isu is the central component in iron-sulfur cluster synthesis. HscA and Ssq1 ensure transfer of the iron-sulfur clusters from Isu to the final protein.

Assembly and disassembly of protein complexes and protein regulation by Hsp70

Some Hsp70s are also involved in the assembly or disassembly of protein complexes and thus in protein regulation. The role of Hsp70s in complex assembly is difficult to distinguish from their role in protein folding. However, the mitochondrial Ssc1 is involved in complex formation of cytochrome c oxidase (see Section 3.3.5.3)^[63,64] and the cavity formation of Hsp60 and Hsp10 (see Section 3.3.5.1).^[65] The role of Hsp70s in disassembly of protein complexes is best studied in the disassembly of clathrin coats. Clathrin coats play an important role in membrane deformation and budding of vesicles during endocytosis. After successful vesicle formation, Hsp70s bind to clathrin. By collisions, they produce enough force to disassemble the network into clathrin trimers.^[66] This is in agreement with the model of entropic pulling that is also proposed for the solubilization of aggregates and protein translocation.

The role of Hsp70 in protein degradation

When the correct tertiary structure of proteins cannot be recovered, they need to be degraded to avoid the formation of aggregates toxic to the cell. Protein degradation is also important for regular cell function. Especially regulatory proteins need to be degraded shortly after fulfilling their regulatory functions. After oxidative stress, Hsp70 binds to oxidized proteins in order to keep them solubilized. It then transfers them to the 20S proteasome for degradation.^[67] Hsp70s are further involved in the chaperone-assisted ubiquitin-proteasome system pathway. In interplay with other proteins, substrates are bound by the Hsp70, ubiquitinated and transferred to the proteasome. (Fernandez-Fernandez 2017) In mitochondria, proteins are not ubiquitinated and the protease Pim1 instead recognizes long unstructured segments in the substrates that are to be degraded. Mitochondrial Hsp70 stabilizes these unfolded segments until they can be transferred to Pim1.^[47]

3.2.2. Secondary and tertiary structure of Hsp70s

The structure of Hsp70 is important for their functions. Hsp70s are highly conserved across species and organelles and show 53 % amino acids sequence identity across 730 Hsp70 sequences.^[68] It is thus not surprising that their tertiary structure is also highly conserved. Hsp70s consist of two domains. Structures of isolated domains of Hsp70s and also structures of both domains are available from crystallography and NMR studies. The structures of Hsp70s can be divided into two major domains, the N-terminal nucleotide binding domain (NBD) and the C-terminal substrate

binding domain (SBD). The two domains are connected by a short and flexible inter-domain linker. The highly conserved linker sequence is hydrophobic and can in some cases be bound like a substrate by another Hsp70.^[69]

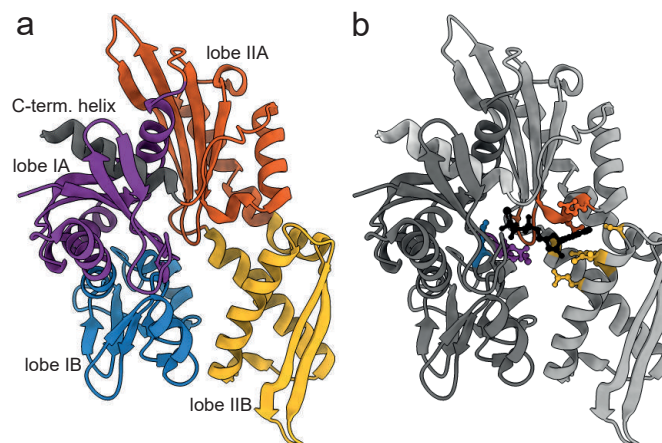


Figure 3.2.: Structure of the NBD of the Hsp70 DnaK bound to ATP. a) The NBD can be divided into two lobes or four subdomains: lobe IA (purple), lobe IB (blue), lobe IIA (orange), and lobe IIB (yellow). A helix (gray) at the C-terminal end of lobe II connects the two lobes. b) The ATP-binding residues are represented and highlighted in the color respective to the colors of the subdomains in a. PDB: 4B9Q

The NBD consists of four subdomains (IA, IB, IIA, IIB; Figure 3.2a) which form two lobes, lobe I and lobe II.^[69,70] The nucleotide is bound between the two lobes, mainly coordinated by residues of lobe II (Figure 3.2b) which contributes 13 out of the total 18 contacts.^[71]

ATP or ADP are bound together with a magnesium ion and stabilized by hydrogen bonds and van-der-Waals contacts. Nucleotide dependent changes in the arrangement of the NBD are small compared to the structural changes in the rest of the protein. However, they fulfill important regulatory functions and are a part of the allosteric conformational network.

The SBD comprises three subdomains: a compact β sandwich, an α -helical lid and an unstructured tail.

The β -sandwich base is made up of eight anti-parallel β -strands (Figure 3.3b). They are arranged in two sheets of four β -strands each.^[3,72] The loops between the β -strands enable substrate binding (Figure 3.3c). Specifically, loops $L_{1,2}$ and $L_{3,4}$ build the channel-like substrate binding groove.^[73] Loop $L_{3,4}$ is stabilized by loop $L_{5,6}$ and loop $L_{1,2}$ by loop $L_{4,5}$. The latter is also involved in allosteric regulation.

The lid domain consists of five α -helices, αA to αE (Figure 3.3a). The helix αA is connected to the β -sandwich together with the first part of the long helix αB .^[73] In the ATP-bound structure,

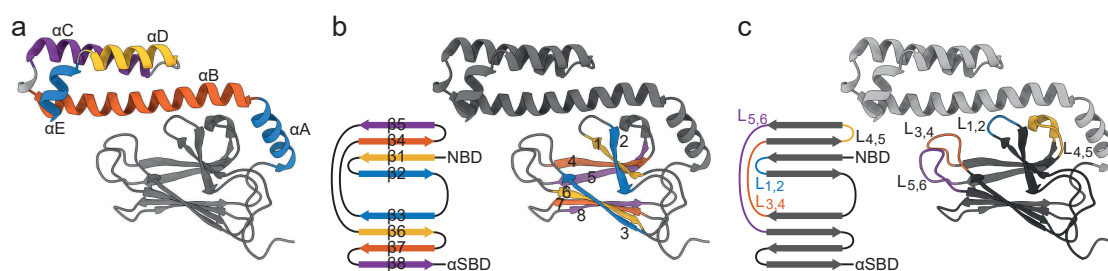


Figure 3.3.: Structure of the SBD of the Hsp70 DnaK in the substrate-bound state. The different features of the SBD are highlighted. a) The lid is comprised of five α -helices. α A (blue) and α B (orange) are in close contact with the base of the SBD and α C (purple), α D (yellow), and α E (blue) build a compact domain at the C-terminal end of α B. b) The base of the SBD is a β -sandwich formed by two β -sheets. Each sheet consists of four β -strands (β 2 (blue), β 1 (yellow), β 4 (orange), β 5 (purple) and β 3 (blue), β 6 (yellow), β 7 (orange), β 8 (purple)). c) The β -strands are connected by loops. The loops $L_{1,2}$ (blue) and $L_{3,4}$ (orange) build the substrate binding pocket and their conformation is influenced by the loops $L_{4,5}$ (yellow) and $L_{5,6}$ (purple). PDB: 2KHO

α A and α B form a continuous helix. This structural change causes opening of the lid. In both structures, the C-terminal part of α B, together with the three helices α C, α D and α E, forms a packed domain around a hydrophobic core.^[73,74]

At the C-terminal end of the α -helical lid, Hsp70s have an unstructured domain of varying length. Some Hsp70s show a conserved sequence at the C-terminal 15 amino acids.^[68] The preceding variable sequence is between 10 and 40 amino acids long.^[68] As this region is disordered, it can not be resolved in crystallographic studies and its exact localization is not known. The exact function of this domain remains unclear, but it might have a function in allosteric communication by connecting the SBD and the NBD. The C-terminal tail is possibly also involved in substrate recognition and sensing of the aggregation state of the substrate.^[68] BiP has been shown to bind its C-terminal sequence as a substrate in the substrate binding groove. Certain co-factors bind to the C-terminus of Hsp70s^[75], especially in the eukaryotic cytosol, where the C-terminal sequence EEVD is highly conserved.

The complete structure of the domains (without the disordered region) of Hsp70s bound to ATP is thought to be conserved between species. The α -helical lid and the β -sandwich base are separated and both docked onto different regions of the NBD (Figure 3.4a).^[4] The linker is bound in a cleft between the subdomains Ia and Ib.^[2]

Also, when bound to ADP and substrate, the structures are similar between multiple homologues of Hsp70. The lid closes upon the substrate binding groove in the SBD. The SBD and NBD are separated and the linker is extended (Figure 3.4b).^[3-5]

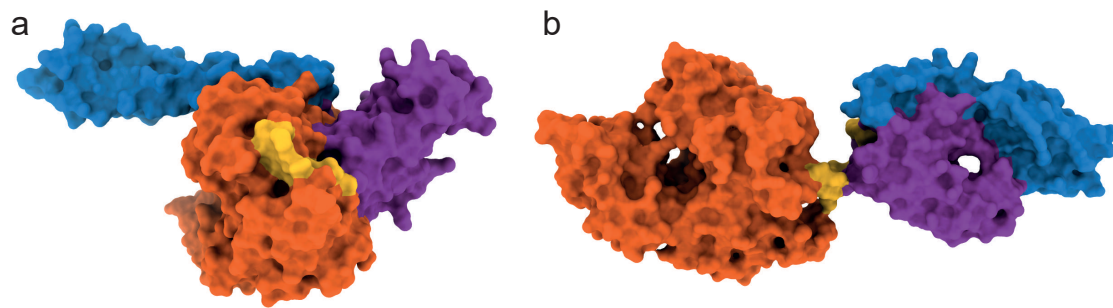


Figure 3.4.: The structure of the Hsp70 DnaK in the presence of ATP or ADP and substrate. a) Hsp70 bound to ATP. The NBD (orange) and β SBD (purple) are docked, the interdomain linker (yellow) is buried in a hydrophobic groove of the NBD. The lid (blue) is wide open and also in contact with the NBD. The substrate binding groove is on the lower right of the SBD. PDB: 4B9Q b) Hsp70 bound to ADP and substrate (which are not resolved). NBD and SBD are undocked and the interdomain linker is extended. The lid is closed upon the substrate binding groove, which is visible as a channel in the structure. PDB: 2KHO

However, for other conditions, e.g. ADP alone, ATP and substrate, or nucleotide free, results from structural studies differ between different Hsp70s.^[69] This is likely due to functional specializations of the Hsp70s. Also, Hsp70s are highly dynamic and show heterogeneous conformations. It is possible that different conformations are favored in crystals for different Hsp70s.

3.2.3. The substrates of Hsp70s

Hsp70s bind a large variety of substrates. Almost all hydrophobic sequences are possible substrates. More specifically, it is usually a sequence of five hydrophobic amino acids surrounded by two positively charged amino acids that are recognized as substrates.^[76] The core of proteins is usually stabilized by such hydrophobic sequences. Because the ions of salts interact less with hydrophobic amino acids, the hydrophobic core stabilizes the tertiary structure of protein the protein. While proteins are being translocated or newly translated, hydrophobic regions of the long unfolded peptides can unspecifically interact with each other to shield themselves from the water and ions in the cell. Such interactions lead to premature misfolding and are often difficult to resolve. Also under heat stress, when partial unfolding or aggregation occurs, these sequences are exposed. Under these conditions, Hsp70s can bind to the exposed hydrophobic sequences to stabilize them until (re)folding can occur. In this way, Hsp70s are reshaping the energy landscape of folding.^[77] While there is a large overlap of possible Hsp70 substrates between species and cell compartments, some differences have been reported. For example, BiP, the Hsp70 of the endoplasmic reticulum, preferably binds aromatic residues, whereas the cytosolic Hsc70 prefers

aliphatic residues.^[78] For the model peptide NRLLLTG bound to DnaK, it was determined that the side chain of the central leucine binds to a small hydrophobic pocket of the binding groove of the SBD.^[73] Also, the surrounding residues are bound to the SBD and stabilized by hydrogen bonds and hydrophobic interactions. The lid closes and binds to the peptide, preventing sliding. If Hsp70s bind to substrates that are partially folded, the lid only closes as far as the substrate allows.^[79,80] This enables an even larger variety of substrates. When bound to ADP, the affinity of the Hsp70s to substrates is in the range of $K_D = 0.1\text{--}1\ \mu\text{M}$. Release rates are increased up to 1000-fold in the presence of ATP leading to lower affinity.^[81]

3.2.4. Allosteric regulation of Hsp70s

During the functional cycle of Hsp70s, large conformational changes take place which are allosterically regulated. Allosteric regulation of the conformational changes of Hsp70s is highly complex. Substrate and bound nucleotide influence the favored conformation. Peptide binding enhances ATP hydrolysis and ATP hydrolysis increases the affinity for the substrate. The information needs to be transferred from the substrate binding groove to the nucleotide binding cleft and vice versa. A large number of small and large structural changes happen during signal transduction. The α -helical lid, the interdomain linker and lobe I of the NBD have been highlighted for allosteric communication. The allosteric regulation of Hsp70s is best studied for DnaK of *E. coli* and will be discussed in further detail.

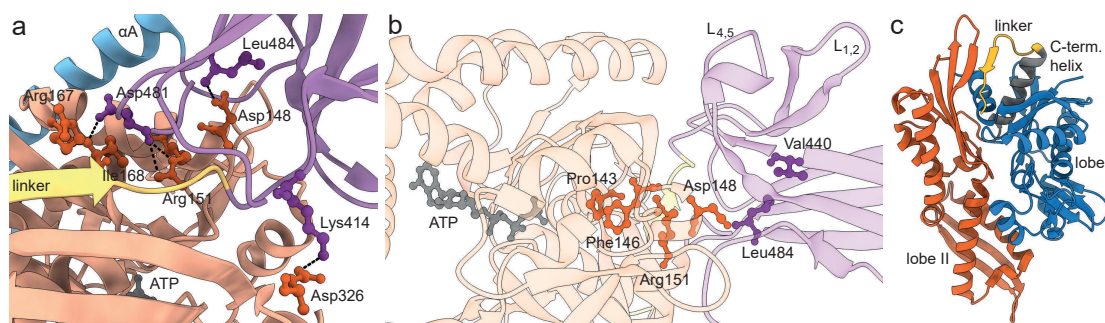


Figure 3.5.: Different aspects of allosteric regulation of the Hsp70 DnaK (PDB: 4B9Q). a) Hydrogen bond network on the interface of the SBD (purple) and NBD (orange). The residues involved in the network are shown as sticks. The black dashed lines indicate the hydrogen bonds formed. b) Allosteric pathway reaching from the bound ATP (gray) to the substrate binding groove. The residues of the pathway are shown as sticks. Residues of the SBD are shown in purple and residues of the NBD in orange. c) The interdomain linker (yellow) regulates the interdomain communication of Hsp70. It does so by binding to a hydrophobic cleft between lobe I (blue) and lobe II (orange) of the NBD in the ATP-bound structure of Hsp70.

The role of the NBD in allostery and specifically lobe I

The residues Asp148, Arg151, Arg167, Ile168, Asp326, Lys414, Asp481, Leu484 of DnaK form a hydrogen bond network at the interface of the SBD and NBD (mainly lobe I) and are important for allosteric regulation of Hsp70s. (Figure 3.5a). Interruption of these hydrogen bonds affects allosteric regulation to different extents.^[82,83] Mutations affect signal transduction differently in both directions, suggesting slightly different pathways. One of the pathways, reaching from the nucleotide binding pocket to the substrate binding groove, is illustrated in Figure 3.5b. The allosteric pathway reaching from the catalytic centre of the NBD to the SBD is made up of residues Pro143, Phe146, Asp148, Arg151, Leu484, and Val440.^[82] All amino acids of the NBD that are involved in this pathway, are located in lobe IA. Thus lobe IA plays an important role in allosteric communication from the NBD to the SBD. Pro143 is closest to the last phosphate of ATP and is a central component for signal transduction and stabilizes the ATP-bound state.^[81] Additionally, mutations in Arg151 lead to a complete loss of allosteric communication. This amino acid is involved in both directions of allosteric communication.^[81]

The role of the interdomain linker

The interdomain linker is an important reporter on the nucleotide state of the NBD. When ADP is bound, the linker is free and the two domains behave independently. When ATP is bound, the linker binds to a hydrophobic cleft between the subdomains IA and IIA of the NBD (Figure 3.5c). This causes domain docking and fixates the catalytic residues in a position that hinders ATP hydrolysis.^[84] The docking can be reversed by binding of substrate. However, the resulting conformation does not favor ATP hydrolysis and the binding of a J protein is needed to arrange the catalytic residues in the optimal conformation for efficient ATP hydrolysis.^[36,85]

The role of the loop $L_{4,5}$ of the SBD

Besides the lobe I in the NBD and the interdomain linker, the loop $L_{4,5}$ of the SBD is an essential part for allosteric signal transduction between domains. Together with the interdomain linker, it is necessary for bidirectional communication and arrangement of the interface between the two domains in the ATP-bound state.^[86] The loop $L_{4,5}$ is in close proximity to the lid (Figure 3.3c) and is probably involved in the opening and closing of the lid. It is also in close contact to the loop $L_{1,2}$ of the substrate binding pocket.

The role of the α -helical lid domain

Removal of the lid leads to an approximately 10-fold decrease in affinity to the substrate. Binding and especially release rates are increased. This can also be observed when Hsp70 is in the ATP-bound state, suggesting an effect of both the presence of the nucleotide and the lid on substrate binding kinetics.^[87] In addition, the ATPase rate of Hsp70 is increased in mutants without the lid indicating an influence in the stabilization of the ATP-bound state.^[88] The mobility of the α -helical lid is further necessary for allosteric regulation. Fixation of the helix αA leads to loss of allosteric communication.^[89]

3.3. Ssc1, the mitochondrial Hsp70 of *Saccharomyces cerevisiae*

Yeast has many Hsp70s located in all cellular compartments. Some are expressed under normal growth conditions while others are only expressed upon temperature change (heat or cold shock) or under other stress conditions.^[90] In yeast mitochondria, three Hsp70 species are present: Ssc1 (Stress Seventy subfamily C 1), Ssq1 (former Ssc2) and Ecm10 (also Ssc3). Ecm10, the least abundant of the three, is not very stable and aggregates fast. It does not appear to bind to proteins and its lid remains open. Even though it has 82 % sequence identity with Ssc1, it is not able to substitute Ssc1. It does not seem to be a functional chaperone for protein folding or translocation and its role is not entirely clear.^[91] Ssq1 has an important role in Fe/S-cluster synthesis. Cells lacking Ssq1 accumulate iron and show a lack of Fe/S containing enzymes. They are also hypersensitive to oxidative agents. High excess of Ssc1 can compensate for missing Ssq1 suggesting at least some functional overlap of these two Hsp70s.^[61] However, Ssq1 cannot compensate for deletion of Ssc1. Ssc1 is the most abundant of the three mitochondrial Hsp70s in yeast. It consists of a 45 kDa nucleotide binding domain (NBD) and a 25 kDa substrate binding domain (SBD). The SBD can be divided into a base consisting of 8 antiparallel β -strands, containing the substrate binding groove, and a lid formed by 5 α -helices, able to close upon the substrate binding groove as described previously. Functional Ssc1 is necessary for cell viability and a knockout is lethal.^[90]

Inside the mitochondrial matrix, Ssc1 has multiple functions. They can be divided into house-keeping tasks to maintain the general function of mitochondria and stress-response related tasks to prevent permanent malfunction of mitochondria after heat shock, cold shock or oxidative stress, which would otherwise lead to cell death. As a classical Hsp70, Ssc1 is in large extent responsible for promoting protein folding.^[56,92,93] It mainly supports proteins by binding to hydrophobic stretches in the peptide sequence exiting from the translocation channel or the ribosome thus stabilizing the unfolded proteins and allowing them to fold slowly once translocation or translation is complete. Proteins that cannot fold on their own are handed over to the Hsp60/Hsp10 system. In this way, Ssc1 prevents aggregation of premature proteins. The same principle applies for partially unfolded proteins during stress conditions or when dissolving aggregates.^[56,92] Ssc1 is further involved in remodeling of complexes or complex formation, as e.g. the cytochrome c oxidase.^[63,64] Proteolytic breakdown, especially by the Pim1/LON protease, also depends on Ssc1.^[94,95] The most important task of Ssc1 might be to drive protein translocation of cytosolically expressed proteins into the mitochondrial matrix.^[56,96,97] Without Ssc1, protein translocation into the matrix does not take place and many essential proteins would be missing. Even Ssc1 itself needs to be imported into mitochondria since it is expressed in the cytosol. This is the main reason why a deletion of Ssc1 is lethal.

3.3.1. Stabilization of Ssc1 by Hep1

Even though Ssc1 itself is a chaperone, it is unable to fold on its own. Ssc1 requires Hep1 (Hsp70 Escort Protein 1) when being recombinantly expressed in *E. coli* and either Hep1 or Mge1 (Mitochondrial GrpE 1) when expressed in yeast.^[98–102] Hep1, also known as Zim17 (Zinc finger Motif protein 17) or Tim15 (Translocase of the Inner Membrane protein 15), is a heat shock protein located in the mitochondrial matrix. It possesses two zinc-finger motifs (hence Zim17), a characteristic feature of J proteins. However, it is only a fractured J protein and does not stimulate ATP hydrolysis in Ssc1.^[103] It is essential for protein translocation, as it ensures the structural and functional integrity of Ssc1, a central part of the protein import motor.^[99]

In vitro, in the absence of nucleotides or in the presence of ADP, Ssc1 tends to oligomerize and aggregate after several hours. It has been reported that the ATPase domain and the interdomain linker are mainly responsible for this aggregation.^[98,101,102,104] Experiments with chimeric proteins have shown that the substrate binding domain of Ssc1 is able to fold on its own and substitution by corresponding parts of DnaK actually enable Ssc1 to fold even in the absence of Hep1 and stay soluble over several hours.^[105] The interaction site with Hep1 is most likely at the ATPase domain of Ssc1. Binding of Hep1 to Ssc1 does not compete with Mge1, so the mechanism of action is not just masking of the aggregation-prone region.^[100] Also, a transient interaction with Hep1 seems to be sufficient for stabilization of Ssc1 because non-stoichiometric amounts of Hep1 are sufficient to prevent aggregation of Ssc1 in the absence of ATP. However, Hep1 is not able to reverse aggregation of Ssc1. Other Hsp70s such as the cytosolic Hsc70, Bip or DnaK, also dimerize, but likely via a different mechanism. Hep proteins seem to only be present in mitochondria, suggesting coevolution with the aggregation propensity of the mitochondrial Hsp70s.^[98] A specialized stabilizing protein emerged rather than evolution of a more stable Ssc1. This implies an important biological function of the aggregation prone regions at the ATPase domain and the interdomain linker of the mitochondrial Hsp70. It is possible that these regions specifically interact with proteins exclusively present in mitochondria. Interestingly, human Hep can stimulate the ATPase rate of the human mtHsp70 and also has some chaperone function in protein folding. However, this is not the case for the interaction of Hep1 and Ssc1 in yeast.^[106]

3.3.2. Ssc1 interaction with substrates

As all other Hsp70s, Ssc1 does not interact with specific amino acid sequences within the substrate protein. The substrate binding groove of Ssc1, itself mostly hydrophobic, can interact with a variety of hydrophobic amino acid sequences. Like most other Hsp70s, Ssc1 recognizes sequences of five hydrophobic amino acids surrounded by two positively charged amino acids. If

Ssc1 binds to hydrophobic segments of long unfolded peptides in order to prevent unproductive folding, the lid can completely close upon the substrate binding groove. During the folding process or under stress conditions, when Ssc1 prevents aggregation, the substrate proteins are already partially folded. Under these conditions, the lid cannot completely close upon the substrate and the exact position of the lid domain depends on the size of the substrate bound.^[79,80] However, while human mtHsp70 can bind substrates without the requirement for the lid, Ssc1 can only bind substrate in the presence of its lid domain.^[106]

The model substrate, P5 (CALLLSAPRR), binds to Ssc1 with a K_D of 43 nM in the absence of nucleotides in the buffer and causes complete monomerization. This monomerization occurs most likely because of a structural change.^[107] Like other Hsp70s, Ssc1 not only binds substrate when bound to ATP, but also when bound to ADP. Dynamic opening and closing of the lid when Ssc1 is in an ADP-bound state enables substrate to access the substrate binding groove.^[93] An open lid accelerates both binding and release rates of the substrate to the SBD of Ssc1. However, substrate release rates are substantially higher in the ATP-bound state, as is also reflected in the binding affinities. The dissociation constant is 100-fold higher in the presence of ATP ($K_D = 20\text{--}31\ \mu\text{M}$) as compared to ADP ($K_D = 0.20\text{--}0.23\ \mu\text{M}$).^[86,91,93] Because of the high substrate release rates in the presence of ATP, it is important that substrate binding is accompanied by ATP hydrolysis. Hydrolysis of ATP to ADP leads to strong binding of the substrate. The basal ATPase rate of Ssc1 is (as for all Hsp70s) rather low. Only between 0.032 and 0.13 ATP is hydrolyzed per Ssc1 per minute.^[4,61,93,104,106–108] This means hydrolysis takes over 8–30 min. A large excess of substrate increases this rate up to 5-fold.^[4,61,107,108] However, ATP hydrolysis is stimulated more efficiently in the presence of J-proteins. The J proteins Mdj1 and Tim14 stimulate ATP hydrolysis of Ssc1 around 7-fold.^[61,93,107,108] *Mapa et al.* detected a stimulation by Mdj1 of up to 30-fold in single-turnover experiments.^[4] Stimulated by J proteins the ATPase rate does not change in the absence or presence of substrate.^[4,107] While Mge1 only slightly increases the rate of ATP hydrolysis, addition of both cochaperones, Mge1 and Mdj1, leads to a 24-fold increase of ATP hydrolysis in steady-state experiments.^[107] There is a large variation in the measured values between the data of the different groups. This can be explained by different buffer compositions, small temperature differences, different protein purification approaches and different experimental setups (single-turnover vs. steady-state). The general trend is that substrate and cochaperones accelerate the ATP hydrolysis rate by one to two orders of magnitude. Moreover, all studies do not detect any further influence of substrate on the hydrolysis rate once cochaperones are present.

3.3.3. Regulation of Ssc1 in protein folding

The functions of Ssc1 are versatile and highly dependent on the presence of nucleotides (especially the availability of ATP) and unstructured or aggregated proteins with hydrophobic sequences. For productive regulation of the functions of Ssc1, however, ATP and substrate are not enough. Because of the different functions of Ssc1 it is important to regulate release and binding of the substrate. Successfully folded proteins should not be handed over to the cell degradation system, neither should freshly imported proteins. Some proteins might require further folding by other components of the mitochondrial chaperone system. Also, there are certain conditions when release of folded substrate will only lead to reaggregation and it should remain bound to Ssc1.^[109] Depending on the state of the cell and the mitochondrion, certain activities of Ssc1 might be more important than others, e.g. protein translocation vs. protein disaggregation. Taken together, the regulation of Ssc1 involves many factors and must be adapted to the current needs of the cell. Not all regulators of Ssc1 are known to date, but some well studied ones include the nucleotide exchange factor Mge1 (mitochondrial GtgE 1, also Yge1, yeast GtgE 1)^[107,110] and J-domain proteins such as Mdj1 (mitochondrial DnaJ 1)^[111,112], the J protein involved in protein folding. There are four other J-proteins present in the mitochondrial matrix of yeast: Tim14 (Translocase of the inner mitochondrial membrane 14, also Pam18), Mdj2, Jac1 (J-type accessory chaperone 1), Jid1 (J-protein Involved in protein Degradation 1), as well as the J-like protein Tim16 (also Pam16). Tim14, Mdj2 and Tim16 are involved in protein translocation and are discussed in detail later. Jac1 interacts with Ssq1 and is essential for Fe-S-cluster biosynthesis.^[60,62,113] Jid1 is a membrane protein and involved in protein degradation in the ER. Its exact working mechanism and its interactions with mitochondrial Hsp70s are not well understood.^[114] It does not appear to interact directly with Ssc1. The major cochaperones are discussed in more detail below.

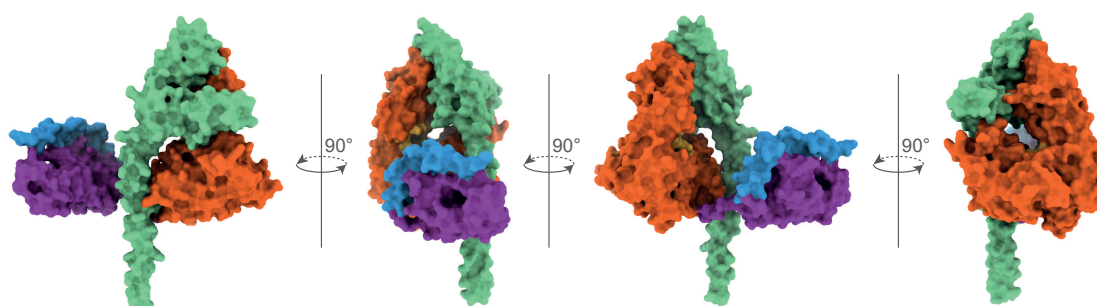


Figure 3.6.: Homology model of the interaction of Ssc1 and Mge1. The SBD of Ssc1 is colored in purple, the lid in blue, the NBD in orange with the nucleotide-interacting residues indicated in yellow. The dimeric Mge1 is shown in green. Based on the structure of GrpE and DnaK (PDB: 4ANI).

3.3.3.1. The nucleotide exchange factor Mge1

The nucleotide exchange factor Mge1 is responsible for the equilibrium between the nucleotide-bound states of Ssc1 and thus influences the ability of Ssc1 to bind to substrate proteins. Mutations in Mge1 result in defects in protein import and subsequent protein folding.^[115] Mge1 binds to the ADP-bound form of Ssc1, promoting nucleotide exchange to ATP and most likely also stabilizing the structure of Ssc1 and thereby preventing oligomerization.^[98] While Mge1 promotes both release of ADP and of ATP, Mge1 is only released upon binding of ATP.^[107] In this way, Mge1 shifts the equilibrium to ATP-bound Ssc1. Mge1 is released from Ssc1 within milliseconds after successful binding of ATP.^[4] This also means that the relative concentrations of ATP and Mge1 will determine the conformation of Ssc1.^[110] However, more recent studies have shown that Mge1 rather stimulates ATP binding than ADP release.^[5] The mechanism of this >60-fold increase in the rate of ATP binding has not yet been unraveled. A homology model based on DnaK and GrpE (PDB: 4ANI, Figure 3.6), however, shows an opening of the nucleotide binding pocket when Mge1 is bound to Ssc1. This possibly makes the binding pocket more accessible for ATP. The strong binding of Ssc1 to Mge1 and the dissociation of the complex by addition of high amounts of ATP has been exploited as a gentle purification method of Ssc1, thus avoiding the use of a purification tag on the already aggregation prone Ssc1.^[116] Mge1 itself is a 26 kDa elongated protein and can only bind to Ssc1 as a homodimer.^[109,110,117] Under elevated temperature, Mge1 denatures to unstructured monomers and no longer interacts with Ssc1. This possibly interrupts substrate release from Ssc1, so that no proteins are released during aggregation prone conditions.^[109] Furthermore, it stops protein import into mitochondria to reduce the amount of unfolded proteins inside the mitochondria and to enable Ssc1 to focus on protein stabilization and disaggregation instead of protein import and folding. It has been speculated that Mge1 behaves similarly under cold-shock conditions.^[109] It has also been reported that Mge1 fails to dimerize under oxidative stress because of the oxidation of a methionine at position 155 and cannot interact with Ssc1.^[117] Another mitochondrial protein, the methionine sulfoxide reductase Mxr2, can restore the function of Mge1 by reduction of MetO at position 155.^[118] Hence, Ssc1 can be regulated directly by cochaperones and also indirectly by proteins that modulate the functionality of the cochaperones. Possibly, Mge1 is also sensitive to other stressors and acts as a kind of thermo and stress sensor, regulating the main activity of Ssc1.

3.3.3.2. The J protein involved in protein folding, Mdj1

The J-protein regulating the role of Ssc1 in protein folding is Mdj1. While depletion of Mdj1 is not affecting the import of precursor proteins, it does affect the successful folding of proteins in the mitochondrial matrix.^[119] One effect of Mdj1 binding to Ssc1 is acceleration of the ATP hy-

drolysis rate of Ssc1 leading to higher substrate affinity and stable binding.^[93] Mdj1 further assists in protection of folded proteins against aggregation and denaturation under stress conditions.^[119] In contrast to Mge1 and Ssc1, Mdj1 is essential to prevent heat-induced aggregation of luciferase in mitochondria. This suggests that Mdj1 is not only a cochaperone of Ssc1, but also acts as a chaperone itself. Indeed, Mdj1 is known to bind to substrates of Ssc1 and thus increase the local concentration of substrate in the proximity of Ssc1. When overexpressed, Mdj1 can partially take over the disaggregation role of Ssc1. It has also been shown that Mdj1, as well as Ssc1, are needed for proteolytic breakdown upon heat shock and thus a complex interplay between the folding machinery and the proteolytic system must exist.^[94] Mdj1 is also essential for maintaining the integrity of mitochondrial DNA as depletion of Mdj1 leads to loss of mitochondrial DNA.^[120]

3.3.4. Regulation of Ssc1 in Protein Translocation

Only 13 of the more than 1000 mitochondrial proteins are expressed from mitochondrial DNA in the matrix of the mitochondria. All other proteins are expressed in the cytosol and need to be imported. Depending on the final destination of the imported proteins, they interact with different components of the mitochondrial protein import machinery. The common entry gateway is the translocase of the outer membrane (TOM, Figure 3.7 gray). Proteins with a cleavable presequence (Figure 3.7 in orange) are targeted either to the inner membrane or the mitochondrial matrix. In both cases, they interact with the presequence translocase of the inner membrane (TIM23, Figure 3.7 blue) in a next step. The characteristic presequence is an α -helically structured sequence, positively charged on one side and containing hydrophobic residues on the other side. This sequence is specifically recognized by the mitochondrial translocation machinery. Proteins or peptide chains intended for translocation with a cleavable presequence are usually termed precursor proteins until the presequence is removed by the mitochondrial processing peptidase and they are correctly folded by the chaperone system. In presence of a membrane potential, this sequence is translocated into the matrix through TIM23. In the case of membrane proteins, the presequence is followed by a hydrophobic sequence serving as a stop signal, which stops translocation and induces membrane insertion.^[121] When the precursor protein is destined for the mitochondrial matrix, it is further translocated through the TIM23 channel and then interacts with the presequence translocase-associated motor (PAM), an essential multi-protein component of the translocase.

PAM provides the necessary driving force for the translocation process. The central unit of the import motor is Tim44 (Figure 3.7 yellow). It anchors Ssc1 at the membrane and positions Ssc1 so that the substrate binding groove is in close proximity to the exit of the translocation channel of TIM23.^[97,108,123] Ssc1 (Figure 3.7 orange) is the second essential part of PAM as it

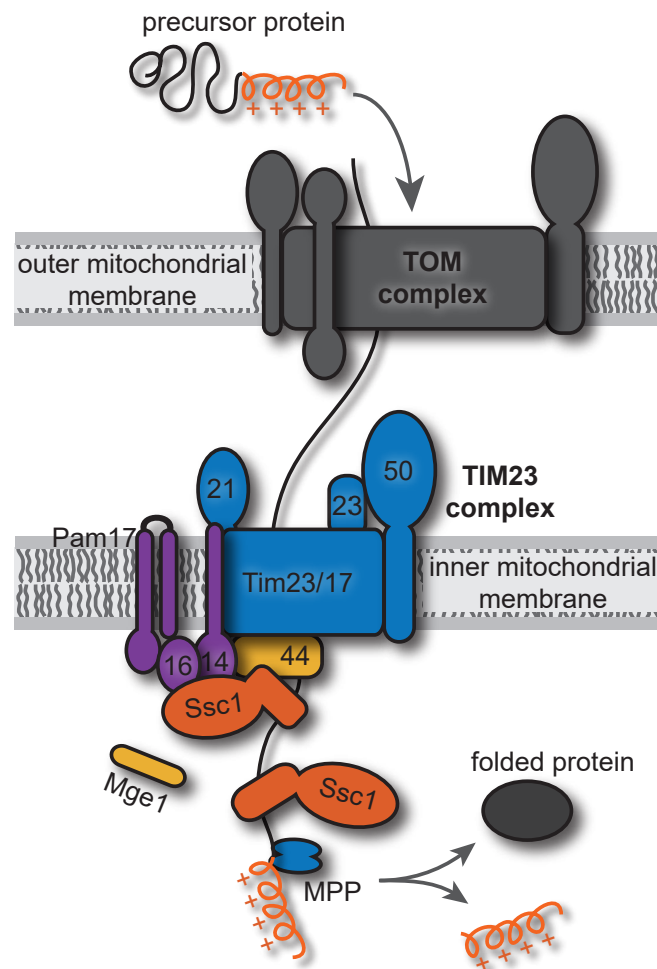


Figure 3.7.: Schematic of the mitochondrial presequence translocase. A precursor protein containing the characteristic mitochondria-targeting presequence is recognized by the TOM complex (gray) in the outer mitochondrial membrane and translocated through the TOM complex to the TIM23 complex (blue), and actively imported by the components of PAM: Tim44 (yellow), Tim14 and Tim16 (purple), Pam17 (purple), Ssc1 (orange) and Mge1 (yellow). Ssc1 can dissociate from the PAM complex for subsequent folding of the precursor protein. MPP (blue) cleaves the presequence. Adapted from [121] and [122].

binds to the peptide chain being translocated. Absence of Ssc1 leads to the complete shutdown of translocation. Another essential protein for protein translocation is the already previously mentioned nucleotide exchange factor Mge1 (Figure 3.7 yellow), which induces dissociation of Ssc1 from Tim44.^[124] Tim14 (Figure 3.7 purple), also known as Pam18, is the J protein of Ssc1 associated with protein translocation and is a membrane protein necessary for stimulation of ATP hydrolysis.^[125] Besides Tim14, the J-like protein Tim16 (or Pam16, Figure 3.7 purple) is also required.^[126] Most likely it evolved from Tim14 and lost some parts of the J-domain and thus its ability to stimulate the ATP hydrolysis of Ssc1.^[127] Mdj2, another J protein, is a membrane

protein and also part of the import motor, however, its depletion does not show a phenotype and it thus seems to not be essential.^[128,129] However, it does stimulate ATP hydrolysis of Ssc1 and is thus a functional J protein. The last associated protein is Pam17 (Figure 3.7 purple), an integral protein of the inner membrane, associated with Tim23. Most likely, Pam17 has a regulatory function by organizing the interaction of Tim14 and Tim16 and increasing the stability of the complex, but its exact role and working mechanism is not yet known.^[130] The presequence is cleaved by MPP (Figure 3.7 blue). Translocation will also be unsuccessful in the absence of Hep1. But as previously mentioned, Hep1 is essential for the correct folding of Ssc1 and increases its stability. Thus, its impact on translocation of proteins is not direct, but rather based on the integrity and function of Ssc1.

3.3.4.1. The peripheral membrane protein Tim44

Tim44 is a peripheral membrane protein exposed to the mitochondrial matrix and associated with the TIM23 complex. It can be isolated in complex together with Ssc1 and the nucleotide exchange factor Mge1.^[131] No ATPase stimulation of Ssc1 by Tim44 has been reported and its main role is to anchor Ssc1 to the translocase of the inner membrane (TIM23)^[108], although it has also been suggested that it might sense and interact with precursors themselves during import. The interaction of Tim44 with Ssc1 has been extensively studied.^[97,108,123,131] Tim44 does not interfere with the stimulation of ATP hydrolysis by Tim14 or peptide and thus binds at a different binding site. It interacts with the β -stranded part of the SBD of Ssc1, but not the substrate binding site. This interaction can occur when Ssc1 is bound to ATP or ADP, but with different affinities and the complex can only be purified together, in the absence of ATP.^[123] The nucleotide state of Ssc1 is sensed by the nucleotide-dependent conformation of the first two helices of the lid (αA and αB). Tim44 can also stably bind to the NBD of Ssc1.^[132] However, while the affinities of Tim44 for both domains of Ssc1 seem to be similar, they are both required for successful regulation of this interaction.^[133] Tim44 is thus a conformational sensitive switch, which binds Ssc1 in its ATP-bound form and releases it upon peptide binding, even without ATP hydrolysis.^[124] However, for stable binding of Ssc1 to the incoming sequence, ATP hydrolysis is required. As mentioned Mge1 can also induce release of ADP-bound Ssc1 from Tim44.^[124,134]

3.3.4.2. The J protein Tim14 and J-like protein Tim16

The J protein Tim14 (Pam18) and the J-like protein Tim16 (Pam16) are found as a subcomplex within the TIM23 complex. The N-terminus of the 18 kDa protein Tim14 reaches into the mitochondrial intermembrane space, while the J-domain is located in the matrix on the other

end of the transmembrane segment. Tim14 stimulates ATP hydrolysis to the same amount as the matrix J protein Mdj1 and deletion leads to disruption of protein translocation.^[108] Tim14 also seems to bind at the same location of Ssc1 as Mdj1 does, suggesting its specific role as a J protein of Ssc1 in protein translocation. In the complex, the J domains of the two proteins interact and both proteins show high similarities with each other. However, Tim16 is missing the signature HPD motif (Histidine, Proline, Aspartic Acid) of J proteins within the loop between two of the helices.^[127] Further, the exposed surface of Tim16 is mainly neutral or negatively charged, which is in contrast to typical J domains, which have a mainly positively charged surface, necessary for interacting with Hsp70s. There is no consensus whether Tim16 regulates the interaction of Tim14 with Ssc1 or whether its sole role is to recruit Tim14 to the translocase.^[127,135] Data suggests that a dimer of two Tim14-Tim16 dimers is formed by the interaction of the two Tim16 proteins. The region of interaction between the two Tim16 proteins is the same as in the interaction of Tim14 with Ssc1.^[127] If two Tim14-Tim16 complexes exist per translocation channel, this also opens the possibility that two Ssc1 are bound and the dimer interface of Ssc1 has a role in protein import.

3.3.4.3. The nucleotide exchange factor Mge1 in protein translocation

Similar to its role in protein folding, Mge1 acts as a nucleotide exchange factor of Ssc1 also in protein translocation. Binding of Mge1 to ADP-bound Ssc1 in the import motor complex leads to release of Ssc1 from Tim44.^[124,134] No such release is detected in the presence of ATP. Mge1 thus increases the occupation of Tim44 with active Ssc1:ATP instead of inactive Ssc1:ADP, which is unable to bind Tim44 and substrate simultaneously.^[124] However, pulldown experiments also showed that Mge1 is in complex with Tim44 and Ssc1 in the presence of ADP.^[131]

3.3.4.4. Role of Ssc1 in protein translocation

The essential parts of the import motor were already mentioned and shortly discussed in Section 3.3.4. Here, the role and working mechanism of Ssc1 in protein translocation will be discussed further. Without functional Ssc1, protein translocation into the matrix is not only impaired but fully inhibited. This is the case also for mortalin, the human mitochondrial Hsp70. In contrast, Bip, the Hsp70 of the ER, is not required for protein import but makes it more efficient.

Import across the inner mitochondrial membrane requires a membrane potential. As the presequence has multiple positive charges, this gradient induces its translocation into the matrix. The membrane potential is also a signal for Tim23 to open the translocation channel for the incoming precursor protein. However, it is not enough for complete translocation. Hence, the import motor

is needed. Interaction of Ssc1 with the positively charged presequence is only weak, whereas binding to binding sites further downstream of the precursor peptide is strong and provides the necessary driving force for successful translocation into the matrix. As long as no Ssc1 is bound to an internal sequence, the precursor protein can still slide back.^[97] The loose binding of Ssc1 to the presequence is probably necessary to ensure its exposure and cleavage by the mitochondrial processing peptidase (MPP) before subsequent folding of the protein.

There are three proposed models of how Ssc1, and the import motor in general, promotes translocation of precursor proteins into the matrix. One is the Brownian ratcheted model, which suggests that the role of Ssc1 is to trap the peptide and prevent it from backsliding. The peptide chain will move inward and outward by Brownian motion until the next possible binding sequence is exposed into the mitochondrial matrix and the next Ssc1 binds and prevents backsliding, thus promoting inward movement over time.^[96] There are two proposed pulling models in which the import motor actively produces inward motion of the peptide chain by a conformational change of Ssc1.^[53,56] One of them suggests a power stroke motion where the induced conformational change produced is large enough to pull the precursor further into the matrix so that the next Ssc1 can bind.^[131] However, no such conformational change in the right direction from the translocation channel has been found so far. The second model, entropic pulling, suggests that release of Ssc1 from the import channel increases its motional freedom. This increase in entropy leads to inward pulling of the precursor protein.^[53,54,136]

3.3.5. Other interacting proteins

Besides the large variety of substrates interacting with Ssc1 in its substrate binding groove, and possibly with the unstructured C-terminal domain attached to the α -helical lid, and the cochaperones interacting with Ssc1 during protein folding and protein translocation, there are many other interaction partners of Ssc1. Most of them form very stable interactions with Ssc1. A lot of interaction partners of Ssc1 have not yet been identified. However, in recent years, advances have been made in identifying and unraveling the various interaction partners of Ssc1. Ssc1 is involved in the ring formation of the Hsp60 chaperonin^[65] and also in the assembly of the cytochrome c oxidase.^[63,64] A recent crosslinking study by *Makepeace et al. (2020)*^[137] showed further interactions of Ssc1 with multiple proteins: e.g. Ecm10 (Ssc3), Atp2, Atp4, Aco1, Ald4 and Cox4. While the interaction with Cox4, a part of the cytochrome c oxidase, has already been intensively studied by *Boettinger et al. (2013)*^[64] and will be discussed in Section 3.3.5.3 in more detail, some of the other interactions are not yet clarified. Atp2 and Atp4 are components of the ATP synthase and Ssc1 could possibly have a similar role in assembly of the ATP synthase as it has in assembly of the cytochrome c oxidase. A possible interaction of Ecm10

with Ssc1 could be dimer formation as part of a regulatory function, e.g. in protein translocation together with the tetrameric Tim14-Tim16 complex. Aco1 is, similar to Ssc1, one of the more aggregation prone proteins of mitochondria, possibly because of oxidative modification of its Fe/S cluster cofactor.^[95,138] To prevent aggregation, Aco1 might thus be a substrate of Ssc1. Ald4 is a mitochondrial potassium-activated aldehyde dehydrogenase and the reason for the interaction with Ssc1 is unclear.

3.3.5.1. Hsp10 and Hsp60

Proteins smaller than 50 kDa, which are not successfully folded by Ssc1 alone, are handed over to Hsp60. Hsp60s are commonly also known as chaperonins and the best studied homologue is GroEL from *Escherichia coli*.^[51] They form large homooligomers consisting of two rings of 7 subunits stacked on top of each other. In this way, they build a large cavity, which can be closed by a complex of 7 subunits of Hsp10 (GroES in *E. coli*) as a kind of lid. The cavity is mostly lined with hydrophobic amino acids, which provide an attractive environment for unfolded proteins. After ATP hydrolysis, a structural change increases the presence of hydrophilic amino acids in the cavity, driving folding of the enclosed protein.^[47,139] Ssc1 has not only been shown to interact with Hsp60 and Hsp10 in the folding pathway of imported proteins but is also involved in maturation of the Hsp60 rings.^[65] While Hsp10 promotes early steps of the Hsp60 complex formation, Ssc1 binds to Hsp60 at different steps of the assembly process. Furthermore, Hsp10 and Ssc1 work together in the ring formation of Hsp60, but their interaction is lost in the presence of ATP. Since the interaction of Ssc1 with Hsp60 and Hsp10 does not depend on the presence of substrates and is also stable if Ssc1 is bound to Mge1, it is most likely not a substrate-like interaction, but a role of Ssc1 outside of protein translocation and folding.^[65]

3.3.5.2. Hsp78, a member of the Hsp100 group

The mitochondrial protein Hsp78 belongs to the group of Hsp100 proteins but is missing the N-terminal domain.^[47] It seems not to be an essential protein under most growth conditions but has been shown to interact with Ssc1. A phenotype of mitochondria lacking Hsp78 was only detected at very high temperature (42 °C) or in combination with mutations in Ssc1. Thus Hsp78 has a role in stabilizing Ssc1 in case of a mutation or under temperatures too high for Ssc1 to retain its tertiary structure.^[140,141] There are also indications that Hsp78 is not involved in preventing aggregation at high temperatures but rather recovery of aggregated proteins in combination with Ssc1.^[142] Other Hsp100 proteins disaggregate proteins by ATP-dependent threading of the peptide through a channel formed by multiple Hsp100 proteins and thus disentangling it.^[47]

3.3.5.3. The role of Ssc1 in the assembly of the cytochrome c oxidase

The cytochrome c oxidase (COX, also known as complex IV) is a large transmembrane complex of the inner membrane and part of the mitochondrial respiratory chain. The three core subunits, Cox1-3, are encoded in the mitochondrial DNA and several other subunits are encoded in nuclear DNA. Interestingly, Ssc1 has been shown to form complexes with proteins of COX from both categories and is involved in different steps of COX assembly. It plays a central role in the formation of respiratory chain complexes. The translation of *COX1* is activated by Mss51 (mitochondrial splicing suppressor protein 51), which forms a stable and ATP-independent complex with Ssc1. Mss51 binds, even when Ssc1 has been preincubated with substrate protein, indicating a different binding site than the substrate binding groove.^[63] Mss51, Ssc1 and Mdj1 form a complex during translation of Cox1 at the mitochondrial ribosome to ensure proper folding of Cox1. Translation of the gene *COX1* is regulated by complex formation of Cox1 with Mss51 to prevent it from binding to the promoter region on the mRNA. This complex contains Ssc1 and Cox14 and remains assembled until incorporation of Cox1 into the COX complex.^[63] Cox4, a subunit of COX that needs to be imported by the mitochondrial translocation system, also forms a stable complex with Ssc1, together with Mge1. Experiments with a temperature sensitive mutant of Ssc1 showed that this complex is different from the complex during protein translocation. However, it is ATP sensitive and dissociates after binding of ATP to Ssc1. When Cox4 cannot be integrated into COX, it remains in complex with Ssc1 and Mge1.^[64] It is not clear where these proteins bind to Ssc1 and what influence they have on the conformation and dynamics of Ssc1.

Taken together, a variety of proteins interact with Ssc1 in a different way than substrates and their influence on the structure and structural dynamics of Ssc1 is not known for most of them. This complicates the study of the conformational state of Ssc1 *in vivo* since it is hard to dissect the interactions of Ssc1 at any given point of time. Specifically for FRET-studies of Ssc1, this means that bulk measurements are hard to interpret based on the high heterogeneity of the system, and single-molecule measurements are also difficult to interpret because most of the interactions are missing in *in vitro* studies.

3.4. Previous FRET experiments of Ssc1

In previous single-molecule FRET experiments by *Mapa et al. (2010)*^[4] and *Sikor et al. (2013)*^[5] two different FRET sensors were established to study the conformational dynamics of Ssc1. The lid sensor (SL) reports on the extent of lid opening and has two fluorescent labels at position 448 in the β -sheet base of the SBD and at position 590 within the α -helical lid of the SBD. The

domain sensor (SD) monitors the interdomain distance and is labeled at the same position in the SBD (residue 448) and at position 341 in the NBD.

Mapa et al. (2010)^[4] carried out solution burst measurements on both sensors. In agreement with the crystal structure of DnaK (PDB: 4B9Q) and the homology model of Ssc1, they observed a high FRET state for the interdomain distance in the presence of ATP and a low FRET state for the lid sensor. In the presence of ADP, the FRET histograms showed broad distributions for both sensors, suggesting that Ssc1 is either heterogeneous or dynamic. Similar distributions were detected in the presence of ATP together with the cochaperone Mdj1 at single-turnover conditions. However, the histograms do differ from the ones recorded in the presence of ADP. Interestingly, bulk FRET measurements suggest complete domain undocking and lid closure in the beginning and then slow equilibration towards the already known ADP-bound conformation. This might be explained by synchronized hydrolysis after addition of Mdj1 and then non-synchronized nucleotide exchange, leading to an average FRET value. When the model substrate P5 is added to ATP-bound Ssc1 in the presence of Mdj1 under single-turnover conditions, the histograms look more defined, with a low FRET efficiency for the domain sensor and a high FRET efficiency for the lid sensor.^[4] This is again in agreement with the crystal structure of DnaK in the presence of ADP and substrate (PDB: 2KHO) and the corresponding homology model of Ssc1. As both substrate and especially Mdj1 stimulate the ATP hydrolysis rate of Ssc1, it can be assumed that Ssc1 is bound to ADP and substrate in the FRET measurement as well. Measurements of release of the Mge1 from the Ssc1 complex upon addition of ATP showed a concentration dependence of the release rate and release occurring on the millisecond time-scale. Release measurements of Mdj1 showed that Mdj1 remains bound to Ssc1 after ATP hydrolysis with a half-life of the complex of around 5 min. However, in presence of Mge1 and/or substrate, release occurs on faster time-scales.^[4] With the analysis methods available, the nature of the dynamic behavior of Ssc1 could not be studied further.

Sikor et al. (2013)^[5] were interested in further study of the dynamic behavior of Ssc1 and did so using single-molecule TIRF experiments. To this end, labeled Ssc1 molecules were encapsulated in vesicles together with nucleotides and substrate. These vesicles were then immobilized on a glass surface for FRET measurements on a TIRF microscope. In the presence of ATP, the results were pretty similar as in the burst experiments. The lid sensor was detected in a static low FRET state (13 % \pm 8 %) and the domain sensor mainly in a high FRET state (91 % \pm 4 %) with some short explorations to an intermediate FRET state (48 % \pm 15 %). As already expected from the solution burst measurements, Ssc1 is highly dynamic in the presence of ADP. Determined with a hidden Markov model (HMM) analysis^[143], lid dynamics occurred between an intermediate FRET state (37 % \pm 8 %) and a high FRET state (89 % \pm 7 %). Interestingly, the dwell time distribution for lid closing cannot be fit by a single-exponential decay, suggesting the presence of multiple closed states. The domain dynamics occurred between a high FRET state (81 % \pm 3 %)

different from the high FRET state observed in the presence of ATP, and an intermediate FRET state ($50 \% \pm 8 \%$), similar to the ATP intermediate FRET state. The dynamics of the lid and the domain sensor occurred on different time-scales, suggesting that they are uncoupled. This hypothesis was further underlined by a recent three-color FRET study by *Voith von Voithenberg et al. (2021)*. Here, all three labeling positions (341, 448 and 590) were used in a single protein to study three instead of just one distance at the same time. Domain and lid motions showed little correlation.^[6] Applying the HMM analysis for the interdomain dynamics, *Sikor et al. (2013)* extracted dwell times for different concentrations of ADP present inside the vesicles. While domain-docking was concentration dependent and faster with higher concentrations of ADP in solution, domain-undocking kinetics did not change significantly. The addition of $5 \mu\text{M}$ Mge1 also did not have an effect on the rates. Addition of a large excess of phosphate (known to increase the affinity of Ssc1 for ADP), however, led to faster docking and slower undocking rates. Taken together, they conclude, that the dynamics correspond to binding and unbinding of ADP and the intermediate FRET state is, in fact, a nucleotide-free state.^[5] In the presence of both ADP and substrate, the lid sensor is in a static high FRET state ($73 \% \pm 5 \%$), different from the high FRET state occupied in the presence of only ADP. The domain sensor shows a static low FRET state ($26 \% \pm 6 \%$) resembling separated domains and an extended interdomain linker. They further investigated the influence of Mge1 on the interdomain distance of ADP- and ATP-bound Ssc1. The short explorations of the intermediate FRET state in the presence of ATP completely disappeared and static high FRET was detected. However, dynamics in the presence of ADP were still visible. A dwell-time analysis showed that Mge1 had no effect on the rate of ADP binding and only a minor effect on the rate of ADP release. When ATP and substrate were added together to Ssc1, cycling of Ssc1 could be detected and binding or release of substrate was always from or to a nucleotide-bound state, and not the nucleotide-free state.^[5]

4. *In vitro* characterization of Ssc1

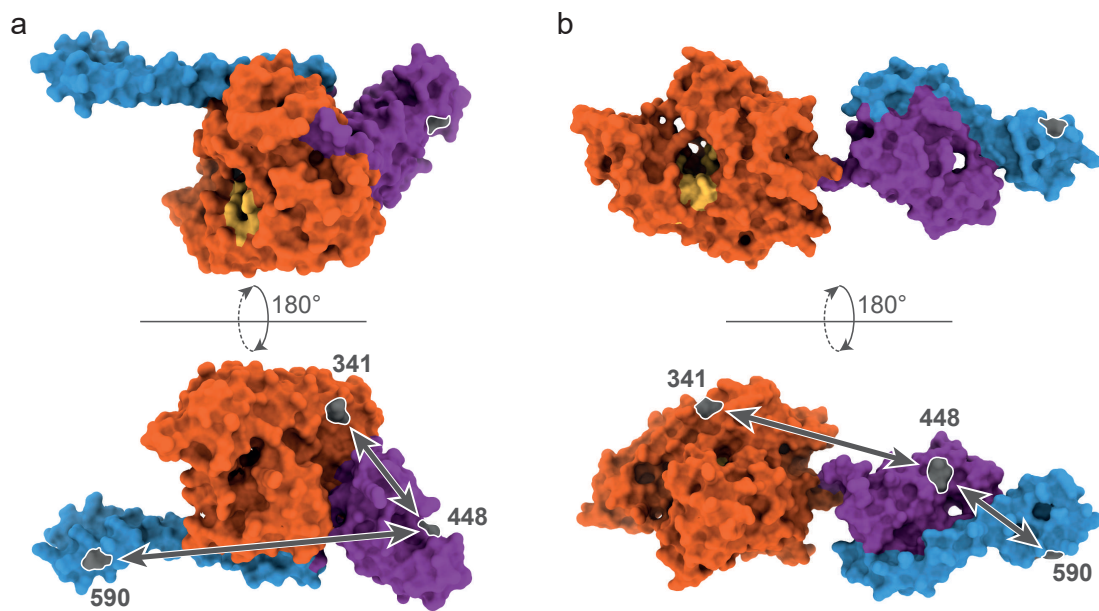


Figure 4.1.: Labeling Positions of the domain sensor and the lid sensor of Ssc1. a) A homology model of ATP-bound Ssc1 based on the structure of DnaK (PDB: 4B9Q). The NBD (orange) and the β -sheet containing base of the SBD (purple) are docked together, and the α -helical lid (blue) is wide open. Residues interacting with the nucleotide are depicted in yellow. The exposed substrate binding groove is on the right side of the structure. Labeling positions D341C and I448C are used for the domain sensor and positions I448C and D590C are used for the lid sensor. b) A homology model of ADP- and substrate-bound Ssc1 based on the crystals structure of DnaK (PDB: 2KHO). The NBD (orange, with nucleotide binding residues in yellow) and the SBD (purple) are separated with an extended linker and the lid (blue) closes upon the substrate binding groove. The residues used for labeling of the domain sensor (341, 448) and the lid sensor (448, 590) are presented in the bottom structure. The homology models were generated using SwissModel.

The conformational dynamics of multi-domain proteins interacting with several components, like nucleotides, substrates and other proteins, are highly complex and not easily unraveled. In order to better understand the working mechanism of the mitochondrial Hsp70, Ssc1, the movement of the two domains and the movement of the lid in respect to the SBD were studied in single-molecule FRET burst experiments. Application of pulsed interleaved excitation (PIE) and multiparameter fluorescence detection (MFD) gives rise to a multitude of information helpful to unravel the conformational changes occurring during the chaperoning cycle of Ssc1.

The labeling positions on Ssc1 used in this study were the same ones as used in previous studies^[4,5] from our group. The mutant Ssc1-D341C-I448C has been shown to reliably report on the interdomain distance of Ssc1 with one cysteine in the NBD and one in the β -sheet subdomain of the SBD. From homology models based on the crystal and NMR structures of DnaK (Figure 4.1) a high FRET efficiency is expected for ATP-bound Ssc1 (Figure 4.1a) and a low FRET efficiency for substrate-bound Ssc1 (Figure 4.1b). Indeed, this is what has been detected previously.^[4,5] Also, the FRET histograms of the lid (Ssc1-I448C-D590C) reflect the conformations expected from the available structures. This mutant has one cysteine in the β -sheet base of the SBD and one in the α -helical lid. ATP-bound Ssc1 shows low FRET and thus an open lid (Figure 4.1a) and substrate-bound Ssc1 has high FRET with the lid closed (Figure 4.1b).^[4,5] In Figure 4.1, the NBD is colored in orange and the amino acid residues interacting with the nucleotide are depicted in yellow. The β -sheet containing the substrate binding-cleft is shown in purple and the α -helical lid in blue. The unstructured C-terminal region continuing from the tip of the lid is not represented here, as it was removed to obtain the crystal structures. The exact structure and location of the C-terminal region under the individual conditions remains unknown.

The dye pair used for this study differs from previous studies by the use of a different acceptor dye. The previously used red dye Atto647N is known to be very hydrophobic. While care has been taken to exclude influences of the dye on the behavior of Ssc1 (functional tests like ATPase activity and anisotropy information from smFRET measurements), it is still possible that the dye changes the dynamic behavior of Ssc1 by interacting with the protein and stabilizing certain conformations. Especially, interactions with the exposed hydrophobic substrate binding cleft or the hydrophobic substrates themselves are possible. Furthermore, this dye could not be used for the *in organello* measurements of this thesis (see Section 5.1.3), as it has been reported that Atto647N sticks to membranes, especially mitochondrial membranes.^[13,144,145] Several dyes have thus been tested and Atto647 has proven to be a good alternative. Atto647 exhibits similar photophysical properties and is more hydrophilic than Atto647N. Also, the Förster radius of the dye pair with Atto532 is the same as for the previous dye and FRET efficiencies are thus expected to be very similar to the ones obtained from the previous studies. While Atto643 has better photophysical properties, it was not available at the time when this measurement series was started, but was used for the experiments in Section 4.6.

4.1. The influence of nucleotides and substrate on the conformation of Ssc1

Ssc1 interacts with substrates in an ATP-dependent manner. Therefore, we studied the influence of the two nucleotides ATP and ADP on the conformational structure of Ssc1. Since the main functions of Ssc1 involve binding of a substrate in the substrate binding pocket, the influence of substrate on the structure of Ssc1 was also studied. The model substrate used was P5, a 10 amino acid long peptide (CALLLSAPRR) and a part of the mitochondrial targeting sequence of the aspartate aminotransferase from chicken.^[107] The sequence consists of mostly hydrophobic sequences that are preferentially bound by the substrate binding pocket of Ssc1. It is a commonly used model substrate for Ssc1 as well as DnaK and thus its binding to Ssc1 is well studied. Previous studies suggest that non-hydrolyzable ATP-derivatives cause structural changes in Ssc1 and cannot replace ATP.^[6] For this reason, ATP was added in high excess to make sure ADP is quickly exchanged for ATP in the case of successful hydrolysis and the majority of Ssc1 was ATP-bound.

4.1.1. Ssc1 in the presence of ATP

ATP-bound Ssc1 shows one main population for both the domain and the lid sensor. The domains are docked close together as can be concluded from the high FRET value of the observed population (Figure 4.2a upper left in purple). In contrast, the lid sensor shows low FRET, meaning the lid is wide open. The lid sensor also shows a second small population with high FRET (Figure 4.2b upper left in purple). This population likely originates from hydrolyzed ATP (thus ADP). While ATP hydrolysis is slow (0.032–0.13 mol ATP per mol Ssc1 per min)^[4,61,93,104,106–108], it is expected to occur over the time course of the 3h measurement. Docked domains and an open lid were expected for ATP-bound Ssc1, as this was suggested already from the homology model based on DnaK (cf. Figure 4.1a) and from previous smFRET measurements.^[4,5] The graph on the left of the lower panel of Figure 4.2a shows an E- τ -Plot of ATP-bound Ssc1. While a part of Ssc1 lies on the static FRET line, some of Ssc1 shows conformational dynamics. Similar sub-millisecond dynamics of the lid are not observed in the E- τ -plot of the lid sensor (Figure 4.2b lower left).

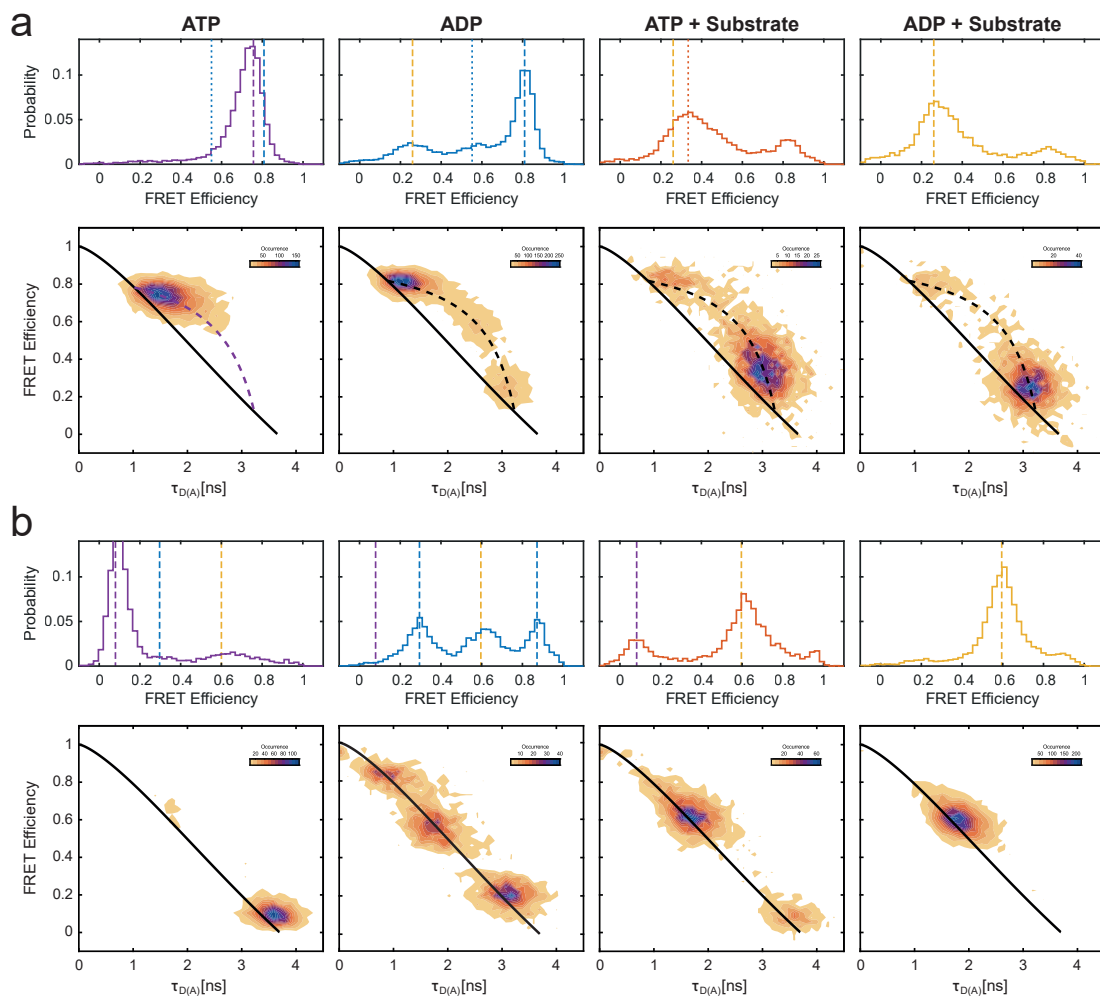


Figure 4.2.: SmFRET histograms and E- τ -plots of Ssc1 in the presence of nucleotide and substrate. a) Top row: SmFRET histograms of the domain sensor of Ssc1 in the presence of ATP (purple), ADP (blue), ATP and substrate (orange), and ADP and substrate (yellow). Bottom row: E- τ -Plots of the domain sensor in the presence of ATP, ADP, ATP and substrate, and ADP and substrate. Populations on the static FRET line (solid line) do not show dynamics while populations on the dynamic FRET line (dashed line) do show dynamics on the millisecond or sub-millisecond timescale. b) Top row: SmFRET histograms of the lid sensor of Ssc1 in the presence of ATP (purple), ADP (blue), ATP and substrate (orange), and ADP and substrate (yellow). Bottom row: E- τ -Plots of the lid sensor in the presence of ATP, ADP, ATP and substrate, and ADP and substrate. The solid line is the static FRET line.

4.1.2. Ssc1 in the presence of ADP

The addition of ADP to Ssc1 mimics conditions post ATP hydrolysis. Both the histograms of the domain and the lid sensor show a clear difference when Ssc1 is bound to ADP as compared to ATP. Three distinct populations are visible in both histograms (Figure 4.2 blue histograms in a and b). Dynamic PDA^[28] results show that half of ADP-bound Ssc1 has docked domains, which can be detected as a high-FRET population of the domain sensor. Furthermore, a low FRET and medium FRET population are observed. The low FRET population represents undocked domains with an extended interdomain linker, as can also be seen in the homology model of Ssc1 when bound to substrate. To further understand the origin of the intermediate FRET population, the E- τ -plot is helpful. The plot shows that this population, in fact, is a population of proteins dynamically transitioning between conformations while diffusing through the confocal volume. This population nicely lies on the dynamic FRET line with the high and low FRET population as end points. The domains of Ssc1 bound to ADP are thus docking and undocking on the sub-millisecond timescale, with half of the proteins remaining in the docked state for longer periods. This finding is in agreement with previous spTIRF experiments in which Ssc1:ADP remained in a high FRET state for seconds with shorter explorations to a lower FRET state.^[5] The three populations of the FRET histogram of the lid sensor differ clearly from the very low FRET population observed when ATP is bound. The intermediate FRET population is also found in the presence of substrate (see section below) and can be assigned to a closed lid. The low FRET population has an interdyer distance between the open and the closed lid conformation. Such a partially closed lid has been previously reported for Bip and DnaK.^[79,89] The third population of ADP-bound Ssc1 shows a high FRET efficiency. The fraction of this population increases over time as can be seen in the time-wise FRET histogram in Figure 4.3a. Here, the smFRET histogram is plotted for 30 min intervals over the 3 h measurement. The low FRET population decreases over this time course while the high FRET population increases. Since the intermediate FRET efficiency is already the result of the closed lid, the question of the underlying structure of the high FRET population arises. One possibility would be a collapsed lid, which leads to a higher proximity of the two dyes than in the closed lid conformation. Another possibility is a dimer or oligomer of Ssc1 leading to an intermolecular high FRET state. Dimeric and oligomeric species of Ssc1 have previously been reported in the absence of nucleotide or in the presence of ADP only.^[98,104,107] It has also been reported that Hep1, the Hsp70 escort protein, which is necessary for *de novo* folding of Ssc1, also stabilizes Ssc1 under these conditions and prevents oligomerization.^[98,104] The addition of Hep1 to Ssc1:ADP almost completely prevents formation of the high FRET population while overall maintaining the rest of the FRET histogram (Figure 4.3b). The presence of Mdj1 together with ADP-bound Ssc1 also reduces the high FRET population (Figure 4.3c). Taken together, this suggests that the high FRET population of ADP-bound Ssc1 originates from Ssc1 dimers. Since Hep1 and Mdj1 bind to a mutually

exclusive binding site on the NBD^[106], this region is most likely the origin of dimerization and both cochaperones shield it. In summary, the domains of ADP-bound Ssc1 switch between a docked and an undocked state. The lid shows no such dynamic behavior on the same timescale. This is in agreement with 3c-FRET experiments which suggest that the dynamics of the lid and the domains are not correlated.^[6]

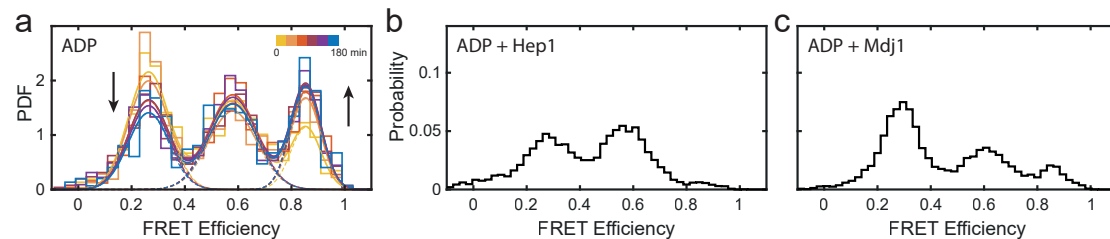


Figure 4.3.: In-depth examination of the high FRET state of the lid sensor. a) A time series of smFRET histograms from the ADP-bound lid sensor of Ssc1 showing an increase of the very high FRET population over the time course of 3 h in time blocks of 30 min. Gaussian probability density functions are shown for each time block. b) SmFRET histogram of ADP-bound lid sensor in the presence of Hep1. c) SmFRET histogram of ADP-bound lid sensor in the presence of Mdj1.

4.1.2.1. The high FRET populations of the domain sensor for ATP- and ADP-bound Ssc1

The FRET efficiency of the high FRET population of the domain sensor for ADP-bound Ssc1 slightly varies from the FRET efficiency of ATP-bound Ssc1 (Figure 4.2a). This small difference also resulted in the need for a different dynamic FRET line for both of the measurements. The interdomain dynamics of most remaining measurements (see below), except in the presence of ATP and Mge1, could be represented with the dynamic FRET line used for ADP. As the labeling position in the NBD is on the back of the ATP-binding groove, small shifts of the amino acids interacting with the nucleotide might also influence this region. It is possible that a rotation of the two domains in respect to each other causes this small difference in FRET efficiencies. Within the scope of this dissertation, efforts have been made to increase this difference in order to reliably differentiate between ATP- and ADP-bound Ssc1 high FRET states (see Section 4.6).

4.1.3. The influence of substrate on the conformation of Ssc1

The addition of substrate P5 to Ssc1 generally causes binding as Ssc1 has a high affinity to hydrophobic peptide sequences. However, the release rate in the presence of ATP is also fast and ATP hydrolysis is necessary for stable binding. The FRET efficiency of the interdomain distance

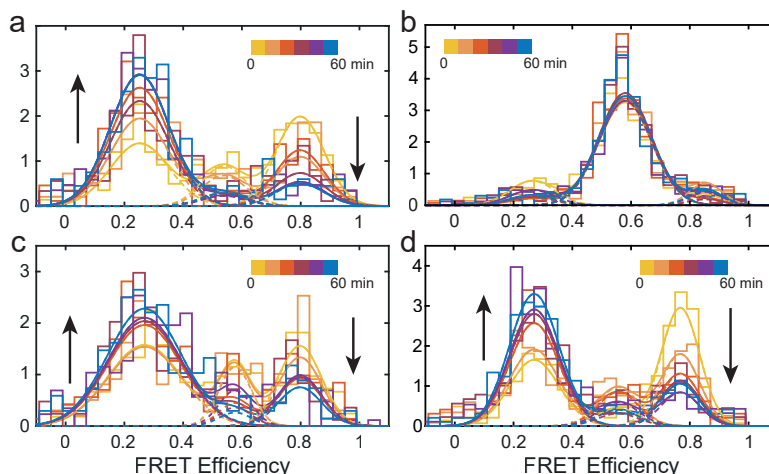


Figure 4.4.: Time series of smFRET histograms of Ssc1 in the presence of substrate. a) A time series of smFRET histograms from the domain sensor of Ssc1 in the presence of ADP and substrate. The fraction of the low FRET population (substrate bound population) increases over the time course from 0–60 min after the start of the measurement in time blocks of 10 min. Gaussian probability density functions are shown for each time block. b) A time series of smFRET histograms from the lid sensor of Ssc1 in the presence of ADP and substrate. No significant change of the histogram over the time course of 60 min is detected. c) A time series of smFRET histograms from the domain sensor of Ssc1 in the presence of ATP, substrate and Mdj1. The substrate-associated population increases during the first 60 min after the start of the measurement in time blocks of 10 min. d) A time series of smFRET histograms of the domain sensor in the presence of ATP, Mdj1 and substrate. The sample was equilibrated for 1 h at single-molecule concentrations in the absence of substrate before the start of the measurement.

drastically decreases in the presence of substrate for both nucleotides. This is due to domain separation. However, the FRET efficiencies of the low FRET populations are not the same for both nucleotides (see Figure 4.2a orange and yellow histograms). While full domain separation is expected in the presence of ADP, as known from the homology model, Ssc1 shows a more dynamic behavior in the presence of ATP and the population is shifted to higher FRET efficiencies. While some dynamic averaging is expected in both cases due to the length and dynamic behavior of the interdomain linker, the low FRET population in the presence of ATP is more clearly located on the dynamic FRET line (Figure 4.2a bottom, second from right). There are two possible explanations for the increased dynamic behavior. Either transient binding of substrate to Ssc1 causes short-lived domain separation, or Ssc1 cycles through ATP hydrolysis, release of ADP and substrate and rebinding of ATP. However, as mentioned previously, ATP hydrolysis is slow in the absence of Mdj1. While a small population of open lid remains in the presence of ATP, binding of the substrate seems to lead to stable lid closure in the presence of either of the nucleotides. The smFRET histogram of the lid sensor of ADP-bound Ssc1 in the presence of substrate is

dominated by one high FRET population associated with a closed lid. This shows that substrate binding can occur even to the ADP-bound form of the Hsp70 and with very high efficiency. The dimeric species of ADP-bound Ssc1 is minor in the presence of substrate since substrate binding causes monomerization. This is either because of competition for hydrophobic surfaces of Ssc1 or because of the structural change and static nature of substrate-bound Ssc1.^[107] The lid sensor of Ssc1 shows almost no dynamic behavior in the presence of substrate.

Taken together, it seems that even though substrate is stably bound by the lid in the presence of ATP, this signal is not enough to lead to stable domain undocking or ATP hydrolysis. With regard to the allosteric communication between the domains, this means that more than one signal is needed for the complete conformational change from open lid and docked domains to closed lid and undocked domains. Of course, it is still possible that the information that ATP is still bound in the nucleotide binding pocket eventually causes the lid to open up again and release substrate. However, only little dynamic lid movement is detected and such dynamics would have to be on a slow timescale not detectable in our burst experiments.

Unique to the four measurements of Ssc1 in the presence of only nucleotides and substrate (ADP and substrate, and ATP and substrate for both domain and lid sensors) were high intensity bursts indicating large aggregates. The occurrence of these aggregates increased with the age of the P5 aliquots (which are stored at -80°C) and slightly decreased when P5 was sonicated before the measurement. Since they were not detected in the presence of cochaperones, fluorescent impurities of P5 can be excluded as the cause of these high intensity bursts. Since P5 is a strongly hydrophobic peptide it is not surprising that it forms higher order oligomers in aqueous solution. Therefore, it is likely that these high intensity bursts originate from P5 aggregates decorated with multiple fluorescently labeled Ssc1 proteins. This is a typical example of multiple Ssc1 working together to stabilize and dissolve aggregated proteins. However, as Ssc1 is only present in μM concentrations and P5 is added at $100\ \mu\text{M}$, Ssc1 is not able to successfully resolve those aggregates. In the measurements with Mdj1 present, those aggregates are a rare occurrence, most likely due to the chaperone function of Mdj1 and it being present at higher concentrations ($5\ \mu\text{M}$) than Ssc1. Thus, it is able to bind P5 and dissolve the aggregates. To decrease the amount of P5 aggregates, P5 was sonicated before use. However, this did not completely dissolve all P5 aggregates. These large burst were filtered out from the analysis.

4.2. The influence of Mdj1 and Mge1 on the conformation of Ssc1

Ssc1 is strongly regulated by its cochaperones. The J protein Mdj1 increases the ATPase activity of the NBD of Ssc1 thus stabilizing substrate interaction and promoting protein folding.^[93] Mdj1

is also known to interact with substrates themselves and recruit them to Ssc1. It has been reported that Mge1 acts as a stress sensor and only binds to Ssc1 in the absence of stress.^[109] In this way, nucleotide exchange and substrate release is thought to be put on hold to avoid release of folded proteins into stress conditions where they are likely to aggregate again. As these cochaperones have such a fundamental influence on the function of Ssc1, it is important to understand the specific impact they have on the structural conformation of Ssc1 and how these interactions influence the working cycle of Ssc1. To this end, the influence of Mdj1 and Mge1 on the structure and conformational dynamics of Ssc1 in different nucleotide states and in the presence and absence of substrate was studied.

4.2.1. Ssc1 in the presence of J protein Mdj1

As expected, addition of Mdj1 to ATP-bound Ssc1 leads to ATP hydrolysis and the smFRET histogram of the domain sensor of Ssc1 (Figure 4.5a left) looks almost identical to the one of ADP-bound Ssc1. Most of the proteins are in a high FRET state with docked domains, while some show undocked domains and some are dynamically switching between the two conformations. The dynamic behavior can also be observed in the E- τ -plot (Figure 4.5a bottom left). The lid sensor however, shows some remaining open lid conformation (low FRET population in Figure 4.5b left). This could either be incomplete ATP-hydrolysis or rebinding of ATP owing to its presence at very high concentration (1 mM). Spontaneous nucleotide release can happen and ATP is more likely to be bound due to the high availability as well as the higher affinity to Ssc1.^[110] The FRET population of the lid sensor assigned to oligomerized Ssc1 is not present in the presence of Mdj1. Both the presence of ATP and Mdj1 have previously been shown to prevent oligomerization of Ssc1.

As the main task of Mdj1 is to stimulate the ATPase activity of Ssc1, not much impact on the FRET histograms of ADP-bound Ssc1 is expected. No influence on the FRET distribution of the interdomain distance is observed (Figure 4.5a second histogram). As already discussed, there is a minor decrease of the very high FRET population of the lid sensor of Ssc1 (Figure 4.3c and Figure 4.5b second histogram in black compared to blue) due to stabilization of ADP-bound Ssc1 and prevention of dimerization or even oligomerization. This suggests transient binding of Mdj1 to Ssc1 even when Ssc1 is ADP-bound. The reason for this binding is unclear and cannot be unraveled by these experiments. One possible explanation is that Mdj1 regularly inspects Ssc1 to gather information on the nucleotide state.

The smFRET histograms of ATP-bound Ssc1 in the presence of substrate already looked fairly similar to ADP-bound Ssc1 even without Mdj1 present (cf. Figure 4.2). Thus no major changes

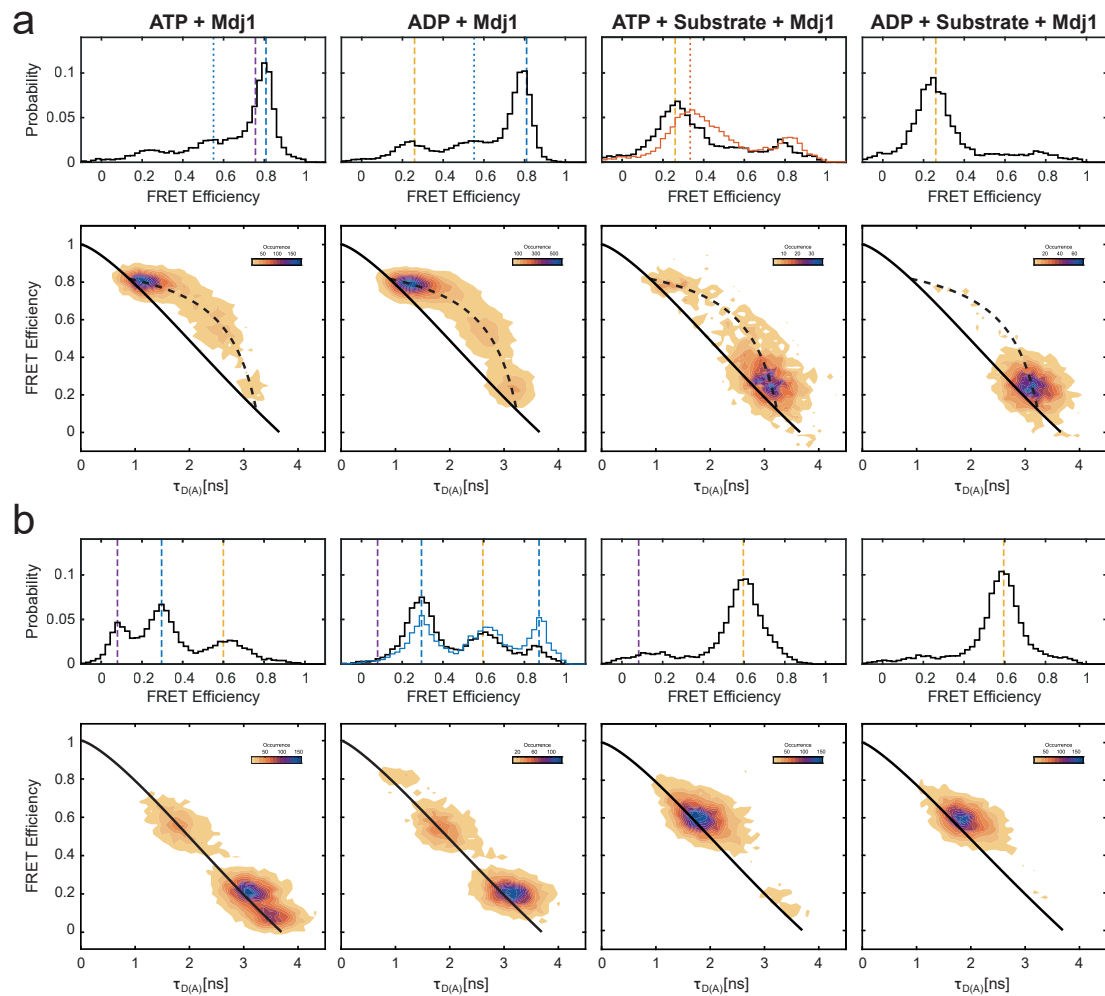


Figure 4.5.: SmFRET histograms and E- τ -plots of Ssc1 in the presence of Mdj1. a) Top row: SmFRET histograms of the domain sensor of Ssc1 in the presence of Mdj1 and ATP, ADP, ATP and substrate, and ADP and substrate. The smFRET histogram of ATP and substrate without Mdj1 is overlaid in orange for comparison. Bottom row: E- τ -Plots of the domain sensor in the presence of Mdj1 and ATP, ADP, ATP and substrate, and ADP and substrate. Populations on the static FRET line (solid line) do not show dynamics on the millisecond and sub-millisecond timescale while populations on the dynamic FRET line (dashed line) are dynamic. b) Top row: SmFRET histograms of the lid sensor of Ssc1 in the presence of Mdj1 and ATP, ADP, ATP and substrate, and ADP and substrate. The smFRET histogram in the presence of ADP without Mdj1 is overlaid in blue for comparison. Bottom row: E- τ -Plots of the lid sensor in the presence of Mdj1 and ATP, ADP, ATP and substrate, and ADP and substrate. The solid line is the static FRET line.

are expected. The low FRET population of the domain sensor, however, is shifted to lower FRET efficiency compared to what is measured in the absence of Mdj1 (Figure 4.5a third histogram, black compared to orange). The population now coincides with the FRET efficiency in the

presence of ADP and substrate, representing fully separated domains. Since Mdj1 stimulates ATP hydrolysis, ADP is expected to be bound to the NBD, which causes conformational changes leading to stable domain separation. This supports the assumption that allosteric communication in Ssc1 is not only mono-directional, but signals from both the substrate binding domain (binding of substrate) as well as the nucleotide binding domain (hydrolysis of ATP) are needed for the structural transition to be stable with a closed lid and undocked domains.

No influence of Mdj1 on the FRET histograms of ADP-bound Ssc1 in the presence of substrate could be observed (Figure 4.5a and b, histograms on the right). This is to be expected, since substrate is already recruited and Ssc1 is already in its ADP-state and no ATP hydrolysis is necessary. It is expected that Mdj1 accelerates substrate binding. However, such a difference could not be determined with this experimental design, since measurements were started a few minutes after addition of Mdj1 or substrate, and thus after successful substrate binding. Since the model substrate P5 is present in a high excess, the influence of Mdj1 on the rate of substrate binding is likely minor.

Our data confirm the role of Mdj1 in the stimulation of ATP hydrolysis. These results further suggest that Mdj1 stimulates ATP hydrolysis not only in the presence of substrate, but also in the absence of substrate. It has previously been shown that the substrate binding rate of ADP-bound Ssc1 is higher than for ATP-bound Ssc1. However, as it was expected that substrate binding precedes ATP hydrolysis the biological implication for ADP-bound Ssc1 being able to bind substrate was unclear. The fact that stimulation of the ATPase activity also happens in the absence of substrate suggests that there is some biological role of ADP-bound Ssc1 in the chaperoning cycle. In addition, Mdj1 seems to interact, at least transiently, with Ssc1 in its ADP-bound form, which leads to stabilization of Ssc1 and the prevention of dimer formation. The exact biological implications of this interaction remain unclear but the transient interactions might be necessary to detect the nucleotide-state of Ssc1 and the stabilization of Ssc1 could be just a byproduct.

4.2.2. Ssc1 in the presence of nucleotide exchange factor Mge1

It is known that Mge1 interacts with both nucleotide states of Ssc1. Thus, it is interesting to see whether Mge1 only affects the nucleotide state of Ssc1 or has a further influence on its conformation and dynamics. The influence of Mge1 on the smFRET histogram of the domain sensor of Ssc1 in the presence of ATP is very subtle (Figure 4.6a left histogram). The dynamic population, showing up as averaged intermediate FRET efficiency, slightly increases compared to Ssc1 with only ATP in solution (Figure 4.2a left histogram). This small increase in the dynamic population is best visible in the associated E- τ -plots and also appears in the summarized PDA

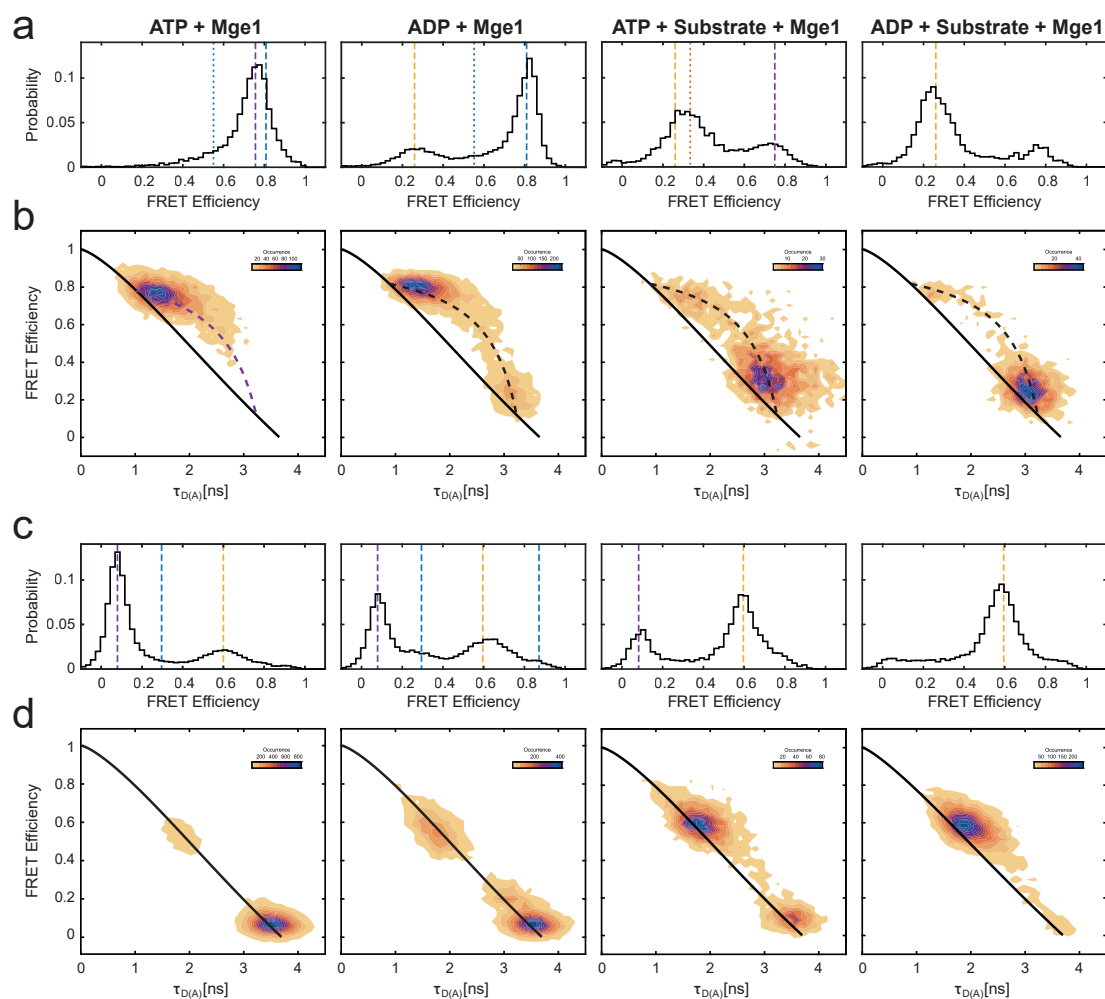


Figure 4.6.: SmFRET histograms and E- τ -plots of Ssc1 in the presence of Mge1. a) Top row: SmFRET histograms of the domain sensor of Ssc1 in the presence of Mge1 and ATP, ADP, ATP and substrate, and ADP and substrate. For comparison, smFRET histograms of ADP as well as ATP and substrate in the absence of Mge1 are shown in blue and orange, respectively. Bottom row: E- τ -Plots of the domain sensor in the presence of Mge1 and ATP, ADP, ATP and substrate, and ADP and substrate. Populations on the static FRET line (solid line) do not show dynamics on the millisecond and/or sub-millisecond timescale while populations on the dynamic FRET line (dashed line) are dynamic. b) Top row: SmFRET histograms of the lid sensor of Ssc1 in the presence of Mge1 and ATP, ADP, ATP and substrate, and ADP and substrate. Bottom row: E- τ -Plots of the lid sensor in the presence of Mge1 and ATP, ADP, ATP and substrate, and ADP and substrate. The solid line is the static FRET line.

results in Figure 4.9a. However, unsurprisingly, most of the proteins still show docked domains, as the ATP in solution is able to interrupt the Ssc1:Mge1 interaction quickly. In the smFRET histograms of the lid sensor (Figure 4.2b and Figure 4.6b left histograms) the fraction of open

lid decreases (very low FRET) and the fraction of closed lid increases (intermediate FRET) in the presence of Mge1 (also see Figure 4.9b). Only a minor fraction of Ssc1 is involved and the biological implications of this lid closing are not immediately obvious. A possible reason could be a structural change subsequent to Mge1 binding or it is related to a previously proposed nucleotide-free state.^[5]

Interactions of Mge1 with ADP-bound Ssc1 are expected to be longer-lived and more clearly visible in the smFRET histograms since reportedly, ADP is less successful in dissociating the two proteins.^[107] The changes in the interdomain distance distribution are only slightly visible. In contrast to ATP-bound Ssc1, the interdomain dynamics of ADP-bound Ssc1 decrease in the presence of Mge1 (cf. Figure 4.9 and Figure 4.6a second histogram; black with, blue without Mge1). Homology models based on the interaction of DnaK and GrpE from *E. coli*^[146] suggest that Mge1 binds between the two domains (NBD and SBD). This provides a reasonable explanation for suppression of the domain movement. Since the domains are docked in the ATP-bound state of Ssc1, binding of Mge1 causes domain separation. Fast release of the complex because of binding of ATP enables domain docking. This results in the increase of the dynamic fraction of Ssc1 in the presence of ATP and Mge1. The change in the distribution of the lid conformations of ADP-bound Ssc1 upon addition of Mge1 is most pronounced. The size of the intermediate FRET population with a FRET efficiency of around 0.6 does not change significantly. However, the population with the high FRET efficiency, which was attributed to oligomeric Ssc1, decreases significantly. As already detected for the addition of Hep1 and Mdj1, the interaction with Mge1 possibly stabilizes ADP-bound Ssc1 and prevents oligomerization. The low FRET population decreases to around one third of the size it was in the absence of Mge1. This partially closed lid conformation does not seem to be favorable when bound to Mge1. Instead, a very low FRET population, associated with a wide open lid, appears and dominates the histogram (Figure 4.6b second histogram). This open lid conformation is otherwise only detected in the presence of ATP. However, no ATP is present in the solution because purified ADP has been used. Mge1 must thus be able to cause a strong conformational shift, opening up the lid of Ssc1, even in the absence of ATP. It is possible that this conformation has no nucleotide bound in the NBD and is primed for fast ATP binding.

The presence of Mge1 has only a minor impact on the FRET histograms of the substrate-bound species of Ssc1. The results of the dynamic PDA of the domain sensor, however, suggest that the low FRET population of Ssc1 in the presence of ATP, substrate and Mge1 has a higher fraction of static, completely separated domains and less of the dynamically switching species (Figure 4.9a, and Figure 4.6a, third histogram, black with, orange without Mge1). This is surprising since it has been previously suggested that besides nucleotide exchange, Mge1 is also involved in substrate release, which would lead to less occupation of the low FRET population. It is possible, that binding of Mge1 inhibits domain dynamics and a high fraction of proteins measured are

detected in an Mge1 bound state. The discrepancy can also be attributed to the fact that, due to the short peptide sequence of only 10 amino acids, there is no folded product, and thus the concentration of possible substrate does not decrease over time. Thus, the fast substrate release is triggered by Mge1 and is compensated by the instant rebinding of substrate. The process of substrate release and rebinding would need to happen faster than the domain separation to result in this smFRET histogram. The E- τ -plots of the lid sensor in the presence of substrate appear more heterogeneous in the presence of Mge1 (Figure 4.2 and Figure 4.6 two histograms and E- τ -plots on the right). One might argue that this heterogeneity appears as dynamics, even after species-wise calculated γ -factors have been applied. Such dynamics could be induced by possible substrate release and rebinding due to the presence of Mge1, but most molecules are in a state with stably bound substrate. Our data show little evidence for the interaction of Mge1 with substrate-bound Ssc1 or influence of Mge1 on the structure of Ssc1 when bound to substrate, and almost no substrate release. These findings imply that there are other factors inducing substrate release, like downstream chaperones (e.g. Hsp90 or Hsp60) or the need for a change of the three-dimensional structure of the substrate. Such a structural change of the substrate could be the driving force for lid opening and substrate release.

4.2.3. Ssc1 in the presence of ATP, substrate, Mdj1 and Mge1

To detect the conformational changes occurring during the full chaperoning cycle of Ssc1, the two FRET sensors were studied in the presence of ATP, substrate and both chaperones, Mdj1 and Mge1. The cycle is now not stalled at a certain point but can actually continue and start over again. When looking at the resulting E- τ -plot (Figure 4.7 bottom left), it is immediately obvious that the domain sensor is highly dynamic. Indeed, dynamic PDA shows that the percentage of the dynamic population is very high (Figure 4.9a). Under these conditions, the sub-millisecond dynamics suggest a very efficient chaperoning cycle. The population of Ssc1, which is stably bound to substrate with a closed lid, remains rather high. But it is lower than for substrate-bound Ssc1 in the presence of ATP and only one of the two cochaperones. This suggests that the presence of both, Mdj1 and Mge1, leads to more substrate release and the two proteins work cooperatively.

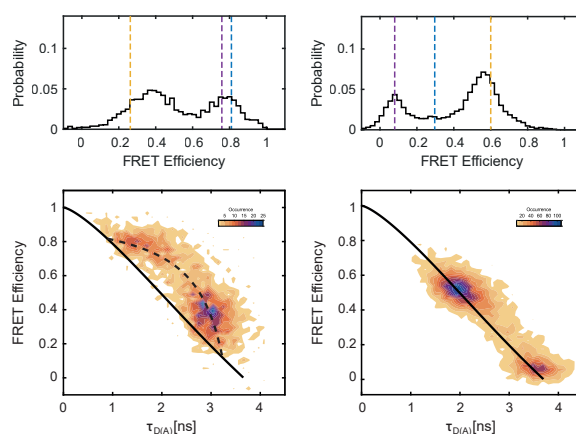


Figure 4.7.: SmFRET histograms and E- τ -plots of Ssc1 ATP, substrate, Mdj1 and Mge1. Sm-FRET histograms (top) and E- τ -plots (bottom) of the domain (left) and lid sensor (right) of Ssc1 in the presence of ATP, substrate, Mdj1 and Mge1. The dashed lines indicate the position of the main population in the presence of ATP (purple), ADP (blue) and ADP and substrate (yellow). In the E- τ -plots, the solid line represents the static FRET line and the dashed line represents a dynamic FRET line.

4.3. Dynamic photon distribution analysis of the sub-millisecond dynamics of Ssc1

To better understand the nature of the dynamic behavior of Ssc1, a dynamic photon distribution analysis (dynamic PDA) was applied. Very interestingly, in 11 out of the 13 tested combinations of solution additives, the dynamics occur between the same two populations of Ssc1. Only the measurement in the presence of ATP, and ATP and Mge1 the high FRET state differs. The domains can be tightly docked (with a slight difference between ATP- and ADP-bound high FRET) or completely extended. Dynamic PDA was fit globally to all 13 conditions. From the E- τ -plots and lifetime fits of the lifetime of the donor fluorophore in presence of the acceptor, the start and end populations of the dynamic structural changes are known. The model contained a static-dynamic mixture in which the two end states can be static or dynamically exchanging. It has been previously shown that Ssc1 is also dynamic on longer timescales^[5]. Molecules appearing static in our measurements on the sub-millisecond to millisecond timescale are thus likely dynamic on slower timescales. Two minor populations at very low and very high FRET were added to account for "impurities". Since PDA accounts for broadening because of shot noise and the heterogeneity of the system, it is able to fit the experimental data well when the right model is applied. This also means that PDA is sensitive to "impurities" and they need to be included in the model. Such occurring "impurities" are not necessarily other fluorescent particles but can also be caused by blinking of the fluorophores and by multi-molecule events. It is important to note that many conditions could also be fit with a static PDA model. However,

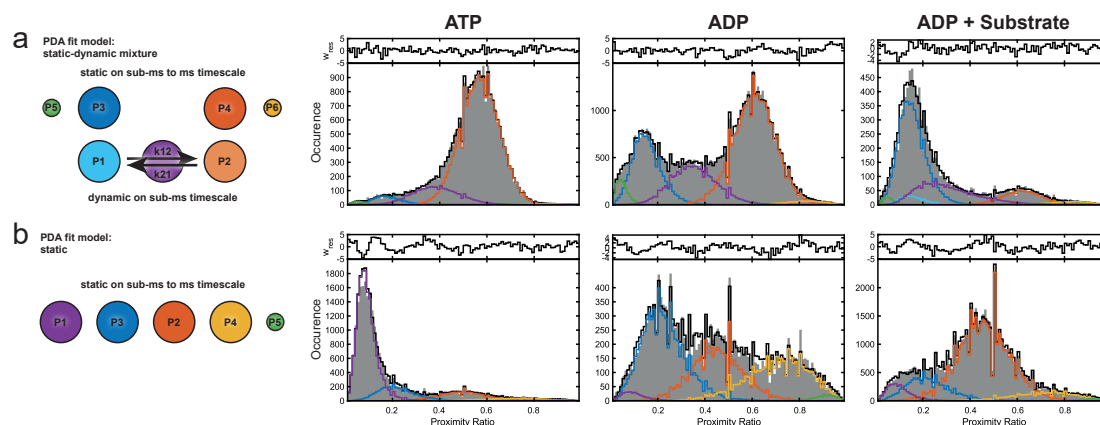


Figure 4.8.: PDA models and exemplary PDA fits. a) Single-molecule proximity ratio histogram and the corresponding dynamic PDA analysis for the domain sensor. Left: A scheme of the dynamic PDA model is shown with a static-dynamic mixture between two FRET states (P3/P1 and P4/P2). The fractions static on the millisecond timescale are P3 (blue) and P4 (orange). Molecules with the same FRET efficiency but dynamic are accounted for with P1 (light blue) and P2 (light orange). Molecules of the dynamic population have an averaged FRET efficiency (between P1 and P2) and are shown in purple. P5 (green) and P6 (yellow) account for "impurities". Right: Dynamic PDA fit results for ATP, ADP and ADP with substrate. b) Single-molecule proximity ratio histogram and the corresponding PDA analysis for the lid sensor. Left: A scheme of the static PDA model is shown with 4 populations (A1–A4) and an additional fifth population, A5 (green), accounting for "impurities". Right: PDA fit results for ATP, ADP and ADP with substrate.

for consistency, all conditions were fit with the same model. Fixing the distance for the high FRET populations (small distance, R2 for both the sensors, see Table A.1 and Table A.2) did not lead to satisfactory PDA fit results and the fit was thus allowed to adopt values $\pm 2.5 \text{ \AA}$ around the value from the first global fit. For the domain sensor this can be explained by the different conformations of the docked domains in the presence of ATP and ADP leading to varying FRET values. In the case of the lid sensor, the population with varying FRET values is the closed lid, where slight changes are also expected depending on the presence and orientation of the substrate influencing the extent of possible lid closure. For the lid sensor, a static PDA Fit with four populations was applied with an additional minor very high FRET population to account for "impurities".

Exemplary PDA fits are represented in Figure 4.8 for the three conditions ATP, ADP and ADP with substrate for the domain sensor (top) and the lid sensor (bottom). All other PDA fits can be found in the appendix. In the PDA histograms of the domain sensor, the end states are represented by the blue and orange populations. The dynamically averaged population is depicted in purple. In the case of slower dynamics, molecules not transitioning between structures while diffusing

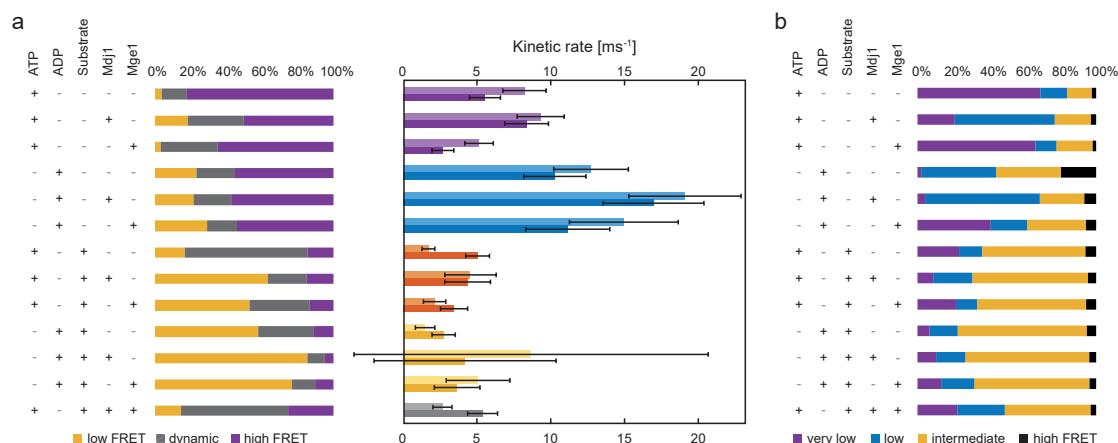


Figure 4.9.: Results of the PDA fit of the smFRET data. a) Analysis of the domain sensor for all 13 conditions. Left: Percentages of the low FRET (yellow), dynamic (gray), and high FRET (purple) populations are shown. Right: Transition rates of the dynamic population of each of the measurements. k_{12} is on top and reports on the rate of the transition from undocked to docked domains and k_{21} is on the bottom and reports on the rate of the transition between undocked and docked domains. Conditions in the presence of ATP are shown in purple, ADP in blue, ATP and substrate in orange, ADP and substrate in yellow, and ATP, substrate, Mdj1 and Mge1 in gray. The error bars are based on the confidence intervals from the PDA fit. b) Analysis of the lid sensor for all 13 conditions. Percentages of the very low (purple), low (blue), intermediate (yellow), high FRET (black) populations are shown.

through the confocal volume, but statistically belonging to the dynamic population, are observable as a smaller population within the static population (e.g. light blue within the blue histogram of ADP and substrate in Figure 4.8). Because a fit based on a static-dynamic mixture was applied, this distinction is made in the representation of the PDA fit results and can also be seen in the graphic representation of the fit model on the left. The amplitude of the dynamic population is set to 1 and the amplitudes of the other populations are given in Table A.1 and Table A.2 in relation to that. The small green and yellow populations in the domain sensor histograms are needed to account for fluorescent impurities and possible multi-molecule events in the very high and very low FRET regions. In the smFRET histograms for the lid sensor the yellow population is the oligomeric population of Ssc1, mainly appearing for ADP-bound Ssc1. The green population also accounts for impurities as for the domain sensor. Such impurities can occur in protein measurements because of the complex purification process, labeling, and buffer components. Their percentage with respect to the total burst events detected, however, remains low, as can also be seen in the summary tables of the PDA fit results (Table A.1 and Table A.2). They were excluded for the calculation of the percentages of the populations represented in Figure 4.9.

4.3.1. Kinetics of the domain dynamics

The first observation is that all obtained kinetics in the dynamic PDA fits are on a similar timescale with sub-millisecond rates. These are quite fast dynamics for detection with burst analysis and thus appear as an averaged but separate population in the smFRET histograms instead of just a bridge between the two populations. This is especially apparent in the histogram of the domain sensor of ADP-bound Ssc1 (Figure 4.2a blue histograms). The middle population appears as a Gaussian population itself. Without the additional dynamic information from the E- τ -plots, it could have easily been mistaken for a third static conformation.

The transition rates in the presence of ATP are on a similar timescale (Figure 4.9a right, purple). In the presence of Mge1 (3rd from top in Figure 4.9), the dynamics are slower, which can be attributed to the already previously mentioned binding of Mge1 between the two domains. The rates in the presence of ADP are faster than in the presence of ATP. This is especially interesting in the presence of Mdj1. Although both samples, ATP and ADP, are expected to be bound to ADP due to ATP hydrolysis, there are differences in the rates. This is likely due to different interactions with Mdj1 because of the different nucleotide state. It is apparent that the rates in the presence of substrate are slower than in the absence of substrate. This highlights the two different origins of conformational dynamics. The dynamics in the absence of substrate possibly stem from exploration conformations. This could be related to allosteric communication to sense conformational changes in the other domain caused by binding of substrate, ATP hydrolysis, binding of ATP or release of ADP. During stable binding of substrate, interdomain communication is not as important. This could be a possible reason for the slower dynamics.

A more detailed analysis of the kinetics of the interdomain dynamics shows two different types of dynamics. One species shows slightly faster docking rates than undocking rates. This is mainly observed in the absence of substrate. The other species shows slower domain docking than undocking. This is especially pronounced in the presence of ATP and substrate or in the presence of ATP, substrate, Mdj1 and Mge1. These conditions are related to cycles of ATP binding, substrate binding, possibly ATP hydrolysis, and finally substrate release.

4.4. Slow domain separation in the presence of substrate

Another interesting finding is that domain separation after addition of substrate occurs over the time span of up to 60 min, as can be seen in the time-wise smFRET histogram of Ssc1 in the presence of ADP and substrate in Figure 4.4a. Each histogram represents a 10 min time

window and the low FRET population slowly increases over time. Such slow dynamic behavior cannot be observed for lid closure (Figure 4.4b), which is apparent immediately after starting the measurement. The time between substrate addition and start of the measurement ranges from 2–5 min. Thus, substrate binding is immediate independently of the nucleotide bound to Ssc1, but domain separation is a slower process. This slow domain separation can be observed for all conditions measured in the presence of substrate and it cannot be attributed to ATP-hydrolysis or the influence of one of the cochaperones. To exclude temperature effects, a sample of Ssc1 was equilibrated in the presence of ATP and Mdj1 at room temperature for 1 h before addition of substrate and start of the measurement. Also in this measurement, a slow domain separation over the time course of 60 min after addition of substrate could be observed (compare Figure 4.4c and d). This observation of immediate lid closure but delayed domain separation is another example of non-correlated conformational changes of Ssc1. Similar observations have been made by *Vogel et al.* where lid closure can be observed before ATP hydrolysis.^[81,83] The smFRET histograms in Figure 4.2, Figure 4.5 and Figure 4.6 in the presence of substrate only include data acquired at least 60 min after measurement start to show steady-state conformations. This is valid for both, the domain and the lid sensor; even though no change was detected for the lid sensor, we wanted to make sure that all protein was at equilibrium before the start of the measurement.

4.5. Proposed model of the chaperoning cycle of Ssc1

Based on the data obtained from the 13 different measurement conditions and the two different FRET sensors (domain sensor and lid sensor), the existing model of the chaperoning cycle of Ssc1 could be revised and improved. The updated model is shown in Figure 4.10.

Ssc1 bound to ATP in the absence cochaperones or substrate is assumed as the start and end point of the chaperoning cycle. The NBD and SBD are docked close together while the α -helical lid is wide open, stretched away from the substrate binding groove in the β -sheet base of the SBD. In this conformation, the substrate binding groove of Ssc1 is easily accessible and in a high energy state, able to use the energy from ATP hydrolysis for e.g. structural changes. The presence of substrate, specifically exposed stretches of hydrophobic amino acid sequences, leads to immediate binding to the peptide and closure of the lid. This step does not require ATP hydrolysis but instead is possible that the hydrophobic interactions of the substrate with the SBD provides the energy for closing of the lid. While binding of substrate by lid closure seems to be instant and stable on the millisecond timescale, the two domains keep moving with respect to each other with domain undocking being faster than domain docking. Under single-turnover conditions or in the presence of Mdj1, Ssc1 is able to hydrolyse ATP and fully transition to a conformation with undocked domains and an extended interdomain linker and the lid remaining

tightly closed upon the bound substrate.^[4] ATP hydrolysis is fast in the presence of the J protein Mdj1 and slow in the presence of only substrate. Mdj1 can also induce hydrolysis of ATP to ADP in the absence of substrate. The conformation of Ssc1 bound to ADP and substrate is very stable and cannot be permanently interrupted by either Mge1 or Mdj1 alone. Substrate release by Mge1 is not visible under the conditions used in these measurements because instant rebinding of substrate occurs. Our results imply that substrate can be released in the presence of both Mdj1 and Mge1 together with ATP. Further experiments with larger model substrates are necessary to see if this hypothesis holds. It is possible that a structural change within the substrate protein is also necessary to indicate successful folding and induce lid opening. Substrate release results in ADP-bound Ssc1, which is highly dynamic with fast fluctuations in the interdomain distance on the sub-millisecond timescale. This species is aggregation prone and can form long-lived oligomers. Previous smTIRF data suggests that the protein can recover from this state^[5] and return to the dynamic ADP-state of Ssc1. Mge1 is now able to induce ADP-release and also causes a structural change leading to lid opening. This structural change possibly enables either ADP-release or ATP-binding. It is further possible that the objective of the lid opening is substrate release assuming that the substrate is folded and the substrate concentration is low enough to prevent instant rebinding. In the next step, ATP binding causes dissolution of the Ssc1:Mge1 complex and Ssc1 is in its original ATP-bound state again.

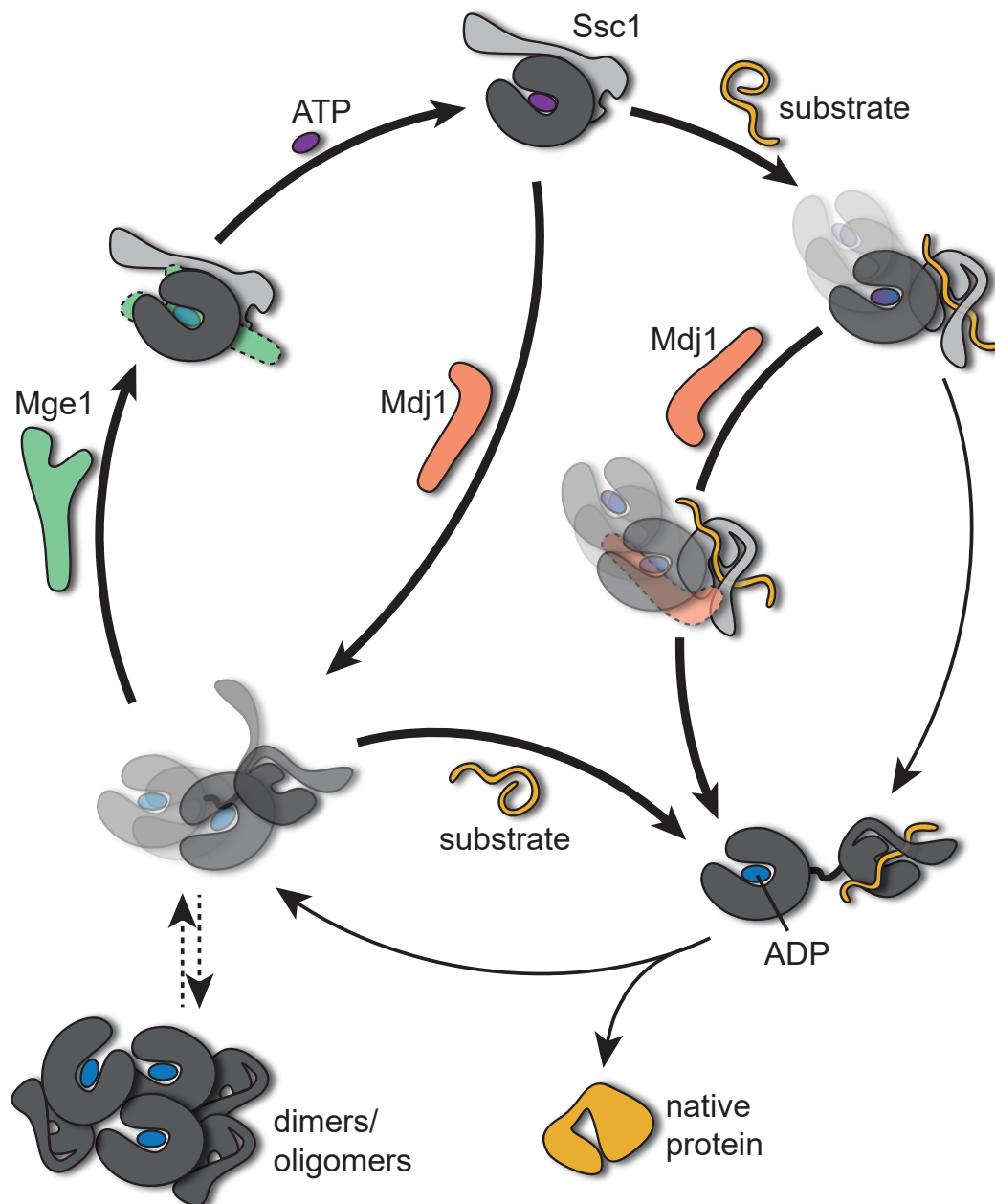


Figure 4.10.: Proposed model for the chaperone cycle of Ssc1. Starting at the top: When bound to ATP (purple), the domains of Ssc1 are docked and the lid is open. In the presence of substrate (yellow), the lid closes. ATP is slowly hydrolyzed to ADP (blue), or the the hydrolysis rate is sped up by Mdj1 (orange; right internal pathway). Mdj1 induced hydrolysis can also occur without substrate (left internal pathway). The combination of substrate binding and ATP hydrolysis leads to full domain separation. ADP-bound Ssc1 without substrate shows fast dynamics of the domains. From this state, collapse of Ssc1 is most likely (black), although seemingly reversible. Mge1 (green) induces a conformational change that leads to the release of ADP and binding of ATP.

4.6. Variations of labeling positions of Ssc1

As discussed in Section 4.1.2.1, the high FRET populations of the domain sensor of Ssc1 have similar FRET values when bound to ADP or ATP. This has also been observed in previous smTIRF experiments.^[5] Based on the obtained single-molecule data, it is difficult to assess how significant the difference in conformation of the NBD is between the ATP and ADP bound states. It is possible that the conformational difference is small and only a few amino acids are shifted. It is also feasible that the arrangement of the domains differs quite significantly between the two conditions and the two labels coincidentally have the same distance. To further understand the domain arrangement when the domains are docked, and to improve the contrast in FRET values between the two nucleotide bound conformations, five new FRET sensors were designed. The labeling sites on the NBD were mainly chosen further away from the label in the SBD than the previous labeling site at position D341. In this way, an attempt was made to lower the FRET efficiency and bring it into a more sensitive range and achieve higher resolution. It was further taken into consideration to not label too close to the nucleotide binding pocket to not interfere with nucleotide binding and release.

The labeling positions chosen for the new Ssc1 mutants are shown in Figure 4.11. The original domain sensor SD (Sensor Domain) of Ssc1 was labeled at positions D341C and I448C. Domain sensor B (SD-B) is labeled at positions Q111C and I448C. Domain sensor C (SD-C) is labeled at positions Q327C and I448C. Domain sensor D (SD-D) is labeled at positions E374C and I448C. Domain sensor E (SD-E) is labeled at positions K337C and I448C. Domain sensor F (SD-F) is labeled at positions S378C and I448C.

SD-B and SD-C were expressed, purified, labeled and measured prior to the other mutants. They were labeled with Atto532 as the donor fluorophore and Alexa fluor 647 as the acceptor fluorophore. Alexa Fluor 647 was chosen instead of Atto647N, which was used in prior experiments, because it is less hydrophobic and a potential influence of the fluorophore on the protein conformation and dynamics is less likely. Before expression of SD-D, SD-E and SD-F, Atto-Tec released the dye Atto643. Atto643 is less hydrophobic than Atto647N but has similar photophysical properties such as high photostability and high brightness. Therefore, the last three domain sensors were labeled with both, Atto643 and Alexa Fluor 647. Interestingly, although labeled in parallel, labeling efficiencies differed between batches. The final measurements of SD-D and SD-F were carried out with the proteins labeled with Atto532 and Atto643. SD-E proved to be difficult to label in general and only by using Alexa647 as the acceptor, could some labeling be achieved. The difficulties in the labeling efficiency hint towards unsuccessful folding of the protein. All proteins were measured in the presence of ATP, ADP, and ADP and substrate.

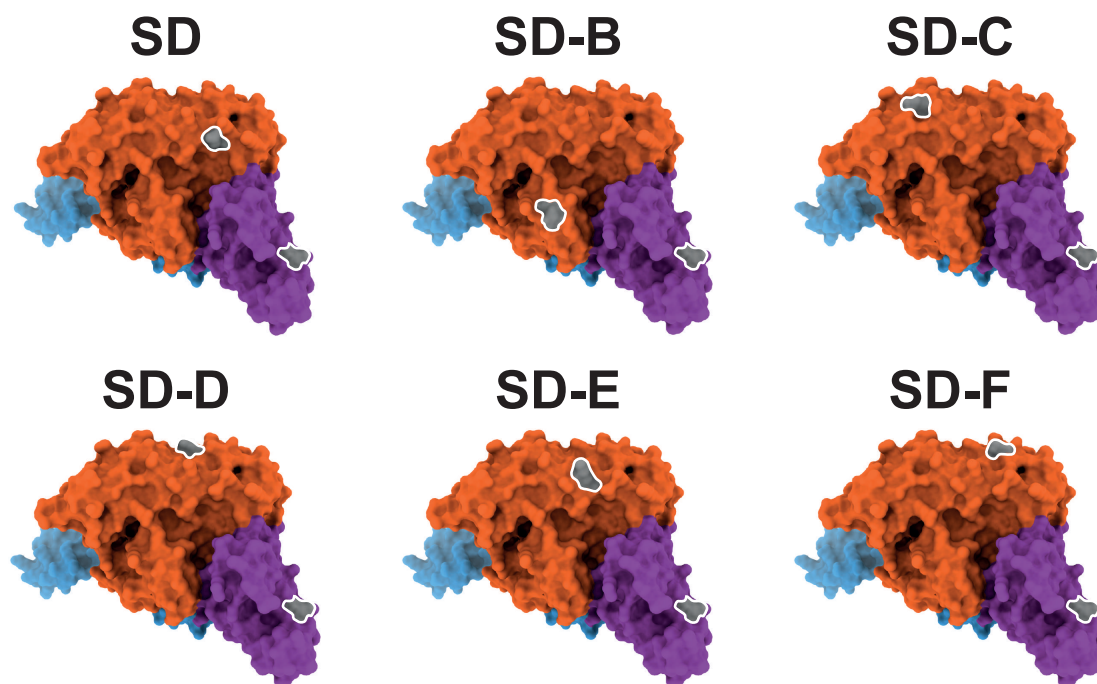


Figure 4.11.: Graphical representation of the labeling positions of the new domain sensors of Ssc1. The labeling positions are shown in gray with a white outline in the ATP-bound structure of Ssc1 when the NBD (orange) and the SBD (purple) are docked. Top row: The original domain sensor SD (Sensor Domain, Ssc1-D341C-I448C), the new domain sensors SD-B (Ssc1-Q111C-I448C) and SD-C (Ssc1-Q327C-I448C). Bottom row: The new domain sensors SD-D (Ssc1-E374C-I448C), SD-E (Ssc1-K337C-I448C) and SD-F (Ssc1-S378C-I448C).

4.6.1. No clear difference in high FRET species of SD-B

The Ssc1 domain sensor SD-B shows a high FRET efficiency when measured in the presence of ATP (Figure 4.12). Because of the docked domains and the chosen labeling position, this is expected. The labeling positions were put at the same distance in the two available structures (left and right of the histograms) as compared to SD. In the presence of ADP, SD-B also shows a high FRET efficiency. The maximum is slightly shifted to higher FRET values, however, no clear separation from the high FRET efficiency of ATP-bound Ssc1 SD-B is possible. When Ssc1 SD-B is bound to ADP and substrate, a low FRET population appears. However, there is still a significant high FRET population left. This suggests the presence of a high FRET "impurity", meaning a species with docked domains or a species with impaired folding and thus appearing as high FRET. The difference in FRET efficiency between ATP and ADP is not big enough to clearly distinguish between the two states or draw conclusions on the exact conformations in the different nucleotide states. Furthermore, the labeling position seems to impair folding or function of the protein.

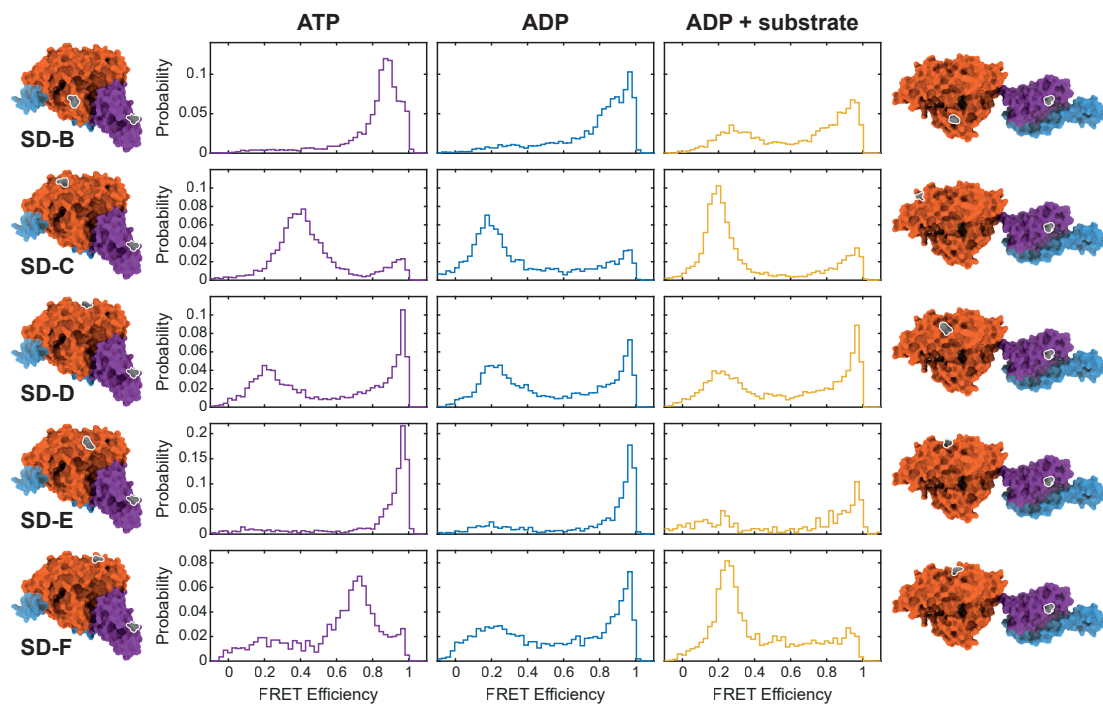


Figure 4.12.: SmFRET histograms of the new domain sensors of Ssc1. On the left, the labeling positions of the mutants are shown in the ATP-bound homology model of Ssc1 based on DnaK (PDB: 4B9Q). In the middle, the smFRET histograms of each of the sensors in the presence of ATP (purple), ADP (blue) and ADP and substrate (yellow) are shown. On the right, the labeling positions are shown in the ADP and substrate-bound homology of Ssc1 based on DnaK (PDB: 2KHO).

4.6.2. SD-C does not show a high FRET species

The smFRET histograms of the Ssc1 domain sensor SD-C show only little high FRET "impurities" caused by aggregated or not properly folded Ssc1 (Figure 4.12). When bound to ATP, SD-C has an intermediate FRET efficiency of around 0.4. The fluorescent labels are placed further apart than for the other mutants and thus this is not surprising. In the presence of ADP, this FRET efficiency is even lower (around 0.2). While this mutant shows the aspired clear separation between ATP and ADP FRET efficiencies, SD-C shows the same FRET efficiency in the presence of ADP and substrate. This takes away the possibility of observing the full cycle of Ssc1 and thus this mutant is also not suitable for following the full conformational cycle of Ssc1.

4.6.3. The function of SD-D is impaired

The Ssc1 domain sensor SD-D proved difficult to handle during expression and purification. However, a good labeling with the fluorescent dyes Atto532 and Atto643 was achieved. The smFRET histogram of Ssc1 SD-D in presence of ATP shows a low FRET and a high FRET population (Figure 4.12). The same histogram is measured in presence of ADP or ADP and substrate. The absence of a conformational change, especially between ATP and ADP with substrate, suggests impaired function of SD-D. With the problems that occurred already during expression, the mutations themselves likely cause this impairment and not only the fluorescent labels.

4.6.4. Defective expression and folding of SD-E

The Ssc1 domain sensor SD-E yielded a low amount of labeled protein for both acceptor dyes Atto643 and Alexa Fluor 647. After further investigation, this was because of the low expression levels of Ssc1 SD-E and impurities of smaller proteins or protein fragments still present after purification. Expression and purification was repeated, however, without success. At this timepoint, problems in overexpression of Mge1 arose. Mge1 is needed for purification of Ssc1, and thus its inavailability also effects the availability of purified Ssc1. SmFRET histograms of the small amount of labeled protein show high FRET in the presence of ATP and ADP together with a small low FRET population in the presence of ADP and substrate (Figure 4.12). However, expression and purification of this protein would need to be repeated once Mge1 is available again.

4.6.5. SD-F is a possible candidate to observe the full cycle of Ssc1

The Ssc1 domain sensor SD-F shows a high FRET efficiency when bound to ATP (Figure 4.12). SD-F also shows a high FRET efficiency in the presence of ADP, however, the two high FRET populations are clearly separated. ADP-bound SD-F also shows some low FRET, which is consistent with previous knowledge of multiple populated conformations of Ssc1 in the presence of ADP. When bound to ADP and substrate, Ssc1 SD-F shows a low FRET efficiency and thus separated domains. Three clearly distinguishable populations could be detected in these measurements and can be assigned to the different conditions. However, all of these smFRET histograms show a high degree of background impurities. Ssc1 SD-F would thus need to be expressed and purified again in order to achieve higher purity. As mentioned in the previous

section, purification of Ssc1 needs Mge1 and Mge1 could not be overexpressed at the time. Thus, a new batch of SD-F could not be synthesized.

4.6.6. Summary

Taken together, the experiments with the different new domain sensors of Ssc1 showed that mutations can have a strong impact on proper folding and function of proteins. For this reason, SD-D and SD-E could not be evaluated further. SD-B showed a similar FRET distribution as the original domain sensor SD-D and is thus not suited for detection of the whole cycle. While SD-C shows a significant difference between ADP and ATP, the FRET efficiency of ADP alone coincides with that of ADP and substrate. Therefore, SD-C is also not suitable to study the full cycle. SD-F does show promising well-separated FRET populations, but the batch measured is not pure enough for high-quality data analysis. In the future, SD-F should be re-expressed, purified, labeled and measured to draw accurate conclusions. In principle this high number of FRET sensors could be used to improve the homology models similar to *Dimura et al. (2016)*^[147] and *Hellenkamp et al. (2017)*.^[148] However, since most of the expressed FRET sensors show impaired function, this was not done.

5. *In organello* smFRET measurements of Ssc1

In vitro measurements allow one to study the interactions with well-defined compositions. By knowing the exact concentrations of all components involved, quantitative conclusions on affinities and kinetic rates can be drawn. The interactions of two, or more, partners can be examined in isolation from the rest of the system. In addition, large complexes can be reconstituted piece by piece and the influence of each component can be studied individually. Moreover, conformations can be measured under various boundary conditions to explore the full possible range of motion.

However, *in vitro* measurements often do not give the true picture of protein's behavior in the cell. Here, many interaction partners are present simultaneously. The information as to which interaction predominates at which point in time can only be obtained from measurements *in vivo* or under *in vivo* like conditions, such as *in organello*. Often, different kinetics are observed *in vivo* compared to *in vitro*. Due to the presence of accelerators or inhibitors, and the different local concentrations of the various components, kinetic rates may vary. In addition, if the resolution is good, the localization of specific interactions can be observed.

With the *in organello* single-molecule FRET measurements of Ssc1 present here, we could contribute further insights into the dynamic behavior and occupation of Ssc1 inside mitochondria. Since establishing these smFRET measurements *in organello* was an important part of the project, the necessary steps will be explained in more detail before discussing the results.

5.1. Stepwise realization of *in organello* smFRET measurements

5.1.1. Import of fluorescently labeled Ssc1 into isolated mitochondria

Rupa Banerjee, from the group of Dejana Mokranjac (LMU Biologie), achieved import of unfolded and fluorescently labeled Ssc1 precursor proteins (Ssc1 with a targeting sequence to

the mitochondrial matrix) into isolated mitochondria. The procedure is explained in great detail in her doctoral thesis.^[149] When the import was carried out, the concentration of added Ssc1 precursor needed to be adjusted for each batch of labeled protein and isolated mitochondria to achieve single-molecule concentrations inside the mitochondria. The remaining external precursor was cleaved unspecifically using proteinase K treatment. This prevented smFRET signals from unsuccessfully imported proteins. Mitochondria were washed after proteinase K treatment to remove as much cleaved peptide as possible. After this procedure mitochondria were taken off the ice and were able to maintain the membrane potential for at least 40 minutes. Because membrane potential is a measure of mitochondrial function, all measurements were performed within this 40-minute period and mitochondria were discarded thereafter.

5.1.2. Specific immobilization of mitochondria

Mitochondria can be immobilized on L-Polylysine since the polymer is positively charged while the mitochondrial membrane is negatively charged. However, a large amount of residual cleaved peptide carrying fluorophores also adhered to the coated surface. For this reason, we switched to specific immobilization of mitochondria, which enables the use of PEG to passivate the glass surface of the cover slides. Surface passivation minimizes unspecific binding of remaining peptide and other impurities. This is particularly important for biological samples, as they carry more co-purified fluorescent impurities than *in vitro* measurements and completely clean measurement slides cannot be expected. The exact immobilization scheme we developed is presented in Figure 5.1a. A small percentage of PEG molecules on the surface carry a biotin, which is able to bind to streptavidin with pM affinity. Streptavidin has a total of four binding pockets for biotin and can act as a linker between two molecules functionalized with a biotin. The strong biotin-streptavidin interaction is commonly used in single-molecule microscopy. Since it is difficult to add a biotin tag to mitochondria, we applied a secondary immobilization step via a biotinylated antibody. We tested two different antibodies against two surface proteins of mitochondria, α Tom22 and α Porin. No immobilization was achieved by biotinylated α Porin (Figure 5.1b), which can have several reasons. Either the non-specific biotinylation of α Porin was not efficient, or the target sequence of Porin is buried in the tertiary structure or degraded by proteinase K. However, immobilization was achieved by the use of biotinylated α Tom22 (Figure 5.1c). Isolated mitochondria are big enough to be visible in brightfield when being illuminated by a halogen lamp from the top of the commercial microscope body. A phase contrast picture of immobilized mitochondria is shown in the left image of Figure 5.1c. In the right image of Figure 5.1c, the autofluorescence of mitochondria after illumination with blue laser light is presented. The autofluorescence of mitochondria in the focal plane can thus be used to locate the mitochondria in our measurements and narrow down the regions of interest. The immobilization

via biotinylated α Tom22 was successful and used for all further measurements.

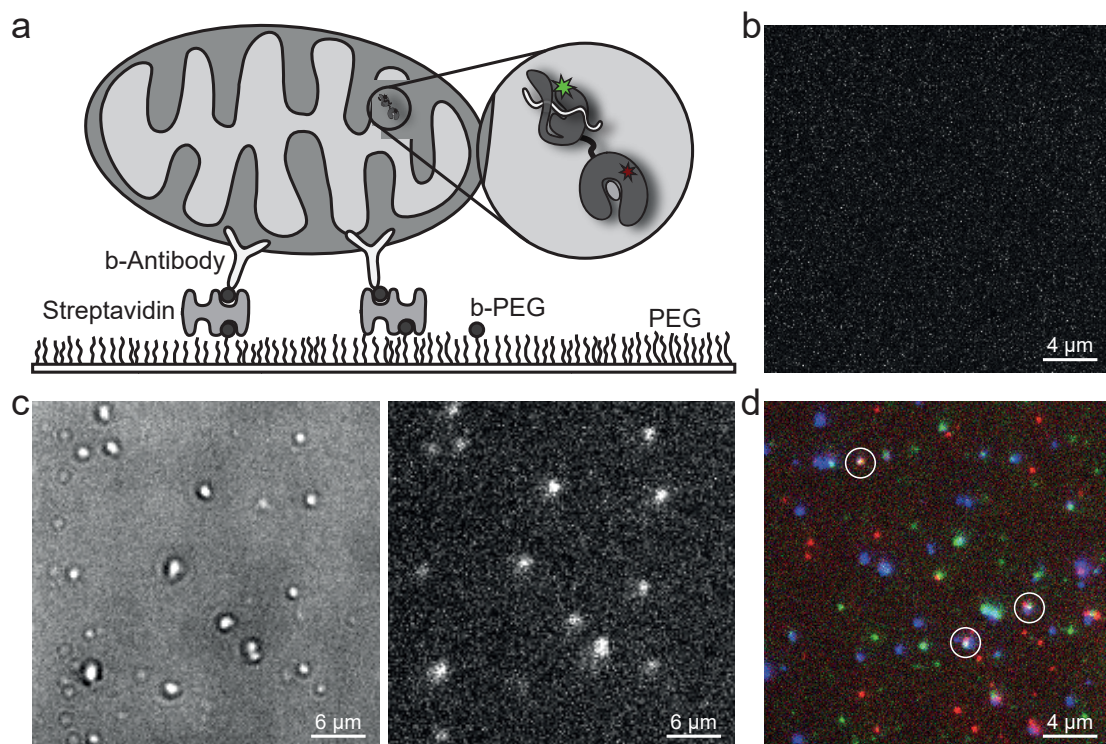


Figure 5.1.: Immobilization of isolated mitochondria for smTIRF experiments. (a) Mitochondria are immobilized on the pegylated glass surface by a biotin-streptavidin-biotin linkage via biotin-PEG-silane and a biotinylated antibody against Tom22. (b) A microscope image after blue excitation of a sample using α Porin for immobilization. No immobilized mitochondria are visible, and no immobilization using α Porin was observed. (c) Mitochondria immobilized via α Tom22 illuminated with the microscope lamp (left) and with the blue laser (right). (d) A section of the field of smFRET experiments *in organello* using HILO illumination. The image is an overlay of fluorescence images after blue, green and red excitation. Within the white circles are examples of colocalization of Atto532 (green), Atto647 (red) and the autofluorescence of the mitochondria (blue, immobilized using α Tom22).

Total internal reflection fluorescence (TIRF) microscopy did not lead to high data quality since simultaneous disappearance of green and red fluorescence after alternating laser excitation (ALEX) could be observed. This is due to diffusion of Ssc1 inside the matrix of the mitochondria out of the approximately 200 nm range of the evanescent field that can be illuminated by TIRF microscopy. Mitochondria detected by brightfield illumination or via autofluorescence using blue excitation (Figure 5.1c) ranged from 600–1200 nm in size and likely have a similar size in the z-direction. Hence, for the measurements here, an angle slightly lower than the critical angle for total internal reflection was necessary. These kinds of measurements are also known as highly and laminated optical sheet (HILO) microscopy^[18] or variable angle epifluorescence microscopy

(VAEM).^[19] This enables an increase of the excitation depth and volume while still maintaining low background illumination. Applying HILO to our measurements allowed us to observe Ssc1 inside mitochondria on longer timescales without losing the signal due to diffusion inside the mitochondrion.

For data analysis, only double-labeled proteins colocalized with the blue autofluorescence of the immobilized mitochondria were used. Proteins outside the mitochondrion are expected to be cleaved by added proteinase K and do not show FRET. Colocalization with the autofluorescence of the mitochondria further suggests the studied proteins are inside the mitochondria and we are in fact measuring *in organello*. To provide higher time resolution, blue excitation was carried out before the actual FRET measurement, followed by alternating excitation with the green and red laser. An exemplary field of view is shown in Figure 5.1d. The autofluorescence of the mitochondria is colored in blue, Atto532 and Atto647 in green and red, respectively. White spots represent a colocalization of mitochondria and a double-labeled protein (marked with white circles in Figure 5.1d). Time traces of such colocalized regions are extracted by the analysis software MITRA for further data analysis. Of course, it is also possible that two single-labeled proteins are colocalizing inside one mitochondrion, but no FRET is expected in such a case and these time traces will be excluded from further analysis.

5.1.3. The influence of dyes

Previous spTIRF experiments of Ssc1 have been performed using Atto532 and Atto647N (both ATTO-TEC GmbH) as a FRET dye pair. The first *in organello* measurements of Ssc1 were performed with Ssc1 labeled with these dyes and showed that Atto647N attached to excess peptide present outside of the mitochondria stuck to the surface of the coverslips. It has also been reported that Atto647N tends to stick to membranes, especially those of mitochondria.^[13,144,145] Such sticking behavior is unwanted since it does not only influence the successful import of Ssc1 precursor into mitochondria, but it also increases unwanted fluorescent background by sticking of peptide residues to the mitochondria and can hinder free diffusion of the folded protein inside the matrix. Since Alexa647 (Thermo Fisher Scientific) has been reported to be more hydrophilic than Atto647N the protein was next labeled with Atto532 and Alexa647. Alexa647 worked well in MFD-PIE burst measurements and reproduced the reported FRET efficiencies (Figure 5.2 orange), when the different Förster Radii are taken into account. However, Alexa647 was too sensitive to the environment inside mitochondria and photobleaching occurred in less than a second. It is important to mention that mitochondria have a low pH, radicals are highly abundant and photostabilization inside mitochondria is not possible without a strong influence on the electrochemical gradient, which potentially results in nonfunctional mitochondria. As a

cyanine dye, Alexa647 is very sensitive to radicals as well as ionic additions. As a particularly photostable dye, we next chose CF640R (Biotium) as the acceptor dye of our FRET pair. The dye showed amazing photophysical behavior with very high brightness and longevity in smFRET measurements on the surface. Unfortunately, solution smFRET burst measurements showed a big influence of CF640R on the FRET efficiency, especially for ADP-bound Ssc1 (Figure 5.2 purple). While measurements with Atto647N (blue) and Alexa647 (orange) showed that most of the proteins are in a high FRET state in the presence of ADP, proteins labeled with CF640R were almost completely captured in a low FRET state. Labeling with CF640R thus clearly influences or even inhibits allosteric communication within Ssc1.

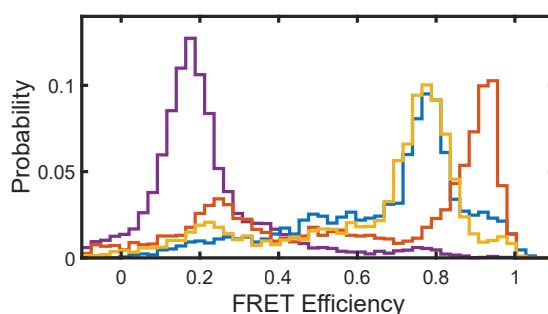


Figure 5.2.: Comparison of different dye pairs on Ssc1. SmFRET histograms of the interdomain distance of Ssc1 in presence of ADP labeled with Atto532 and Atto647N (blue), Atto647 (yellow), Alexa647 (orange) and CF640R (purple).

Atto647, while less photostable than Atto647N, also showed promising photophysical properties and is less hydrophobic than Atto647N. It performed well as an acceptor dye in solution burst measurements and reproduced the FRET histogram of the protein labeled with Atto532 and Atto647N (Figure 5.2 yellow compared to blue) reasonably well. In surface immobilized *in organello* smFRET measurements, Atto647 showed reasonable photobleaching times and was thus chosen for our system. Similar conclusions were drawn by *Plochowietz et al. (2014)*^[150] in *in vivo* experiments. At the time of these studies, Atto643 was not available yet and at later time points large amounts of data were already collected using Atto647 making a switch not worthwhile. It is likely that Atto643 would outperform Atto647 in the here presented *in organello* smFRET measurements. The best choice of dyes for this type of measurement in the future would be dyes with intramolecular photostabilizers as studied by T. Cordes and S. Blanchard.^[151–153] Such dyes are designed for exactly this application and are becoming commercially available and more convenient to use.

5.1.4. Single-molecule trace quality *in organello*

For a quantitative analysis of single-molecule FRET experiments it is essential to have a high signal-to-noise ratio and low background. Furthermore, long observation times are beneficial to increase the statistics. Exemplary traces of single Ssc1 proteins *in organello* are shown in Figure 5.3. Even though the fluorophores could not be stabilized by the addition of photostabilizers like Trolox or Cyclooctatetraene, the fluorescence traces show high signal intensity and low background noise. Other photophysical properties, like blinking and photobleaching, are not optimal and limit the observation times. Especially the green fluorophore, Atto532, populates long-lived dark states and permanently bleaches in several seconds. This can be seen in the upper panel of Figure 5.3, which shows the fluorescence of Atto532 and Atto647 after excitation at 532 nm. As an alternative, Cy3B could be used in the future, which showed higher photostability and comparable brightness in *in vivo* experiments.^[150] Nonetheless, data quality is high enough for further FRET analysis and exemplary FRET traces are presented in the lower panels of Figure 5.3. To exclude blinking of the acceptor dye Atto647 during collection of smFRET data, the fluorescence of Atto647 after excitation at 647 nm is shown in the middle row of Figure 5.3. Since almost all smFRET traces of *in organello* Ssc1 showed no dynamics, the resulting smFRET histograms were built on molecule-wise FRET efficiencies (Figure 5.4). This means that the FRET efficiency is averaged over all frames per molecule and only one value is used per molecule for the final FRET histogram.

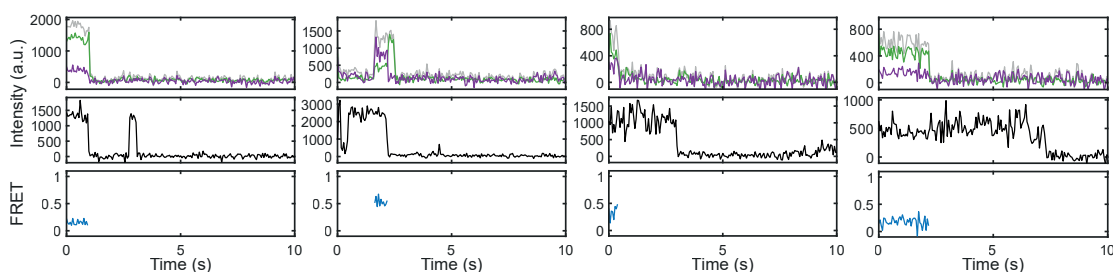


Figure 5.3.: Exemplary single-molecule traces of Ssc1 inside mitochondria. Top: Signal of Atto532 (green) and Atto647 (purple) after green excitation; Middle: Atto647 signal after red excitation; Bottom: Calculated FRET efficiency.

5.2. Conformational state of Ssc1 *in organello*

We were interested in the conformational state of Ssc1 inside mitochondria and the influence of the other proteins present. Since the used mitochondria are isolated, their energy levels can be manipulated by solution additives and can be compared to conditions used for *in vitro* measurements. ATP, NADH, phosphocreatine and creatine kinase were added to energize

mitochondria and produce high levels of available ATP. For ATP depletion experiments, apyrase and oligomycin were added to hydrolyse the available ATP and to block the ATP synthase, respectively. Within minutes, all ATP should be used up while no new ATP is being produced, thus simulating an ATP-deficient environment. A condition without any additional compounds in the buffer was not measured since the mitochondria are already in an ATP and NADH containing buffer during the import of the labeled Ssc1. Thus, it would not be possible to unravel the actual conditions for the mitochondria during the measurements. These two conditions, ATP and ATP depletion, can be compared to ATP and ADP *in vitro* with possible substrates being present in mitochondria at all times. Two different FRET sensors have been used previously and are well established (see Section 4). The mutant Ssc1-I448C-D590C reports on the amount of lid opening from the β -sandwich base of the SBD. The interdomain distance between the NBD and SBD is monitored by the mutant Ssc1-D341C-I448C. It is known that substrates of different sizes result in opening of the lid to different extents. This complicates the comparison of the data from the lid sensor to preexisting *in vitro* data. Since substrates inside mitochondria are present not only as extended peptide chains, but also partially folded, the mutant reporting on the lid distance would show a heterogeneous mixture of states. For this reason, we first carried out *in organello* measurements with the domain sensor of Ssc1. This mutant shows two well defined conformations, separated domains or docked domains, and dynamic switching between the two.

5.2.1. Conformation of Ssc1 *in organello* with ATP excess

The *in vitro* data (as presented in Section 4 and Figure 5.4c histogram on the right) shows that Ssc1 populates a high FRET state in the presence of ATP. This high FRET state is the result of closely docked domains. A similar conformation was expected for the *in organello* data of Ssc1 under ATP conditions. Instead, a broad FRET distribution is seen (Figure 5.4a left histogram) with a maximum at low FRET values. This low FRET state is associated *in vitro* with the substrate-bound state and separated domains (Figure 5.4c left). Besides the low FRET state, an intermediate FRET state is populated. When measured under ATP depletion conditions, Ssc1 can also be observed in a low FRET state with a small fraction of a high FRET state (Figure 5.4a middle histogram). While the low FRET state seems to be the same for both conditions, the higher FRET values differ. While it is convenient to assume the low FRET state of the *in organello* measurements corresponds to the substrate bound state, as measured *in vitro* (Figure 5.4c left), there are other possibilities for the predominance of separated domains. Besides a large number of possible substrates, there are also cochaperones and other interaction partners of Ssc1 present in mitochondria. These interaction partners could possibly induce domain separation by binding between the two domains. For the cochaperones Mge1 and Mdj1, no such conformation changes

could be detected in *in vitro* smFRET measurements, but the interaction with Tim44 could not yet been studied with smFRET. Also, other less well-studied or still unidentified interaction partners are present inside mitochondria. To unravel the origin of the observed low FRET state, we carried out a series of control measurements.

5.2.2. Functionality studies of imported Ssc1

First, it is important ensure that Ssc1 is fully functional after import. To this end, we lysed mitochondria containing imported, fluorescently labeled Ssc1 and diluted it in buffer containing an excess of ATP. Subsequently, single-molecule burst measurements of the imported and lysed Ssc1 were carried out. The obtained histogram (Figure 5.4b black histogram) clearly shows that Ssc1 is able to bind ATP and adopt the docked domain conformation, as seen by the high FRET efficiency. However, a small part remains in the intermediate FRET efficiency state. This intermediate FRET population is a dynamic population. Therefore, Ssc1 is binding and releasing the remaining substrates in the solution and is fully active. We conclude from this measurement that the fluorescently labeled Ssc1 used for the *in organello* measurements is fully functional after import into isolated mitochondria.

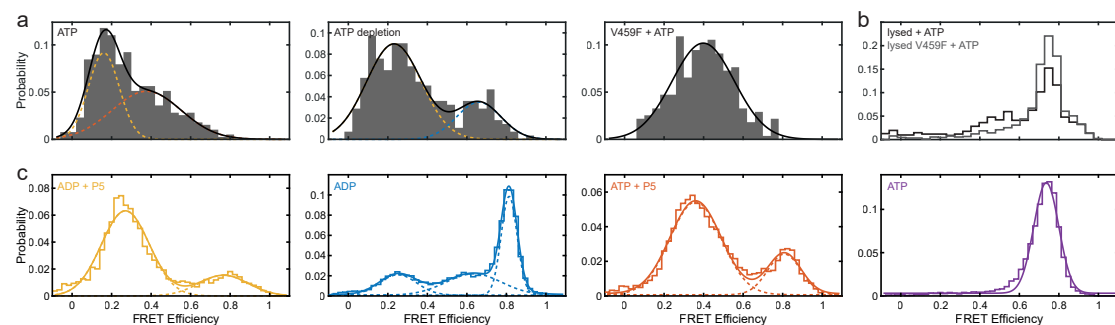


Figure 5.4.: *In organello* smFRET histograms of the domain sensor of Ssc1. (a) *In organello* data of Ssc1 under ATP (left) and ATP depletion (middle) conditions, as well as Ssc1 V459F under ATP conditions. (b) *In vitro* smFRET histograms of Ssc1 and Ssc1 V459F in solution after import into mitochondria, lysis of those mitochondria and dilution in buffer with 5 mM ATP.

5.2.3. Ssc1 is mostly substrate-bound *in organello*

Based on the extensive *in vitro* experiments (Section 4), Mdj1 and Mge1 could be excluded as the reason for the low FRET population *in organello*. Control experiments showed that Ssc1 is fully functional. Thus, it is most likely that the low FRET population indeed is substrate-bound Ssc1.

In this case, the low FRET population is expected to disappear in a mutant that is deficient in substrate-binding. One such mutant is Ssc1-V459F, where a valine in the substrate binding pocket is replaced by a phenylalanine.^[135] Similar mutants have been well studied for other Hsp70s like DnaK. *In organello* FRET data of Ssc1-V459F under ATP conditions does indeed not show a low FRET population but only a broad intermediate FRET population (Figure 5.4a right histogram), the same population, which was already present in WT-Ssc1 measurements. To ensure that this mutant is also correctly folded and able to bind ATP, the same control measurement after lysis as performed before was carried out. Ssc1-V459F was measured after import into and lysis of the mitochondria and diluted in ATP containing buffer as a control. The resulting FRET histogram looks exactly like *in vitro* measurements of Ssc1 in the presence of ATP and is completely shifted to the expected high FRET state (Figure 5.4b gray histogram) with no intermediate FRET population remaining. The data shows that Ssc1-V459F is correctly folded *in organello*, can still bind ATP and is only deficient in substrate binding.

The absence of the low FRET population for Ssc1-V459F, together with the control measurements shown in Figure 5.4b supports the assumption that most Ssc1 inside mitochondria is in the substrate-bound state already known from *in vitro* measurements. The fact that Ssc1 is not in the ATP-bound state, and thus not available for substrate binding, has considerable biological implications. When most of the Ssc1 inside mitochondria is occupied with substrate, there is little to none available to ensure successful translocation of precursors into the matrix. This further raises questions about the regulation of Ssc1 in regards to protein translocation. How is Ssc1 recruitment to the translocase of the inner membrane regulated? Which signal triggers substrate release and starts import? Where is all this substrate coming from, why does Ssc1 stay bound to it over longer timescales? Of course, it is possible that isolated mitochondria are stressed and thus more proteins are in need for binding and stabilization by Ssc1. In this case, the Ssc1 chaperone system is clearly at its capacity limit.

5.2.4. The high FRET population under ATP depletion conditions

To unravel the meaning of the second FRET population under ATP depletion conditions, it is helpful to look at the *in vitro* data of Ssc1. The high FRET state of the *in organello* ATP depletion measurements has a lower FRET efficiency than the high FRET states of either ATP (Figure 5.4c right) or ADP (Figure 5.4c second from left) *in vitro*. However, Ssc1:ADP not only populates two states resembling the docked (high FRET) and undocked (low FRET) domains, but also another population in between. This population has been shown to be dynamic on the sub-millisecond timescale. In Section 4, we propose that Ssc1 bound to ADP is in a stalled state and exploring a full range of inter-domain motion. Since the ATP synthase is blocked under ATP depletion

conditions and the ATP inside the mitochondria is used up rather quickly, it is reasonable to assume that the observed state resembles the ADP-bound conformation of Ssc1. In the *in vitro* burst measurements, the dynamic population averages around a FRET value of 0.6. The time resolution of the *in organello* surface measurements is lower, so further averaging with the longer lived high FRET state around 0.8 can occur. This leads to the observed average FRET efficiency of 0.67 and disappearance of the high FRET state. While most of the Ssc1 molecules observed are substrate-bound, a smaller population might already have successfully aided in protein (re) folding and thus released substrate. Since no ATP is remaining after ATP depletion, Ssc1 has to remain in an ADP-bound state, at least until it detects another unfolded protein or peptide. Thus, our conclusion is that the observed second FRET state under ATP depletion conditions in the *in organello* measurements is resulting from dynamic ADP-bound Ssc1 proteins, currently not bound to substrate.

5.2.5. The intermediate FRET population in the presence of ATP

It has been shown that Ssc1 behaves highly dynamic in the presence of ATP and substrate, and even more so, when the two cochaperones Mdj1 and Mge1 were also present *in vitro* (Section 4). While the domain dynamics of ADP-bound Ssc1 averaged around a FRET efficiency of 60 % in burst measurements, dynamics induced by ATP and substrate had a lower average FRET efficiency because of slower domain undocking. The intermediate FRET population in the *in organello* measurements is likely caused by fast release and rebinding of the same or the next substrate. This population also has the same FRET efficiency as the remaining FRET population of the Ssc1 mutant V459F, which might be transiently interacting with substrate but is not able to stably bind substrate. The hypothesis that the intermediate FRET population is interacting with substrate and this interaction introduces domain dynamics is further supported by the control measurement of lysed mitochondria (Figure 5.4b black). Here, labeled Ssc1 was imported into mitochondria. Subsequently, the mitochondria were lysed and diluted in ATP-containing buffer. Solution burst measurements showed a intermediate FRET population next to the high FRET population of ATP-bound Ssc1. This intermediate FRET population is a dynamic population. These dynamics can be caused by binding and release of remaining substrate in the lysate.

The observation of a high amount of substrate-bound Ssc1 suggests that substrate release is not favored inside the mitochondria. There are multiple possible reasons for this. It has been reported that Mge1 does not interact with Ssc1 under certain stress conditions. Possibly, isolated mitochondria are more stressed than mitochondria in an intact cell and Mge1 is not present in its active dimeric form, thus unable to bind to Ssc1 and induce nucleotide exchange. Substrates inside mitochondria are longer peptides and proteins, which take more time to fold and thus are

not released as easily as the short 10 amino acid long model substrate P5, which was used in the *in vitro* experiments. And, of course, the vast amount of other proteins present in mitochondria can have an impact on the regulation of the chaperoning cycle and function of Ssc1.

5.3. Conformation of the lid sensor of Ssc1 *in organello*

As previously mentioned, the extent of lid opening of Ssc1 depends on the size and structure of the substrate bound. For this reason, the substrate-bound structure is not well defined when different substrates are present. Inside mitochondria, substrates can be extended peptide chains as well as partially or fully folded proteins. After establishing that most of Ssc1 inside mitochondria is substrate bound with measurements of the domain sensor, we were next interested in the state of the lid. To this end, *in organello* measurements were carried out with the lid sensor under ATP and ATP depletion conditions. For this, the precursor protein of the lid sensor, with the mitochondrial targeting sequence, was labeled with Atto532 and Atto647.

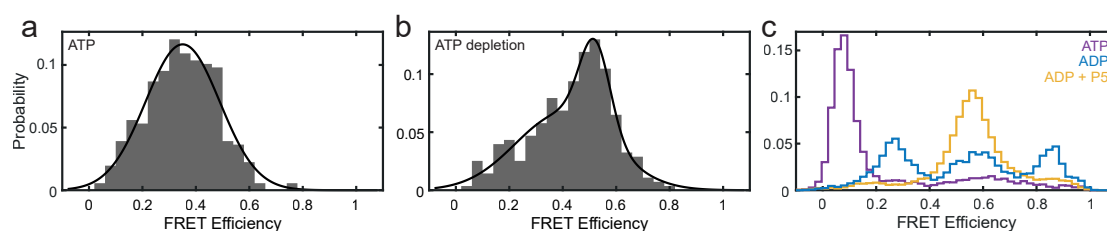


Figure 5.5.: *In organello* smFRET histograms of the lid sensor of Ssc1. (a) SmFRET histogram of the *in organello* measurements of Ssc1 under ATP conditions. (b) SmFRET histogram of the *in organello* measurements of Ssc1 under ATP depletion conditions. (c) *In vitro* smFRET histograms of the lid sensor of Ssc1 in the presence of ATP (purple), ADP (blue) and ADP and substrate (yellow).

In the presence of an excess of ATP, the lid sensor shows a broad distribution of FRET efficiencies (Figure 5.5a). Under ATP depletion conditions, the maximum of the smFRET efficiency distribution is at a higher FRET value and two populations can be detected (Figure 5.5b). The maximum of the FRET population in the presence of ATP *in organello* lies in between the open lid conformation known from *in vitro* measurements in the presence of ATP (Figure 5.5c purple) and the closed lid conformation in the presence of ADP and substrate (Figure 5.5c yellow). Thus the lid is in an intermediate open state *in organello* or is dynamically switching between an open and a closed lid on a fast timescale ($\ll 25$ ms). However, in previous *in vitro* TIRF experiments^[4], the dynamics of the lid were slow enough to be observed. It is thus more likely that the intermediate open state originates from partially folded substrates where the lid cannot close completely. However, since no precursor proteins are imported during the measurements,

this species cannot be observed here. While the FRET efficiency of the low FRET population of the *in vitro* measurement of ADP (Figure 5.5c blue) is similar to the conformation observed in the presence of ATP *in organello*, it is unlikely that Ssc1 is present in an ADP but not substrate-bound state *in organello*. The intermediate open lid is also present *in organello* when ATP is depleted and is in nice agreement with a closed lid. This closed lid conformation is mainly adopted in the presence of unfolded substrate (Figure 5.5c yellow), but can also be adopted in the absence of substrate (Figure 5.5c blue). For both conditions, no open lid can be detected *in organello*. In agreement with the data obtained from the domain sensor, this shows that Ssc1 is not present in the ATP-only bound state, but always has substrate bound as well.

5.4. Tracking of Ssc1 paths inside mitochondria

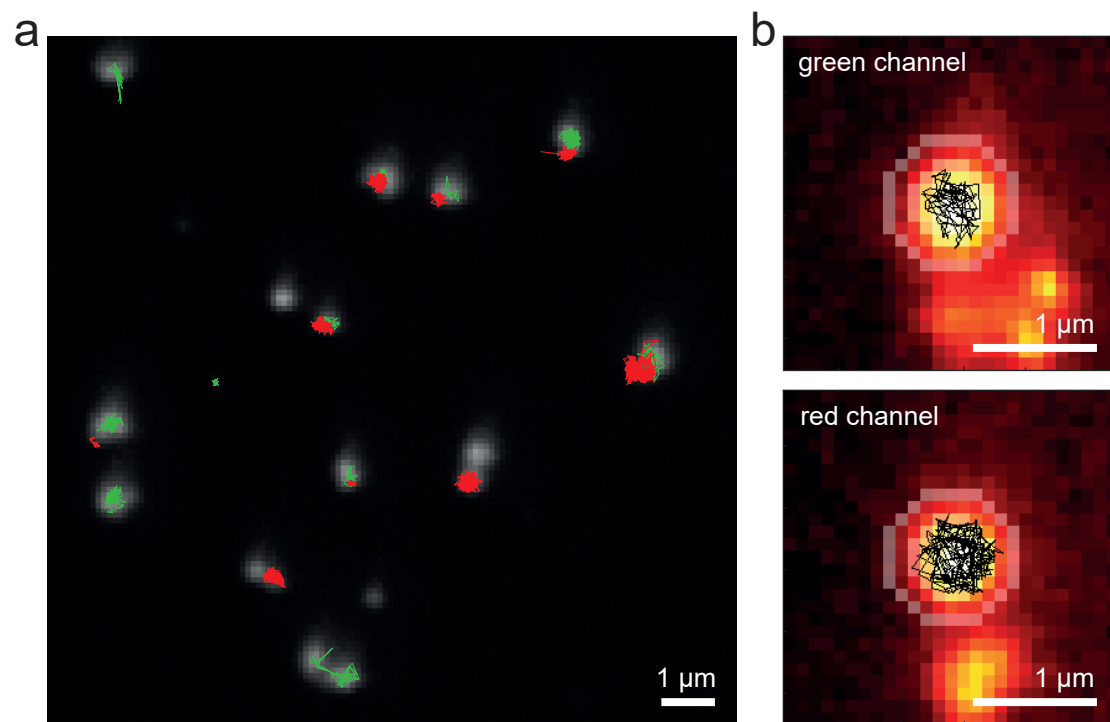


Figure 5.6.: Trajectories of tracked molecules inside mitochondria. a) Exemplary field of view with mitochondrial autofluorescence and with tracks based on the green and red signal of single Ssc1 molecules. The shift between the colors is because of minor shifts in the detection path, which are later corrected for with camera mapping. b) Zoom in on the tracks of a single molecule detected in the green (top) and red (bottom) channel.

When taking a closer look at the accumulated movies, it became apparent that many of the fluorescent spots are moving. These moving Ssc1 molecules are colocalized within mitochondria.

The mitochondria themselves are stably immobilized and do not show movement. This indicates that we are detecting the movement of Ssc1 inside the mitochondria. Because the different functions of Ssc1 are associated with different interaction partners, an influence of the diffusion behavior of Ssc1 can be expected. Especially, when bound to the TIM23 complex, a membrane complex, Ssc1 is not able to diffuse freely in the matrix. In contrast, Ssc1 can diffuse freely in the matrix when not bound to substrate or bound to small proteins which are not membrane associated. It is therefore tempting to investigate whether differences in the mobility of Ssc1 are associated with differences in the smFRET histograms. Thus, one can investigate if there are conformational differences for Ssc1 with different diffusional behavior.

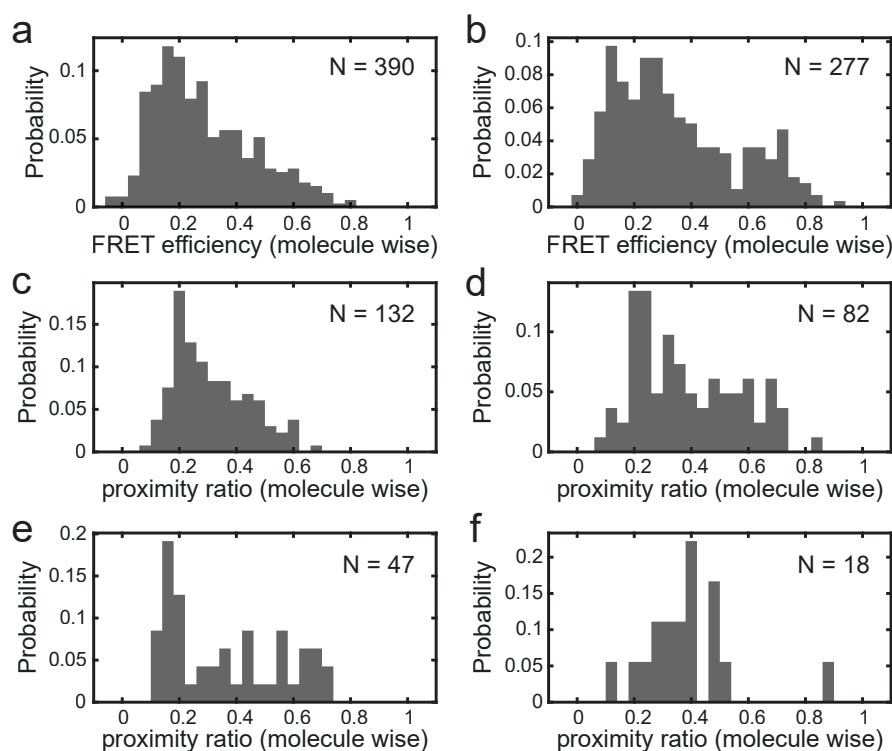


Figure 5.7.: Mobility-dependent *in organello* smFRET histograms of the domain sensor of Ssc1. The smFRET histograms of the ATP (a) and ATP depletion (b) conditions extracted with the standard algorithm are shown. SmFRET histograms of proximity ratios of the moving molecules under c) ATP conditions and d) ATP depletion conditions. Because of the minor influence of the correction factors in these experiments, FRET efficiency and proximity ratios can be directly compared. SmFRET histograms of the proximity ratios of the non-moving molecules under e) ATP conditions and f) ATP depletion conditions. The number of molecules, N, comprising each histogram is given.

To this end, single molecules were tracked applying a wavelet algorithm provided by Philipp Messer.^[154] For tracking, the ALEX signal on the red camera was used because of the highest signal intensity. However, since we wanted to correlate the movement of Ssc1 with the FRET

efficiency, the molecules were also tracked on the green camera (Figure 5.6). Colocalized tracks were used for further analysis. The tracks from the green fluorophores were mapped onto the red camera to extract the FRET signal from these locations. Single-molecule FRET traces were further divided into two categories based on their diffusion behavior. This was achieved by assessing the single-molecule tracks (Figure 5.6b) based on their diffusion behavior and also by examining the movie of each of these molecules to verify the tracks. The molecule-wise proximity ratios of the molecules are presented in Figure 5.7, and compared to the smFRET histograms from the previous analysis. The total smFRET traces obtained from the tracking analysis is less than the traces obtained from the standard method because of stricter selection criteria (e.g. minimum trace length, correct tracking, etc.). There is a clear difference between the smFRET histograms. The moving Ssc1 under ATP conditions (Figure 5.7c) mainly populate low and intermediate FRET efficiencies. High FRET efficiencies (>0.6) are only populated in the non-moving fraction of Ssc1 (Figure 5.7e). Based on the FRET efficiency, these molecules have docked domains. Because of their low mobility, it is reasonable to assume that they are bound to the translocation complex and in the substrate-free conformation, since no protein is being imported during the measurement. In turn, the results from the FRET-tracking analysis also show that all mobile Ssc1 interacts with substrate, either transiently (intermediate FRET) or stably bound (low FRET). Also under ADP depletion conditions, there is a difference between the smFRET histograms of moving (Figure 5.7d) and non-moving (Figure 5.7f) Ssc1. A low and a high FRET population can be identified for the mobile fraction, while only an intermediate FRET population can be identified for the non-moving fraction. This suggests substrate-free Ssc1 in the ADP-bound state is diffusing in the matrix. There are multiple possible explanations for the low to intermediate FRET conformations observed for non-moving Ssc1. First of all, they could be bound to large protein aggregates. They could also be bound to the translocase and a precursor protein, which is stuck in the translocation channel from the import of labeled Ssc1 into the mitochondria. Lastly, they can also be bound to one of the other proteins Ssc1 interacts with, some of them also associated with the inner mitochondrial membrane.

To get an idea of the difference in diffusion coefficients between the moving and non-moving molecules, a probability distribution of square displacements (PDS) analysis^[155] was carried out. The analysis was carried out for red detection of the ALEX signal and green detection separately (Figure 5.8). Differences in diffusion coefficients are most likely due to differences in localization precision between the two channels. For the category of moving molecules, the analysis yielded diffusion coefficients in the range of $0.040\text{--}0.051\ \mu\text{m}^2\ \text{s}^{-1}$ (Figure 5.8a). For the non-moving molecules, diffusion coefficients in the range of $0.0080\text{--}0.024\ \mu\text{m}^2\ \text{s}^{-1}$ were calculated. In both cases, the calculated diffusion coefficients are most likely a lower boundary of the actual diffusion coefficients. The mitochondria in the measurement define a small confined space and the time resolution is insufficient. Nonetheless the PDS analysis verified a difference in mobility between the two selected species.

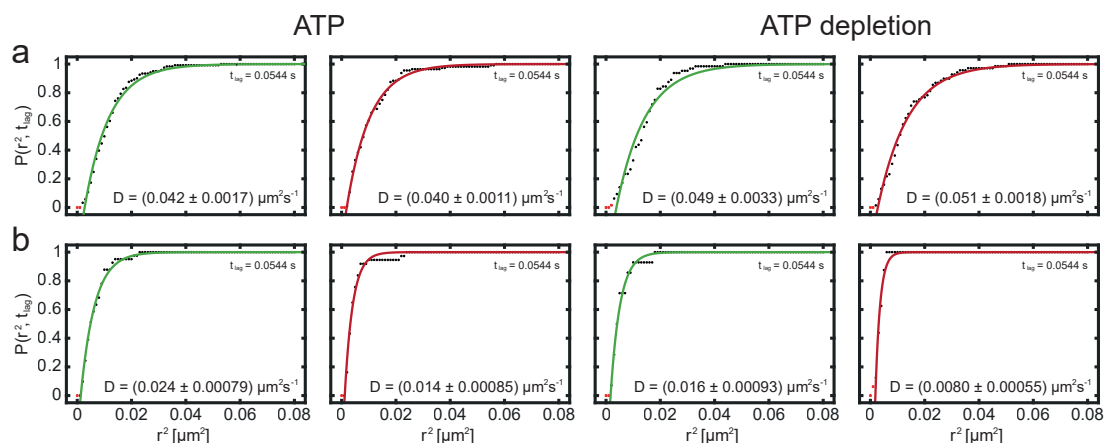


Figure 5.8.: Analysis of the probability distribution of square displacements (PDS) of the tracked Ssc1 for $t_{lag} = 0.0544$ s. Fits are shown in the color of the detection. Excluded datapoints are indicated with red crosses. a) PDS of the moving fraction of Ssc1 under ATP conditions (left two graphs) and ATP depletion conditions (right two graphs). b) PDS of the non-moving fraction of Ssc1 under ATP conditions (left two graphs) and ATP depletion conditions (right two graphs).

Taken together, the single-molecule tracking analysis enabled us to see a correlation between the mobility of Ssc1 and the FRET efficiency. We could conclude that a small fraction of Ssc1 is bound to the translocase and is not substrate-bound. Furthermore, mobile Ssc1 without substrate-bound only exists under ATP depletion conditions and thus when bound to ADP.

6. Conclusion and Outlook

Maintenance of the proteome is essential for cell survival. This also holds true for the proteome of mitochondria. Ssc1, the mitochondrial Hsp70 of yeast, ensures this by its diverse maintenance and stress related functions. Ssc1 is involved in translocating cytosolically expressed proteins into the mitochondrial matrix, in *de novo* protein folding, protein complex assembly and disassembly, stabilization of proteins to prevent aggregation, dissolving of protein aggregates and protein degradation. These diverse functions need to be timed and regulated. This is, to a large extent, achieved by interactions with cochaperones, such as the nucleotide exchange factor Mge1 and J proteins like Mdj1 or Tim14. Furthermore, the availability of ATP and the presence of substrate have an impact on Ssc1. All these binding partners have an influence on the structure and conformational dynamics of Ssc1.

With *in vitro* single-molecule FRET measurements of Ssc1, we were able to show that Ssc1 transitions on the sub-millisecond timescale between two domain conformations, docked and undocked domains. At the same time, the lid can adopt four distinct conformations, which are static on the sub-millisecond timescale. The four states can be assigned to a wide open lid, a partially closed lid, a closed lid and a collapsed lid where the dye distance is smaller than that of the closed lid. The latter state could be assigned to dimers of Ssc1. Our experiments show that Mdj1 effectively stimulates ATP hydrolysis, even in the absence of substrate. We could show that, besides the release of nucleotide, Mge1 induces a conformational change causing opening of the lid. This shows a possible mode of action of Mge1 in release of substrate. However, in our experiments, efficient substrate release could not be observed, most likely due to the short model substrate used. Thus, a change in the three-dimensional structure of the substrate might be needed as a signal for successful folding. A global kinetic analysis of the conformational dynamics of the domain sensor of Ssc1 with dynamic PDA gave transitional rates on the sub-millisecond timescale. Rates were fastest in the presence of ADP, and slowest in the presence of substrate. This shows two different types of conformational dynamics. A kind of idle behavior in the absence of substrate, with exploration of possible contacts that are important in allosteric communication, and conformational dynamics that are related to substrate binding and release. Besides fast interdomain dynamics, slow dynamics on the second timescale could be detected in the presence of substrate. While lid closure is immediate, showing successful binding of substrate,

complete domain separation can take up to 60 min. The presence of sub-millisecond and second dynamics in the domain sensor and absence of similar dynamics in the lid sensor strengthen previous reports of uncorrelated dynamics in Ssc1.

With the goal of observing the complete conformational cycle of Ssc1 on a single protein, efforts were made to increase the difference between the high FRET efficiencies of ATP- and ADP-bound Ssc1. The mutant Ssc1 SD-F might be a possible candidate.

We established *in organello* smFRET measurements with specific immobilization of the mitochondria on a glass coverslide in order to study the conformation of Ssc1 in its physiological environment. Surprisingly, Ssc1 is mostly in a substrate-bound state or transiently interacting with substrate. Only when depleting the mitochondria of ATP, could we detect Ssc1 bound to ADP but not substrate. This implies that Ssc1 inside mitochondria is highly occupied with protein folding and the prevention of aggregation. By tracking single Ssc1 proteins inside mitochondria, the relation between the mobility and the conformation of Ssc1 could be studied. This enabled us to detect a small fraction of Ssc1 in an ATP-bound and substrate-free state, most likely bound to the translocation complex. Together, these findings suggest that most Ssc1 inside these mitochondria is occupied with substrate and only a small fraction is available for protein translocation. When exposed to stress, the need for stabilization of proteins by Ssc1 increases which might lead to an interruption of protein translocation.

The application of smFRET measurements *in vitro* enabled us to study the influence of nucleotides, substrate and the cochaperones Mdj1 and Mge1 on the conformation and dynamics of Ssc1. It would be interesting to also study the influence of other proteins interacting with Ssc1, such as the translocation associated Tim14 and Tim44, or substrate proteins.

The *in organello* smFRET measurements of Ssc1 gave important insights on the occupation of Ssc1 inside mitochondria. Labeling of other components of the Hsp70 machinery, such as Tim44, with a third color could give additional information on the regulation of Ssc1. Furthermore, it would be interesting to import precursor proteins during the measurement and move the equilibrium from folding and stabilization of proteins to translocation.

7. Materials and Methods

7.1. Molecular biology and biochemistry

7.1.1. Materials

Chemicals used in this work were purchased from Sigma-Aldrich, Thermo Fisher Scientific, Carl Roth GmbH, Qiagen, New England Biolabs and ATTO-TEC.

7.1.1.1. Buffers and solutions

Buffers and solutions were prepared with Milli-Q water and are listed in Table 7.1.

Table 7.1.: Media, buffers and solutions.

name	components
LB medium (1 L volume)	15.5 g Luria broth base, Miller
LB agar	LB medium 15 g L ⁻¹ agar-agar
1x TAE (Tris-acetate-EDTA) buffer	100 mM Tris-HCl pH 8.5 1 mM EDTA 0.1 % (v/v) acetic acid
1x running buffer for SDS-PAGE (1 L total volume)	2 g Tris-base pH 8.3 14.4 g glycine 1 g SDS
Coomassie Brilliant Blue staining solution	0.1 % CBB R-250 10 % acetic acid 40 % methanol
Ssc1 expression buffer (autoclaved)	50 mM Tris-HCl pH 7.5 250 mM KCl 5 mM MgCl ₂ 5 % glycerol
Lysis buffer	100 mL Ssc1 expression buffer 100 µL 0.2 M TCEP 100 µL 5 M imidazole 1 mL 100 mM PMSF
Wash buffer (25 mM imidazole)	40 mL Ssc1 expression buffer 40 µL 0.2 M TCEP 200 µL 5 M imidazole 400 µL 100 mM PMSF
Elution buffer A (10 mM ATP)	10 mL Ssc1 expression buffer 10 µL 0.2 M TCEP 10 µL 5 M imidazole 100 µL 100 mM PMSF 389 µL 256 mM ATP
Elution buffer B (500 mM imidazole)	20 mL Ssc1 expression buffer 20 µL 0.2 M TCEP 2 mL 5 M imidazole 200 µL 100 mM PMSF
Storage buffer	20 mM Hepes/KOH pH 7.4 100 mM KCl 5 mM MgCl ₂ 5 % glycerol 0.2 mM TCEP
Ssc1 working buffer	20 mM Tris-HCl pH 7.5 80 mM KCl 5 mM MgCl ₂

7.1.1.2. Plasmids and primers for site-directed mutagenesis

All primers were ordered from metabion.

Table 7.2.: Primers used in this work for site-directed mutagenesis.

primer name	sequence (5' to 3')
Ssc1-341D	phosphate-GAACTGTCGACCCAGTCAAGAAGG
Ssc1-341D-rev	phosphate-TCTTAACTAGTGGGGCTGTCAAAGTCTC
Ssc1-327C	phosphate-CTCCAGGGCTTGTTTCGAGACTT
Ssc1-327C-rev	phosphate-AACTTCATGTTGATATGCTTTGGACCTG
Ssc1-111C	phosphate-CGCTGAAGTGTGTAGAGATATCAAGC
Ssc1-111C-rev	phosphate-TCTTCGAAACGACGACCAATC
Ssc1-176C	phosphate-GCTTATTTCAACTGCTCTCAAAGACAAGC
Ssc1-176C-rev	phosphate-TGGGACAGTGACAACAGCATTCT
Ssc1-337C	phosphate-GCCCCACTAGTTTGTAGAACTGTCCG
Ssc1-337C-rev	phosphate-TGTCAAAGTCTCGAATTGAGCCC
Ssc1-378C	phosphate-CGAAACCGTTAAATGTTTGTGG
Ssc1-378C-rev	phosphate-ACAACCTTAGGCATTCTGGACATACC
Ssc1-374C	phosphate-GCCTAAGGTTGTCTGTACCGTTAAATCT
Ssc1-374C-rev	phosphate-ATTCTGGACATACCACCGACCAA
Ssc1 2-3 seq fw	CACTGAAATCAACCTGCC
Ssc1 2-2 seq fw	GTCACTGTCCCAGCTTATT
Ssc1 VT seq fw	GTATTGCCACACGTTTGC
Ssc1 VT2 seq fw	GTTCCGTCATCGGTATCG

7.1.2. Site-directed mutagenesis

In a first step, starting from the plasmid pET-Duet-1-Hep1-Ssc1-C341-C448, C341 was mutated back to D341 from the wildtype sequence. Then point mutations to cysteins were introduced according to Table 7.3. Point mutations were introduced using the Phusion Site-Directed Mutagenesis Kit (Thermo Fisher Scientific). Polymerase chain reaction (PCR) amplification was performed according to the kit protocol in a 50 μ L reaction mixture containing 1x Phusion buffer, 200 μ M dNTP (each), 0.5 μ M of forward and reverse primer, 40 ng plasmid template and 0.02 U/ μ L Phusion Hot Start II DNA Polymerase. Forward and reverse primers are listed in Table 7.2. The applied PCR program is shown in Table 7.4.

PCR products were then circularized by ligation with T4 DNA ligase. For this, 5 μ L of the PCR product was combined with 0.5 μ L T4 DNA ligase and 4.5 μ L 1x Rapid Ligation Buffer for a

Table 7.3.: Plasmids created in this work.

Plasmid	Protein Name	Probe Name
pET-Duet-1-Hep1-Ssc1-C448		A#6
pET-Duet-1-Hep1-Ssc1-Stop448		C#1
pET-Duet-1-Hep1-Ssc1-C111-C448	SD-B	I#3
pET-Duet-1-Hep1-Ssc1-C111-Stop448		J#1
pET-Duet-1-Hep1-Ssc1-C327-C448	SD-C	F#2
pET-Duet-1-Hep1-Ssc1-C327-Stop448		N#1
pET-Duet-1-Hep1-Ssc1	WT	E#1 and G#1
pET-Duet-1-Hep1-Ssc1-C327		M#4
pET-Duet-1-Hep1-Ssc1-C176-C327-Stop448	3c-NBD	O#1
pET-Duet-1-Hep1-Ssc1-C176-C327	SNBD	P#3 (only in Top10 or BL21)
pET-Duet-1-Hep1-Ssc1-C374-C448	SD-D	S#1
pET-Duet-1-Hep1-Ssc1-C374-Stop448		T#1
pET-Duet-1-Hep1-Ssc1-C337-C448	SD-E	Q#1
pET-Duet-1-Hep1-Ssc1-C337-Stop448		R#3
pET-Duet-1-Hep1-Ssc1-C378-C448	SD-F	U#1
pET-Duet-1-Hep1-Ssc1-C378-St448		V#1

Table 7.4.: PCR protocol used for site-directed mutagenesis.

	temperature	time	
initial denaturation	98 °C	30 s	1x
denaturation	98 °C	30 s	
annealing	variable temperature	30 s	25x
extension	72 °C	200 s	
final extension	72 °C	7 min	1x
hold	4 °C	hold	

total volume of 10 μ L. The mixture was incubated at room temperature for 5 min and then stored at -20 °C.

7.1.2.1. Agarose gel electrophoresis

To verify the success of the PCR amplification, 5 μ L of the PCR product was mixed with 1 μ L of 6x DNA loading dye and loaded on a 1 % agarose (in 1x TAE; 40 mM Tris-acetate, 1 mM EDTA) gel together with a 1 kb DNA ladder. Gels were run in 1x TAE buffer at 100 V for 40–50 min. The gels were then stained with SYBR Gold and imaged with UV light in a Bio-Rad gel documentation system.

7.1.3. Preparation of chemically competent bacteria

Chemically competent *E. coli* cells were prepared from BL21 AI cells and TOP10 cells. Two sterilized solutions of 100 mM MgCl₂ and 100 mM CaCl₂ were prepared. First, a preculture of 10 mL was grown overnight. The next day, 5 mL of the preculture were used to inoculate 500 mL of LB medium. Cells were grown at 37 °C for 1–2 h until an *OD*₆₀₀ of 0.6 was reached. They were put on ice for 30 min and then transferred into a precooled centrifuge bottle and centrifuged for 35 min with 2000 g at 4 °C. The supernatant was discarded and cells were gently resuspended in 200 mL MgCl₂ solution (100 mM). The cells were split into 8 small, precooled centrifuge bottles (50 mL volume) and centrifuged for 15 min at 2000 g and 4 °C. The supernatant was discarded, cells were gently resuspended in 12.5 mL CaCl₂ solution (100 mM) and each two bottle were combined. Cells were kept on ice for 20 min and then centrifuged for 15 min at 2000 g and 4 °C. The supernatant was again discarded and the cells were resuspended in 250 μL CaCl₂ solution (100 mM, with 15 % glycerol). Aliquots of 100 μL were transferred into precooled cryo vials and stored at –80 °C

7.1.4. Transformation in *E. coli*

For transformation of plasmid DNA into *E. coli*, approximately 50 μL of chemically competent *E. coli* cells (TOP10 for plasmid preparation, BL21 AI for recombinant protein expression) were thawed on ice. After addition of 1–2 μL of ligation product or purified plasmid DNA, transformation mixtures were incubated on ice for 30 min. Cell wall recovery was induced by a 45 s heat shock at 42 °C. Cells were then stored on ice. In the next step, 1 mL LB medium was added and cells were incubated and shaken (350 rpm) at 37 °C for 1 h. To increase the concentration, cells were centrifuged at 2000 rpm for 2 min and 900 μL of supernatant were removed. The cells were resuspended carefully in the remaining 100 μL of LB medium. For positive selection, cells were then plated on LB agar plates containing ampicillin and incubated overnight at 37 °C. Only cells containing the plasmid, and thus the encoded antibiotic resistance, were able to grow and form colonies.

7.1.5. Plasmid isolation

After incubation on ampicillin-containing LB agar plates, four colonies were picked per plate and each was inoculated in 3 mL LB medium (100 μg mL⁻¹) and cultured overnight at 37 °C. Of these cultures, 500 μL were combined with 160 μL of sterile glycerol and stored at –80 °C as

bacterial glycerol stocks. From the remaining bacterial cultures, plasmid DNA was isolated using either a QIAprep Spin Miniprep Kit (Qiagen) or a Monarch Plasmid Miniprep Kit (New England Biolabs). Eluted plasmid DNA was quantified by measuring the absorption at 260 nm using a NanoDrop spectrophotometer.

7.1.6. Next generation sequencing

Next generation sequencing of the obtained plasmid DNA was performed by GATC Biotech (SUPREMERUN tube Barcode). Samples of 20 μL plasmid DNA (30–100 $\text{ng } \mu\text{L}^{-1}$) and 20 μL sequencing primer (10 $\text{pmol } \mu\text{L}^{-1}$) were prepared and send to GATC.

7.1.7. Protein expression

Hep1 is needed for the correct folding and stability of Ssc1. Thus, recombinant Ssc1 proteins were coexpressed with histidine-tagged Hep1. After transformation of purified plasmid DNA in *E. coli* BL21AI cells (Section 7.1.4), colonies from plates were grown in 25 mL LB medium (100 $\mu\text{g mL}^{-1}$ ampicillin) overnight at 37 °C. The precultures were then used to inoculate 0.5–1 L of LB medium (100 $\mu\text{g mL}^{-1}$ ampicillin) and cultured at 37 °C. At an OD_{600} of around 0.5, protein expression was induced with 1 mM IPTG and 0.2 % arabinose. Expression was carried out at roughly 26 °C (lowest temperature achievable in the incubator) overnight.

7.1.8. Protein purification

Cells from the overnight expression were harvested by centrifugation at 4000 rpm for 20 min at room temperature. After resuspension in 5–10 mL lysis buffer, they were pelleted again by centrifugation at 4000 rpm as a washing step. Cells were then resuspended in 8–10 mL lysis buffer and disrupted by sonication with 5x 30 pulses (duty cycle 50 %, output control 3) on ice. Soluble proteins were separated from cell debris by centrifuging for 30 min at 12 000 rpm and 4 °C. Purification was then carried out separately for Mge1 and Ssc1.

7.1.8.1. Purification of Mge1

Mge1 was expressed with a His-Tag. For purification of Mge1, 3–5 mL NiNTA superflow beads were washed with water and equilibrated with lysis buffer. Mge1 supernatant was added to the NiNTA beads and incubated while rotating for 1 h at 4 °C. The beads were then washed twice with 10 mL lysis buffer, once with 10 mL wash buffer and again with 10 mL lysis buffer by centrifuging the beads for 7 min at 5000 rpm. Each supernatant was collected for SDS-PAGE. When Mge1 was used to purify Ssc1 on the same day, then the flow-through of the Ssc1 expression was now added to the Mge1-NiNTA. Otherwise, the beads were then loaded onto a gravity flow column and washed with 5 mL of Ssc1 expression buffer (10 mM Imidazole, 2 mmol dm⁻³ ATP). Mge1 was then eluted with 10 mL elution buffer (500 mM Imidazole). The remaining NiNTA beads were washed with water and then stored in EtOH at 4 °C. From each fraction, 9 µL were collected for SDS-PAGE. The buffer of the remaining eluted fractions was exchanged to storage buffer using Corning 10 kDa spin centrifugal filters. Mge1 was then stored at –80 °C.

7.1.8.2. Purification of Ssc1

NiNTA superflow beads were washed with water and equilibrated with lysis buffer. The Ssc1-Hep1-expression supernatant was added to 3–5 mL NiNTA superflow beads to remove his-tagged Hep1 by binding to the beads. The mixture was incubated and rotated for 2 h at 4 °C. The beads were then loaded onto a gravity-flow column and the flow-through was collected. Taking advantage of the strong affinity of Ssc1 to the nucleotide exchange factor Mge1, the flow-through was then added to the washed Mge1-NiNTA beads. The beads were rotated during incubation for 1 h at 4 °C. During this time, Hep1-NiNTA was washed with 10 mL wash buffer and Hep1 was then eluted with 10 mL elution buffer (500 mM Imidazole). The remaining NiNTA beads were washed with water and then stored in EtOH at 4 °C. The incubated Ssc1-Mge1-NiNTA beads were added to a gravity-flow column and washed with 15 mL lysis buffer. They were then washed with 20 mL wash buffer and Ssc1 was eluted with 10 mL elution buffer A. Mge1 was then eluted with 10 mL elution buffer B. NiNTA beads were washed with water and then stored in EtOH at 4 °C. For each fraction, 9 µL was collected for SDS-PAGE. The buffer of the remaining eluted fractions (Hep1, Ssc1, Mge1) was exchanged to storage buffer using Corning 10 kDa (Hep1, Mge1) or 30 kDa (Ssc1) spin centrifugal filters. The proteins were then stored at –80 °C. Ideally, Ssc1 was labeled with organic fluorophores right after purification and prior to freezing.

7.1.9. SDS gel electrophoresis

The quality of purification was assessed using SDS-PAGE (sodium dodecyl sulfate polyacrylamide gel electrophoresis). Samples of 9 μ L were collected from the flow-through, wash and elution fractions and each were combined with 9 μ L 2x SDS loading buffer and denatured at 100 °C. Appropriate volumes were loaded onto a 12 % SDS-PAGE gel (Table 7.5) together with a PageRuler prestained protein ladder. Gels were run in 1x running buffer at 100 V for the stacking gel and 150 V for the separating gel for approximately 45–60 min. The gels were then stained with Coomassie Brilliant Blue to visualize the protein bands.

Table 7.5.: Preparation of 12 % SDS-PAGE gels.

	separating gel	stacking gel
H ₂ O	3.75 mL	2.9 mL
1.5 M Tris-SDS	2.8 mL	–
0.5 M Tris-SDS	–	1.2 mL
30 % Acrylamide	4.7 mL	0.8 mL
TEMED	13 μ L	6 μ L
APS 20 %	45 μ L	30 μ L

7.1.10. Labeling of proteins with organic fluorophores

Ssc1 SD and SL, as well as Ssc1 for *in organello* measurements, was labeled by Rupa Banerjee.^[149] For all other Ssc1 double-cysteine mutants, stochastic labeling of the cysteines was performed by adding a 2–5 x excess of Atto532 maleimide and Alexa Fluor 647 or Atto643 maleimide. Dyes were premixed, protein was added (to yield 50 μ M) and the volume adjusted to 50 μ L with Ssc1 working buffer. The reaction mixture was incubated for 1–2 h shaking (350 rpm) at room temperature. Dye excess was removed using a PD MiniTrap G-25 column and subsequent concentration with a Sartorius Vivaspin 30 kDa centrifugal filter. Labeled Ssc1 was frozen in storage buffer and stored at –80 °C.

7.1.11. Import of labeled Ssc1 into isolated mitochondria

7.1.11.1. Purification and labeling of presequence-containing Ssc1

Expression, purification and labeling of presequence-containing Ssc1 is described in detail in the doctoral thesis of Rupa Banerjee.^[149] Proteins were labeled with Atto532 (Atto-Tec) as the donor fluorophore and Atto647N, (Atto-Tec), Alexa Fluor647 (Thermo Fisher Scientific), CF640R (Biotium) and Atto647 (Atto-Tec) as acceptor fluorophores. For the final *in organello* measurements, Atto647 was used as the acceptor dye and was added in 10-fold excess for labeling while Atto532 was added in 2-fold excess. Proteins were stored at -80°C in 50 mM Tris-HCl pH 7.0, 3 M urea until import into mitochondria.

7.1.11.2. Import of presequence-containing Ssc1 into isolated mitochondria

The import of presequence-containing and fluorescently labeled Ssc1 into isolated mitochondria is described in detail in the doctoral thesis of Rupa Banerjee.^[149] For different batches of isolated mitochondria and labeled protein, different dilutions were tested to achieve single double-labeled proteins inside mitochondria. Proteinase K was added after the import was stopped to digest any remaining labeled proteins outside of the mitochondria. Cleavage of labeled proteins prevents FRET signals from proteins located outside the mitochondria during subsequent single-molecule FRET measurements. Mitochondria were then centrifuged and washed to remove excess of labeled proteins and stored on ice until immobilization for the smFRET experiments. Immobilization for *in organello* sm FRET experiments is described in Section 7.2.3.3. Fluorescence quenching of DiSC₃(5) dye was used to determine the membrane potential of the isolated mitochondria. The analysis of the fluorescence recovery showed that the mitochondria were able to maintain the membrane potential for a minimum of 40 min after the import procedure. For this reason, smFRET measurements were carried out up until 40 min after start of the immobilization at room temperature.

7.2. Biophysical and analysis methods

7.2.1. MFD-PIE measurements

7.2.1.1. 2-color MFD-PIE microscope

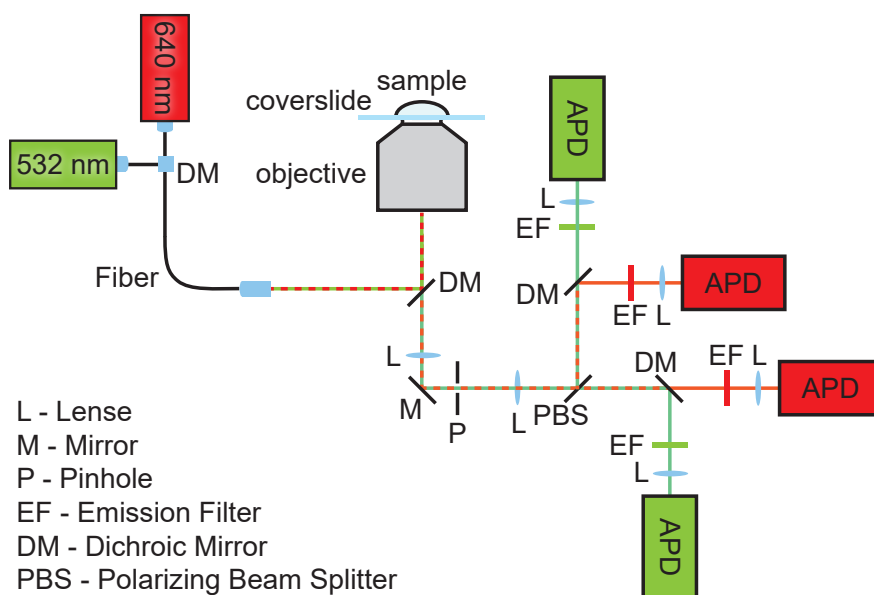


Figure 7.1.: Schematic of the 2-color confocal MFD-PIE microscope. The two pulsed lasers are combined in a single-mode fiber and alternately excite the sample. Fluorescence signal of the sample is collected by the objective and guided to the detection pathway by a dichroic mirror (DM). The signal is focused onto a pinhole (P) by a lens (L) and separated based on its polarization by a polarizing beam splitter (PBS). The signal is further separated by dichroic mirrors based on its wavelength, spectrally selected by emission filters (EF) and focused by lenses onto avalanche photodiodes (APD) for detection.

Measurements of freely diffusing samples labeled with Atto532 and/or either Alexa Fluor 647, CF640R, Atto647N or Atto647 were measured on a custom-built^[79] dual-color confocal microscope with pulsed-interleaved excitation (PIE)^[20,21] and multi-parameter fluorescence detection (MFD).^[22] The power of the two lasers with the wavelengths 532 nm (PicoTA Toptica) and 640 nm (PicoQuant LDH-D-C-640) measured before the objective was 100 μ W.

7.2.1.2. Calibration, preparation of the sample chamber, and sample dilution

Each day, PBS and measurement buffer were measured to determine the instrument response function (IRF) and the scatter component of the FRET measurements. Furthermore, a dye sample of Atto532 and Atto655 was measured to ensure good alignment of the detection pathway and to determine the brightness and the confocal volume. For the smFRET measurements, droplets of 20 μL BSA (1 mg mL^{-1} , New England Biolabs) were put in 8-well or 4-well Labtek I slides and incubated for 10 min to passivate the surface. Next, the BSA solution was removed and replaced by 20 μL of the sample of interest in its measurement buffer. The concentration of fluorescently labeled Ssc1 for burst measurements was 10–50 μM , depending on the sample quality, so that around 5 bursts of photons occurred in 1 s. Nucleotides ATP and purified ADP were added at final concentration of 1 mM, model substrate P5 (CALLLSAPRR) at 100 μM and the cochaperones Mdj1 and Mge1 at 5 μM . Burst measurements lasted for 3–5 h.

7.2.2. Burst selection and data analysis

Data acquired on the confocal MFD-PIE microscope were analyzed with the the open-source software PAM (PIE Analysis with Matlab).^[156] Single bursts were selected by an all-photon burst search applying a sliding time window of 500 μs , a minimum burst size of 100 photons and 20 photons per time window. Burst selection was further refined with the ALEX-2CDE filter.^[157] The correction factors for direct excitation, crosstalk and γ were determined using photon counts based on an approach from *Coullomb et al.*^[158] The static FRET line was determined based on a single-exponential fit of the lifetime of the donor fluorophore from the donor-only population present in the sample. The dynamic FRET line was determined based on a double-exponential fit of the lifetime of the donor fluorophore from the dynamic population. For the E- τ -plots of the lid sensor γ was determined population-wise by taking different acceptor lifetimes into account. This can be done based on the relationship between the γ -factor, the detection efficiencies (η_A, η_D) and the quantum yields (Φ_D, Φ_A) of the acceptor and donor fluorophores

$$\gamma = \frac{\Phi_A \eta_A}{\Phi_D \eta_D} \quad (7.1)$$

and the relationship of the natural lifetime τ_n of a fluorophore with the measured lifetime τ and the quantum yield.

$$\tau_n = \frac{\tau}{\Phi} \quad (7.2)$$

For the two measurements of the domain sensor of Ssc1 in the presence of substrate and either ATP or ADP, two individual measurements were combined for the resulting smFRET histograms since statistics were low due to aggregation of P5. Multiple Ssc1 proteins bind trying to resolve these aggregates leading to high intensities and security shutdown of the APDs. For this reason, P5 was sonicated before measurements and the aggregates in the solution were spun down with a table top centrifuge and the supernatant was measured on the MFD-PIE setup. However, because of the aggregates, less protein remained diffusing freely in the solution, leading to lower statistics.

For the measurements of the domain sensor, where P5 was added as a substrate, it became apparent that changes in FRET efficiency were occurring for up to an hour. When we are interested in equilibrium measurements, we only used data collected after 60 min. Although the lid sensor did not show such slow FRET changes after addition of substrate, we also did not use the first 60 min of the measurements to be on the consistent.

7.2.2.1. Dynamic photon distribution analysis (PDA)

To determine a FRET efficiency, all photons collected within a given timebin are used. When the protein undergoes a conformational change within a time bin, an averaged signal will be calculated. Hence, a dynamic population will cause a bridge between the two end conformations it dynamically switches between. Due to the shot-noise limited Gaussian shape of many of the dynamic populations of the measurements in this thesis, it was assumed that the dynamics are on a timescale much faster than the diffusion time. Because the end populations are still visible in most cases, this suggests a static-dynamic mixture. For this reason, a 2-state system with a static-dynamic mixture was applied for dynamic PDA, with two additional static populations to account for "impurities". Since dynamic PDA includes parameters accounting for shot-noise, and other statistical parameters, all data points are included in the fit. For this reason, possible "impurities" need to be included in the model. Further, one can use the different averaging caused by the dynamics, from histograms with different time bin to fit the transition rates. This is possible, because PDA accounts for noise and the heterogeneity of the system. Histograms with time bins of 0.7, 1.0, 1.5 and 2 ms were exported to PDAFit. Due to the complexity of the model chosen and the global fit of the data, the fit proces was divided into 4 steps. Because the domains of Ssc1 transitions between two well-defined structures, the measurements with ATP or ADP and P5 were analyzed first, to obtain the position of the end populations. In the next step,

the 1 ms dataset of all 13 measurements of the domain sensor were globally fitted. This was done to get a first idea of the distances, populations widths and amplitudes. Time constants were left free in this step. It became clear, that the high FRET can not be fit with on global value, so a window of $\pm 2.5 \text{ \AA}$ was added in the next step. Next, the four histograms with different bin sizes were fit globally to obtain the transition rates. This was done individually for the 13 different conditions. Here, a range of 5 \AA was given for each of the distances for better accuracy, since the rates change slightly depending on the exact distance. All values were fit globally in this step. Next, the distances of the 1 ms datasets of all 13 conditions were fitted globally again. The transition rates obtained from the previous step were fixed for each condition. This step yielded the final distances and widths of the populations. In a last step, the final transition rates were obtained by fitting again the four histograms with different bin sizes of each condition globally, with everything but the transition rates and amplitudes fixed. Error bars of the transition rates are based on confidence intervals from the fit.

The static lid data was fit globally for all 13 conditions with 5 static populations. Four of these populations (except the very low FRET population) and all five the population widths were fit globally based on a dataset with 1 ms bin width.

7.2.3. HILO measurements

7.2.3.1. Single-molecule objective-type TIRF/HILO microscope

Single-molecule total internal reflection fluorescence (TIRF) measurements were carried out on a custom-built three-color objective-type TIRF microscope with alternating laser excitation (ALEX).^[159] The incident angle of the laser beam can be alternated by moving a motorized stage on which the mirrors are mounted that direct the beam into the microscope body. This changes the location at which the beam enters the 60x oil immersion objective (Apo TIRF 60x/1.49 Oil, Nikon, Düsseldorf, Germany) and thus the angle at the glass water interface. The laser lines at 491 nm (Cobolt Calypso, 50 mW, Solna, Sweden), 532 nm (Cobolt Samba, 100 mW), 561 nm (Calypso Jive, 50 mW) and 647 nm (Cobolt MLD, 120 mW) are coupled into a single-mode fiber (optimized for 532/647 nm, OZ Optics, Carp, Canada) with dichroic mirrors. In this work only the laser lines 491 nm, 532 nm and 647 nm were used. An acousto-optical tunable filter (AOTFnC.400-650-PV-TN, Pegasus Optik, Wallenhorst, Germany) between the lasers and the fiber is used for millisecond ALEX. The laser beam is collimated and expanded after the fiber exit and directed to the two mirrors on the motorized stage, that direct the laser into the microscope body.

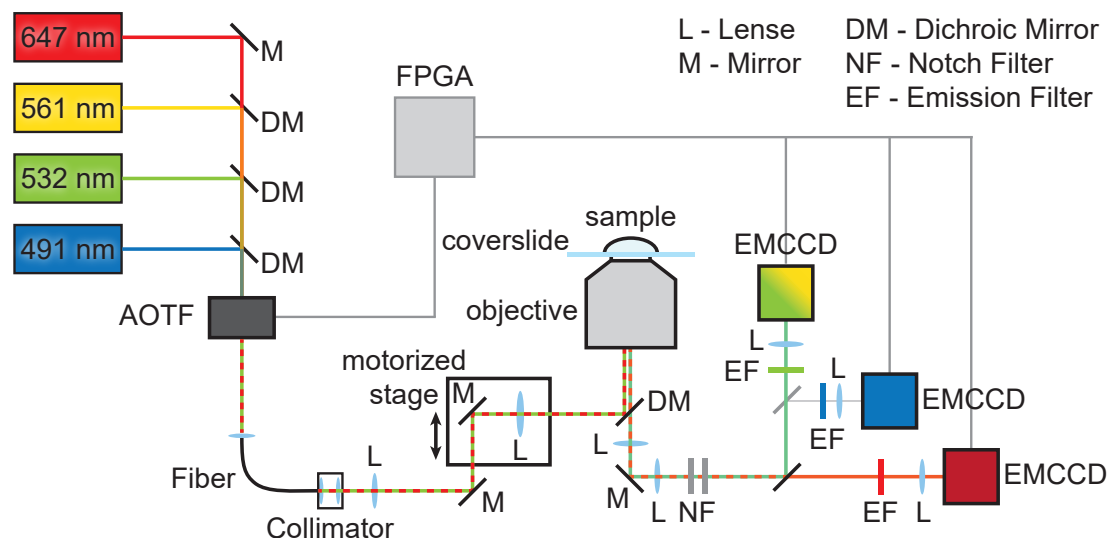


Figure 7.2.: Schematic of the single-molecule TIRF microscope. The lasers are combined by dichroic mirrors (DM), and coupled into a single-mode fiber after passing an acousto-optical tunable filter (AOTF). At the exit of the fiber, the beam is collimated and expanded. A second lens (L) focuses the beam on the backfocal plane of the objective and the TIRF angle can be adjusted with the mirrors (M) on a motorized stage. Fluorescence signal separated from the excitation pathway with a dichroic mirror and guided to the cameras. The signal passes two notch filters (NF) to remove remaining excitation light. The signal is split according to wavelength using dichroic mirrors, spectrally defined with emission filters (EF) and focused on electron multiplying charge coupled device (EMCCD) cameras. The cameras and the AOTF are synchronized with an field-programmable gated array (FPGA).

The collected fluorescence signal is separated from excitation light by a dichroic mirror (z532/633rpc, AHF Analysentechnik, Düsseldorf, Germany) and guided to the side port of the microscope body. Remaining excitation light is filtered out by a 488/647 (AHF) and a 532/10 notch filter (AHF). The signal is then split by a long-pass dichroic mirror (630DCLP, AHF). The blue/green emission can be split again by an optional second long-pass dichroic mirror (560DCXR, AHF). However, the autofluorescence signal of the mitochondria could be detected on the green camera and thus the third camera was not necessary. The fluorescence signal is focused onto electron multiplying charge coupled device (EMCCD) cameras (Andor iXON, Andor Technology, Belfast, UK) with achromatic lenses. An HQ 705/100 emission filter (AHF) is used in front of the red camera and an HQ 595/50 emission filter (AHF) in front of the green camera to clean up the emission light. Cameras and AOTF are synchronized by a field-programmable gated array (FPGA, cRIO-9073, National Instruments, Austin, TX, USA).

7.2.3.2. Cleaning and surface passivation of glass coverslides for TIRF microscopy

Glass coverslides (Marienfeld, High Precision Microscope Cover Glasses, 24 mm × 60 mm, (170 ± 5) μm, No. 1.5H) were cleaned with Acetone (HPLC grade) and in a second step with pure Ethanol in a sonication bath. After drying, the surface was coated over night at 55 °C in a solution of 50 mL toluene with 5–10 v% PEG-Silane (ABCR, 3-[Methoxy(polyethyleneoxy)propyl]-trimethoxysilane, 90 %, 6–9 PE–units) and 3–5 mg Silane-PEG-Biotin (Nanocs, 3400 Da). On the next day, slides were washed in pure Ethanol twice for 3 min, rinsed twice with milliQ water and dried with compressed air. Slides were either used right away (Section 7.2.3.3) or stored under vacuum.

7.2.3.3. Assembly and preparation of probe chambers for *in organello* smTIRF microscopy

A piece cut from a red silicon sheet (2.4 mm thickness) with a hole (8 mm diameter) in the middle was put on the washed and dried coverslide and fixated with a coat of epoxy glue around the edges. The hole acts as the probe chamber. The probe chamber was incubated with 100 μL of 0.2 mg mL⁻¹ streptavidin (Sigma-Aldrich, from *Streptomyces avidinii*) for 15 min. Afterwards, the chamber was washed with PBS three times to remove unbound streptavidin. In the next step, biotinylated antibody (αTom22, or αPorin) was added to the chamber and incubated for at least 15 min and washed with PBS three times to remove left over antibody and then washed once with SI buffer.

The prepared batch of mitochondria (see Section 7.1.11) was taken off the ice, diluted in 100 μL SI buffer and added to the chamber. After 10 min of incubation at room temperature, the chamber was washed with SI buffer 3–4 times. In the last washing step the buffer with additives respective to the measurement condition, either ATP or ATP depletion, was added on top. The sample was measured immediately for approximately 25 min. After 40 min had elapsed since taking the mitochondria off the ice, the measurements were stopped and the sample was discarded.

7.2.3.4. Single-molecule *in organello* HILO measurements

For the *in organello* measurements, the blue laser line was used at maximum power before the objective, which corresponds to 18 mW to excite the autofluorescence of the mitochondria. After excitation for 50 frames using the blue laser, the sample was excited alternately with green

(532 nm) and red (647 nm) laser light at 30 mW and 20 mW, respectively. The timescale of ALEX was either 25 ms or 50 ms with an additional 2.2 ms for frame transfer. 600 frames were collected per color adding up to a total of 1250 frames including blue excitation for mitochondria localization.

7.2.4. Trace analysis

The acquired movies were analyzed with a home-written Matlab based software (Mitra). In a first step, a map between the locations of the two cameras was created for each measurement day based on an image of a zero mode wave guide. The 50 frames with blue laser excitation were used to localize the mitochondria and every pixel above a certain intensity was marked. This was necessary because mitochondria are larger than the diffraction limit and have different shapes and sizes. The program is generally designed to choose the brightest pixel or the center of mass as the location of the object. Since mitochondria autofluorescence is used as a criterion for selection of double-labeled proteins, the whole mitochondrion needs to be taken into account. The intensity threshold varied depending on the coverslide background and possible bright fluorescent impurities. Furthermore, it depended on the state of the optical setup and possible brightness gradients in the field of view. Typically it was set between 0.2 and 0.25 of the maximum brightness of the 50 frames. The subsequent 1200 ALEX frames were used to look for colocalization with dual-labeled proteins. Green excitation and green detection was used for detection of green fluorophores and red excitation and red detection for detection of red fluorophores. Here, a mask was applied for detection of single fluorophores in the sum image. Intensity in a radius of 2 pixels around the central pixel was averaged for the fluorescence signal of the fluorophore. The background was calculated per molecule as an average of the pixel intensity in a circular ring around the detected fluorescent signal, with a radius of 4 pixels from the central pixel and subtracted from the intensity. Traces were exported for signals overlapping in the green and red detection channels as well as with mitochondrial localization determined using blue excitation. After trace extraction, traces were sorted manually into categories for FRET and for correction factor calculations. Crosstalk was calculated from suitable traces and the peak position of a Gaussian fit to the narrow distribution of this parameter was applied for all other traces, where crosstalk could not be calculated directly. Direct excitation was calculated and also exhibited a narrow distribution. However, consistent with the previous camera-based smFRET experiments of Ssc1, it was not included in the data correction. Gamma was determined by a linear fit of the relation between the inverse of the stoichiometry and the FRET efficiency (see Section 2.4.5.1) of all molecules used for FRET analysis.^[29] Careful data examination and application of different methods for gamma determination and fitting resulted in this being the most robust method based on the sometimes low statistics per day and the overall data quality (especially short trace lengths).

FRET was calculated based on the formulas described in the introduction (Formulas 2.12 through 2.23). SmFRET histograms shown are molecule-wise (i.e. averaged over all frames detected for an individual molecule), since dynamics that could be distinguished from noise were rarely detected and averaging over the whole trace reduced the influence of the noise.

7.2.4.1. Tracking analysis

For tracking of single Ssc1 proteins diffusing inside mitochondria, a script written by Philipp Messer^[154,160], was implemented into Mitra in Matlab. Molecules were identified in each frame using a multiscale wavelet analysis. The image is decomposed into planes of different resolutions. Since the fluorescent molecules were small, the planes 1 through 3 were used which are the planes with higher resolution. A threshold was applied to differentiate signal from noise. For green detection a threshold of 0.91 proved to be most successful and a threshold of 0.93 for red detection. Using a nearest neighbour approach with a tolerance of up to 5 pixels detected positions were combined into trajectories. To correlate mobility and FRET efficiency, trajectories were not only created for the ALEX channel that should have the highest intensity, but also for the green camera. To extract FRET, trajectories detected on the green and red camera were connected to FRET pairs by applying the mapping mask and allowing a distance of up to 4 pixels between the average location. Because of slow blinking behavior and diffusion in z-direction, out of the volume detectable with HILO, molecules were sometimes not detected for several frames until appearing again. To still be detected as the same molecule, a frame skip of 50 following frames was allowed. For signal extraction, a larger mask was applied than before, with signal detection in a radius of 3 pixels around the center pixel. This yielded the highest quality traces. For background calculation, a circle at 4 to 5 pixels around the center pixel was used.

The traces obtained were then further sorted based on quality and occurrence of FRET. The molecules of the traces showing FRET were then looked at in further detail to see if the trajectories match the actual position of the particle. Traces were then categorized into moving and non-moving molecules and, in rare cases, into a category with molecules changing their mobility during acquisition.

Probability distribution of squared displacements (PDSD) analysis

Because of the short length of the single-molecule tracks, classic mean squared displacements (MSD) analysis could not be performed. Instead, a probability distribution of square displacements (PDSD) analysis was applied.^[155] For this, the square displacements of the first time lag

($t_{lag} = 0.0544$ s) were used. The probability $P(r^2, \tau)$ was then fit to

$$P(r^2, \tau) = 1 - \exp(-(r^2 - a)/4D\tau) \quad (7.3)$$

to obtain the diffusion coefficient D .

A. Supplementary Figures and Tables

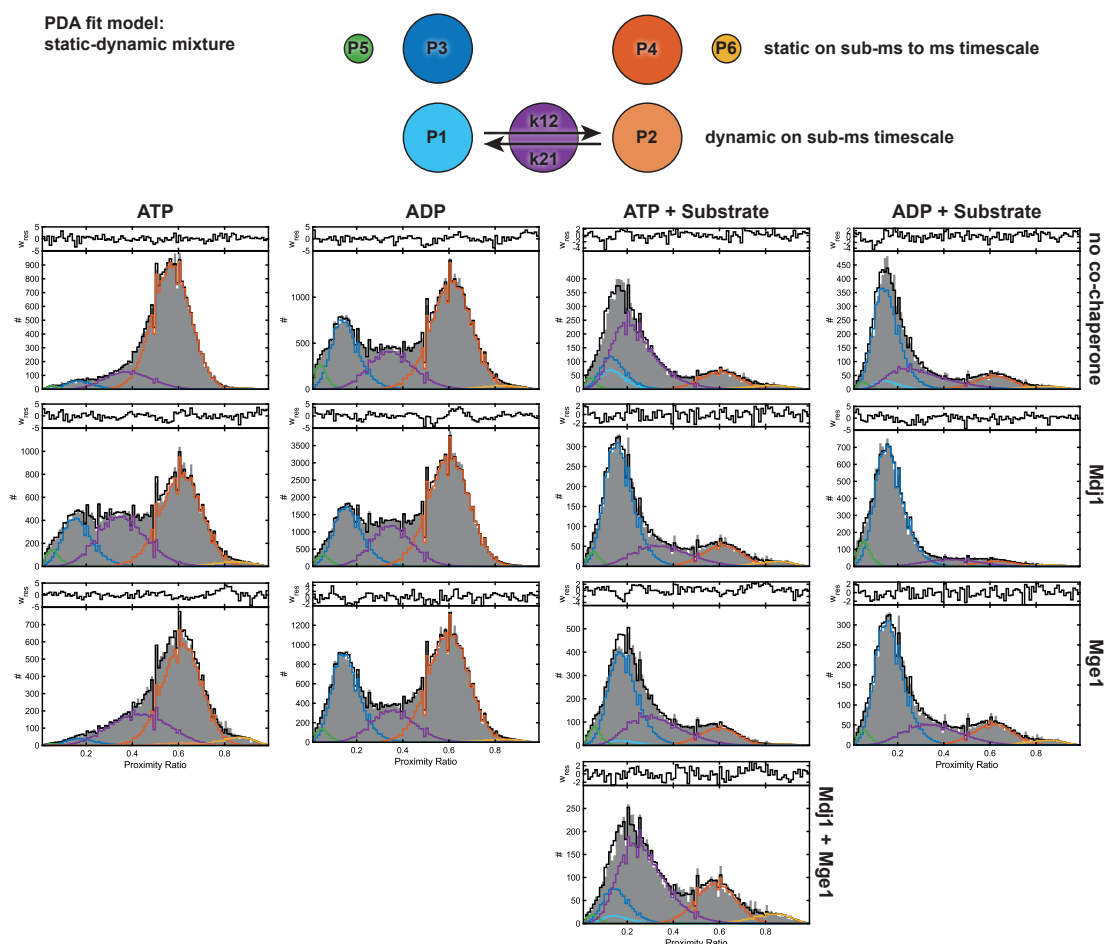


Figure A.1.: Global dynamic PDA fits of the domain sensor of Ssc1. Top: Schematic representation of the fit model. A static-dynamic mixture between two FRET states is assumed. This means that the low and high FRET species are partially static (P3 and P4) but are also part of the dynamic population as P1 and P2 besides the completely averaged species (purple). Histograms: Resulting histograms (stairs) of the dynamic PDA fit compared to the experimental data (gray). Blue and orange are the static species P3 and P4, respectively. Purple is the dynamically averaged FRET species. For slower kinetics ($<3 \text{ ms}^{-1}$) FRET efficiencies are not completely averaged and P1 (light blue) and P2 (light orange) are visible as part of the dynamic population. The green (P5) and yellow (P6) populations account for impurities and have no biological relevance. The columns are from left to right: ATP, ADP, ATP and substrate, ADP and substrate. The rows are from top to bottom: without cochaperones, with Mdj1, with Mge1, with both cochaperones (Mdj1 and Mge1).

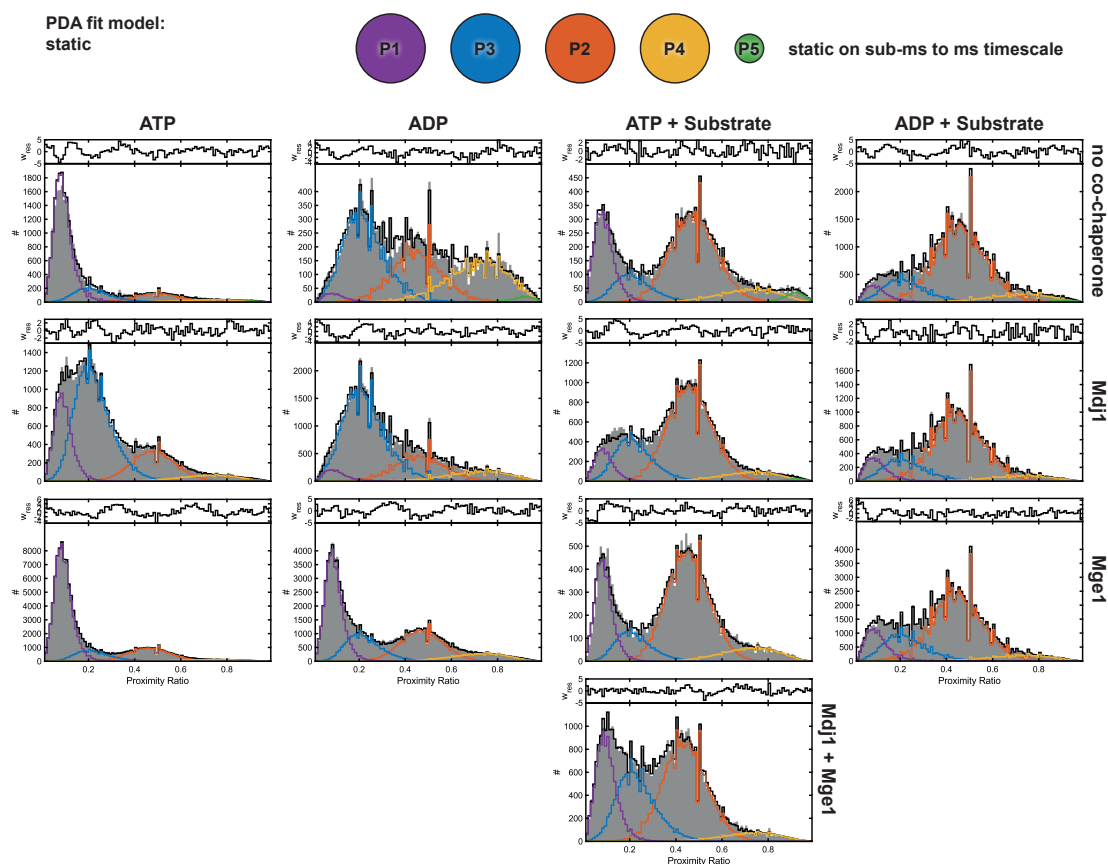


Figure A.2.: Global PDA fits of the lid sensor of Ssc1. Top: Schematic of the PDA fit model. 5 static populations are assumed. A1 through A4 have biological, A5 accounts for impurities. The columns are from left to right: ATP, ADP, ATP and substrate, ADP and substrate. The rows are from top to bottom: without cochaperones, with Mdj1, with Mge1, with both cochaperones (Mdj1 and Mge1).

Table A.1.: Results of the global dynamic Photon Distribution Analysis of the domain sensor of Ssc1. The distances R1/R3, R5 and R6, the widths $\sigma1/\sigma3$, $\sigma5$ and $\sigma6$ were fit globally for all conditions. The widths $\sigma2/\sigma4$ were fit semi-globally, for all conditions except ATP. Kinetic rates k12 and k21, the distance R2/R4 and amplitudes A3, A4, A5 and A6 were fit for each condition based on 4 different bin sizes (0.7 ms, 1 ms, 1.5 ms, 2 ms) and with the global values fixed. Global fits were carried out on the datasets with 1 ms bin time.

Domain Sensor	[ms-1]	[Å]	[Å]	[ms-1]	[Å]	[Å]	[Å]	[Å]	[Å]	[Å]	[Å]	[Å]	[Å]	[Å]	[Å]	[Å]	[Å]	
ATP	8.2	71.7	4.5	5.5	51.1	2.3	0.28	71.7	4.5	5.9	51.1	2.3	0.0064	104.4	1.0	0.0058	39.8	3.3
ATP Mdj1	9.3	71.7	4.5	8.3	48.6	2.2	0.59	71.7	4.5	1.6	48.6	2.2	0.030	104.4	1.0	0.022	39.8	3.3
ATP Mge1	5.1	71.7	4.5	2.7	49.7	2.2	0.10	71.7	4.5	2.0	49.7	2.2	0.0039	104.4	1.0	0.044	39.8	3.3
ADP	13	71.7	4.5	10	47.9	2.2	1.1	71.7	4.5	2.6	47.9	2.2	0.038	104.4	1.0	0.017	39.8	3.3
ADP Mdj1	19	71.7	4.5	17	49.1	2.2	1.0	71.7	4.5	2.7	49.1	2.2	0.020	104.4	1.0	0.0044	39.8	3.3
ADP Mge1	15	71.7	4.5	11	48.5	2.2	1.8	71.7	4.5	3.3	48.5	2.2	0.021	104.4	1.0	0.013	39.8	3.3
ATP P5	1.7	71.7	4.5	5.0	47.4	2.2	0.25	71.7	4.5	0.22	47.4	2.2	0.027	104.4	1.0	0.033	39.8	3.3
ATP P5 Mdj1	4.5	71.7	4.5	4.3	48.7	2.2	3.0	71.7	4.5	0.72	48.7	2.2	0.035	104.4	1.0	0.031	39.8	3.3
ATP P5 Mge1	2.1	71.7	4.5	3.4	50.4	2.2	1.6	71.7	4.5	0.39	50.4	2.2	0.045	104.4	1.0	0.0075	39.8	3.3
ADP P5	1.5	71.7	4.5	2.7	47.8	2.2	1.9	71.7	4.5	0.37	47.8	2.2	0.019	104.4	1.0	0.024	39.8	3.3

Table A.2.: Results of the global Photon Distribution Analysis of the lid sensor of Ssc1. The distances R1, R3, R4 and R5 and the widths σ_1 , σ_2 , σ_3 , σ_4 , and σ_5 were fit globally based on a dataset with 1 ms bin size. The distance E2 and the amplitudes A1, A2, A3, A4 and A5 were fit per condition.

Condition Sensor	Lid	Population P1			Population P2			Population P3			Population P4			Population P5			χ^2_{red}
		A1	R1 [Å]	σ_1 [Å]	A2	R2 [Å]	σ_2 [Å]	A3	R3 [Å]	σ_3 [Å]	A4	R4 [Å]	σ_4 [Å]	A5	R5 [Å]	σ_5 [Å]	
ATP	0.68	91.5	7.0	0.14	54.8	3.3	0.15	70.5	5.1	0.024	44.3	2.6	0.0067	36.1	1.6	3.55	
ATP Mdj1	0.21	91.5	7.0	0.20	55.7	3.3	0.56	70.5	5.1	0.029	44.3	2.6	0.0043	36.1	1.6	1.88	
ATP Mge1	0.66	91.5	7.0	0.20	56.5	3.3	0.12	70.5	5.1	0.019	44.3	2.6	0.0024	36.1	1.6	4.46	
ADP	0.019	91.5	7.0	0.35	56.0	3.3	0.41	70.5	5.1	0.19	44.3	2.6	0.017	36.1	1.6	2.19	
ADP Mdj1	0.042	91.5	7.0	0.25	55.9	3.3	0.64	70.5	5.1	0.065	44.3	2.6	0.0026	36.1	1.6	3.78	
ADP Mge1	0.41	91.5	7.0	0.33	55.9	3.3	0.20	70.5	5.1	0.056	44.3	2.6	0.0060	36.1	1.6	4.67	
ATP P5	0.22	91.5	7.0	0.56	55.8	3.3	0.13	70.5	5.1	0.057	44.3	2.6	0.027	36.1	1.6	1.99	
ATP P5 Mdj1	0.087	91.5	7.0	0.64	56.7	3.3	0.22	70.5	5.1	0.044	44.3	2.6	0.0089	36.1	1.6	4.61	
ATP P5 Mge1	0.21	91.5	7.0	0.60	56.9	3.3	0.12	70.5	5.1	0.055	44.3	2.6	0.0029	36.1	1.6	4.39	
ADP P5	0.067	91.5	7.0	0.71	56.7	3.3	0.16	70.5	5.1	0.051	44.3	2.6	0.010	36.1	1.6	4.59	
ADP P5 Mdj1	0.10	91.5	7.0	0.69	57.1	3.3	0.16	70.5	5.1	0.038	44.3	2.6	0.0027	36.1	1.6	2.39	
ADP P5 Mge1	0.13	91.5	7.0	0.64	57.2	3.3	0.19	70.5	5.1	0.037	44.3	2.6	0.0027	36.1	1.6	4.28	
ATP P5 Mdj1 Mge1	0.22	91.5	7.0	0.48	58.0	3.3	0.27	70.5	5.1	0.030	44.3	2.6	0.0014	36.1	1.6	2.70	

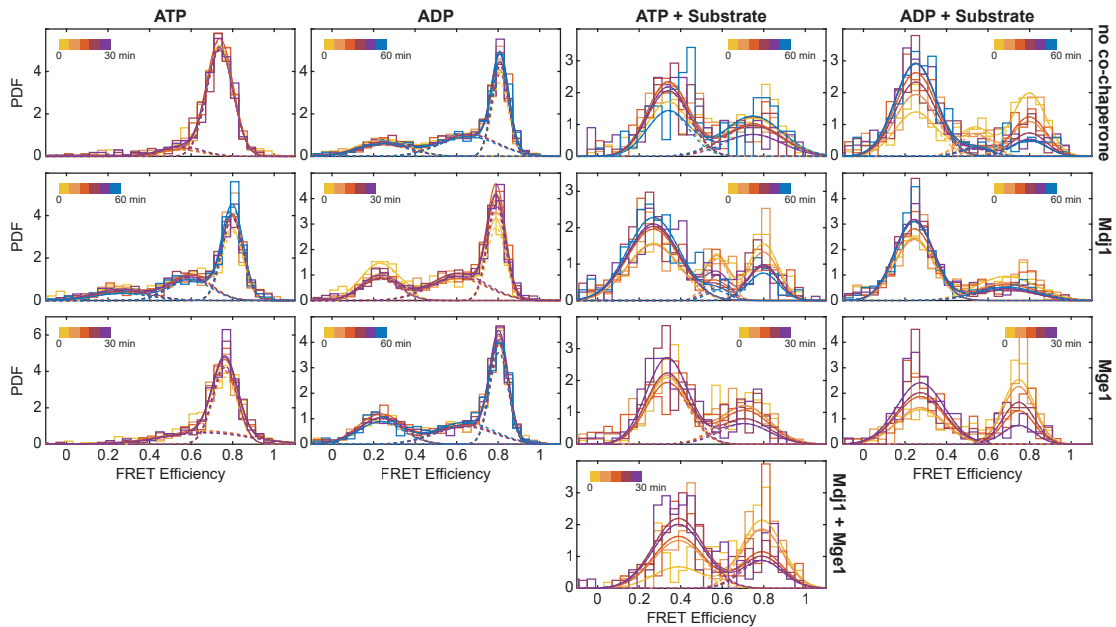


Figure A.3.: Time-wise FRET histograms of the domain sensor of Ssc1 to follow slow structural changes. The first 30 or 60 min of each measurement are dissected into multiple histograms to be able to observe slow conformational changes. The columns are from left to right: ATP, ADP, ATP and substrate, ADP and substrate. The rows are from top to bottom: without cochaperones, with Mdj1, with Mge1, with both cochaperones (Mdj1 and Mge1).

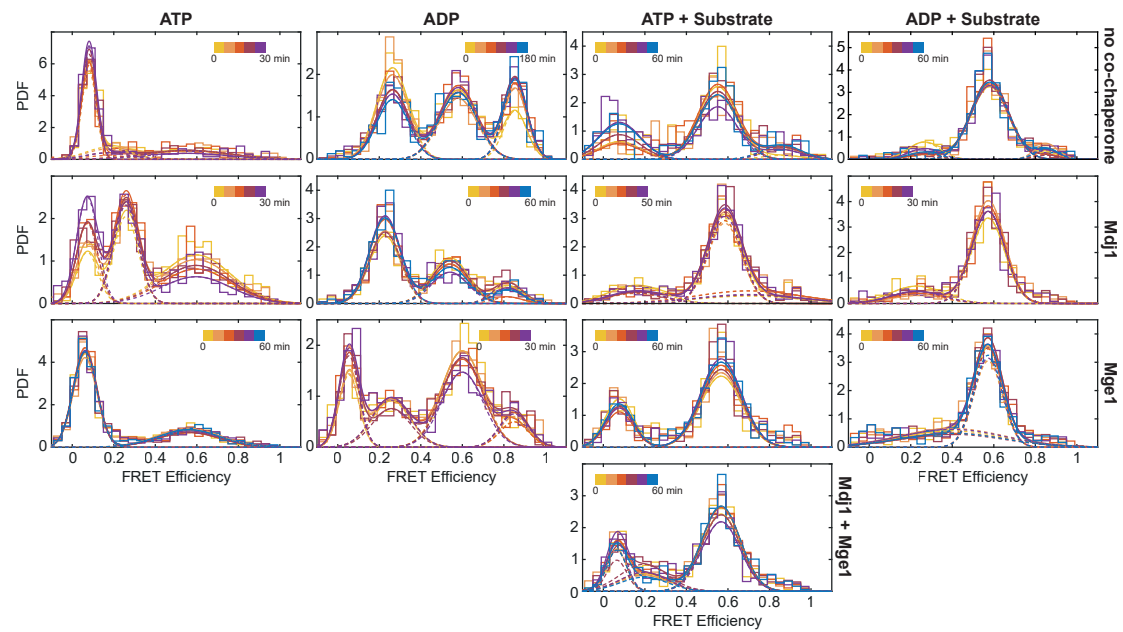


Figure A.4.: Time-wise FRET histograms of the lid sensor of Ssc1 to follow slow structural changes. The first 30 or 60 min (180 min for ADP) of each measurement are dissected into multiple histograms to be able to observe slow conformational changes. The columns are from left to right: ATP, ADP, ATP and substrate, ADP and substrate. The rows are from top to bottom: without cochaperones, with Mdj1, with Mge1, with both cochaperones (Mdj1 and Mge1).

B. List of Figures

2.1. Jablonski diagram showing the basic processes involved in fluorescence.	5
2.2. Jablonski diagram of FRET between a donor and an acceptor fluorophore.	7
2.3. Widefield illumination, TIRF and HILO/VAEM.	10
2.4. An overview of a typical TIRF experiment.	11
2.5. An overview of a burst measurement.	13
2.6. Exemplary E- τ -plot.	15
2.7. Dynamic PDA fit of a series of proximity ratio histograms generated at different time bins.	15
3.1. Exemplary structures of the different classes of heat shock proteins.	22
3.2. Structure of the NBD of the Hsp70 DnaK bound to ATP.	26
3.3. Structure of the SBD of the Hsp70 DnaK in the substrate-bound state.	27
3.4. The structure of the Hsp70 DnaK in the presence of ATP or ADP and substrate.	28
3.5. Different aspects of allosteric regulation of the Hsp70 DnaK.	29
3.6. Homology model of the interaction of Ssc1 and Mge1.	35
3.7. Schematic of the mitochondrial presequence translocase.	38
4.1. Labeling Positions of the domain sensor and the lid sensor of Ssc1.	46
4.2. SmFRET histograms and E- τ -plots of Ssc1 in the presence of nucleotide and substrate.	49
4.3. In-depth examination of the high FRET state of the lid sensor.	51
4.4. Time series of smFRET histograms of Ssc1 in the presence of substrate.	52
4.5. SmFRET histograms and E- τ -plots of Ssc1 in the presence of Mdj1.	55
4.6. SmFRET histograms and E- τ -plots of Ssc1 in the presence of Mge1.	57
4.7. SmFRET histograms and E- τ -plots of Ssc1 ATP, substrate, Mdj1 and Mge1.	60
4.8. PDA models and exemplary PDA fits.	61
4.9. Results of the PDA fit of the smFRET data.	62
4.10. Proposed model for the chaperone cycle of Ssc1.	66
4.11. Graphical representation of the labeling positions of the new domain sensors of Ssc1.	68
4.12. SmFRET histograms of the new domain sensors of Ssc1.	69

5.1. Immobilization of isolated mitochondria for smTIRF experiments.	74
5.2. Comparison of different dye pairs on Ssc1.	76
5.3. Exemplary single-molecule traces of Ssc1 inside mitochondria.	77
5.4. <i>In organello</i> smFRET histograms of the domain sensor of Ssc1.	79
5.5. <i>In organello</i> smFRET histograms of the lid sensor of Ssc1.	82
5.6. Trajectories of tracked molecules inside mitochondria.	83
5.7. Mobility-dependent <i>in organello</i> smFRET histograms of the domain sensor of Ssc1.	84
5.8. Analysis of the probability distribution of square displacements of the tracked Ssc1.	86
7.1. Schematic of the 2-color confocal MFD-PIE microscope.	98
7.2. Schematic of the single-molecule TIRF microscope.	102
A.1. Global dynamic PDA fits of the domain sensor of Ssc1.	108
A.2. Global PDA fits of the lid sensor of Ssc1.	109
A.3. Time-wise FRET histograms of the domain sensor of Ssc1 to follow slow structural changes.	110
A.4. Time-wise FRET histograms of the lid sensor of Ssc1 to follow slow structural changes.	111

C. Literature

- [1] C. Sánchez-Rico, L. Voith von Voithenberg, L. Warner, D. C. Lamb, M. Sattler, “Effects of Fluorophore Attachment on Protein Conformation and Dynamics Studied by spFRET and NMR Spectroscopy”, *Chemistry – A European Journal* **2017**, *23*, 14267–14277.
- [2] R. Kityk, J. Kopp, I. Sinning, M. P. Mayer, “Structure and Dynamics of the ATP-Bound Open Conformation of Hsp70 Chaperones”, *Molecular Cell* **2012**, *48*, 863–874.
- [3] E. B. Bertelsen, L. Chang, J. E. Gestwicki, E. R. P. Zuiderweg, “Solution conformation of wild-type E. coli Hsp70 (DnaK) chaperone complexed with ADP and substrate”, *Proceedings of the National Academy of Sciences* **2009**, pnas.0903503106.
- [4] K. Mapa, M. Sikor, V. Kudryavtsev, K. Waegemann, S. Kalinin, C. A. M. Seidel, W. Neupert, D. C. Lamb, D. Mokranjac, “The Conformational Dynamics of the Mitochondrial Hsp70 Chaperone”, *Molecular Cell* **2010**, *38*, 89–100.
- [5] M. Sikor, K. Mapa, L. V. von Voithenberg, D. Mokranjac, D. C. Lamb, “Real-time observation of the conformational dynamics of mitochondrial Hsp70 by spFRET”, *The EMBO Journal* **2013**, *32*, 1639–1649.
- [6] L. Voith von Voithenberg, A. Barth, V. Trauschke, B. Demarco, S. Tyagi, C. Koehler, E. A. Lemke, D. C. Lamb, “Comparative analysis of the coordinated motion of Hsp70 from different organelles observed by single molecule three-color FRET”, *Proceedings of the National Academy of Sciences* **2021**.
- [7] E. Betzig, “Nobel Lecture: Single molecules, cells, and super-resolution optics”, *Reviews of Modern Physics* **2015**, *87*, 1153–1168.
- [8] S. W. Hell, “Nobel Lecture: Nanoscopy with freely propagating light”, *Reviews of Modern Physics* **2015**, *87*, 1169–1181.
- [9] W. E. Moerner, “Nobel Lecture: Single-molecule spectroscopy, imaging, and photocontrol: Foundations for super-resolution microscopy”, *Reviews of Modern Physics* **2015**, *87*, 1183–1212.
- [10] J. Capoulade, M. Wachsmuth, L. Hufnagel, M. Knop, “Quantitative fluorescence imaging of protein diffusion and interaction in living cells”, *Nature Biotechnology* **2011**, *29*, 835–839.
- [11] P. F. Aramendia, R. M. Negri, E. S. Roman, “Temperature Dependence of Fluorescence and Photoisomerization in Symmetric Carbocyanines. Influence of Medium Viscosity and Molecular Structure”, *The Journal of Physical Chemistry* **1994**, *98*, 3165–3173.
- [12] M. Levitus, S. Ranjit, “Cyanine dyes in biophysical research: the photophysics of polymethine fluorescent dyes in biomolecular environments”, *Quarterly Reviews of Biophysics* **2011**, *44*, 123–151.

- [13] L. D. Hughes, R. J. Rawle, S. G. Boxer, “Choose Your Label Wisely: Water-Soluble Fluorophores Often Interact with Lipid Bilayers”, *PLOS ONE* **2014**, *9*, e87649.
- [14] H. C. Kolb, M. G. Finn, K. B. Sharpless, “Click Chemistry: Diverse Chemical Function from a Few Good Reactions”, *Angewandte Chemie International Edition* **2001**, *40*, 2004–2021.
- [15] C. S. Heil, A. Rittner, B. Goebel, D. Beyer, M. Grininger, “Site-Specific Labelling of Multidomain Proteins by Amber Codon Suppression”, *Scientific Reports* **2018**, *8*, 14864.
- [16] L. Kyung Jin, K. Deokhee, P. Hee-Sung, “Site-Specific Labeling of Proteins Using Unnatural Amino Acids”, *Molecules and Cells* **2019**, *42*, 386–396.
- [17] T. Förster, “Zwischenmolekulare Energiewanderung und Fluoreszenz”, *Annalen der Physik* **1948**, *437*, 55–75.
- [18] M. Tokunaga, N. Imamoto, K. Sakata-Sogawa, “Highly inclined thin illumination enables clear single-molecule imaging in cells”, *Nature Methods* **2008**, *5*, 159–161.
- [19] C. A. Konopka, S. Y. Bednarek, “Variable-angle epifluorescence microscopy: a new way to look at protein dynamics in the plant cell cortex”, *The Plant Journal* **2008**, *53*, 186–196.
- [20] A. N. Kapanidis, N. K. Lee, T. A. Laurence, S. Doose, E. Margeat, S. Weiss, “Fluorescence-aided molecule sorting: Analysis of structure and interactions by alternating-laser excitation of single molecules”, *Proceedings of the National Academy of Sciences* **2004**, *101*, 8936–8941.
- [21] B. K. Müller, E. Zaychikov, C. Bräuchle, D. C. Lamb, “Pulsed Interleaved Excitation”, *Biophysical Journal* **2005**, *89*, 3508–3522.
- [22] C. Eggeling, S. Berger, L. Brand, J. R. Fries, J. Schaffer, A. Volkmer, C. A. M. Seidel, “Data registration and selective single-molecule analysis using multi-parameter fluorescence detection”, *Journal of Biotechnology* **2001**, *86*, 163–180.
- [23] V. Kudryavtsev, M. Sikor, S. Kalinin, D. Mokranjac, C. A. M. Seidel, D. C. Lamb, “Combining MFD and PIE for Accurate Single-Pair Förster Resonance Energy Transfer Measurements”, *ChemPhysChem* **2012**, *13*, 1060–1078.
- [24] J. Hendrix, D. C. Lamb in *Methods in Enzymology*, Vol. 518, (Ed.: S. Y. Tetin), Academic Press, **2013**, pp. 205–243.
- [25] A. Gansen, A. Valeri, F. Hauger, S. Felekyan, S. Kalinin, K. Tóth, J. Langowski, C. A. M. Seidel, “Nucleosome disassembly intermediates characterized by single-molecule FRET”, *Proceedings of the National Academy of Sciences* **2009**, *106*, 15308–15313.
- [26] S. Kalinin, A. Valeri, M. Antonik, S. Felekyan, C. A. M. Seidel, “Detection of Structural Dynamics by FRET: A Photon Distribution and Fluorescence Lifetime Analysis of Systems with Multiple States”, *The Journal of Physical Chemistry B* **2010**, *114*, 7983–7995.
- [27] M. Antonik, S. Felekyan, A. Gaiduk, C. A. M. Seidel, “Separating Structural Heterogeneities from Stochastic Variations in Fluorescence Resonance Energy Transfer Distributions via Photon Distribution Analysis”, *The Journal of Physical Chemistry B* **2006**, *110*, 6970–6978.

- [28] I. V. Gopich, A. Szabo, “Single-Molecule FRET with Diffusion and Conformational Dynamics”, *The Journal of Physical Chemistry B* **2007**, *111*, 12925–12932.
- [29] N. K. Lee, A. N. Kapanidis, Y. Wang, X. Michalet, J. Mukhopadhyay, R. H. Ebright, S. Weiss, “Accurate FRET Measurements within Single Diffusing Biomolecules Using Alternating-Laser Excitation”, *Biophysical Journal* **2005**, *88*, 2939–2953.
- [30] H. Wallrabe, A. Periasamy, “Imaging protein molecules using FRET and FLIM microscopy”, *Current Opinion in Biotechnology* **2005**, *16*, 19–27.
- [31] R. Crawford, J. P. Torella, L. Aigrain, A. Plochowitz, K. Gryte, S. Uphoff, A. N. Kapanidis, “Long-Lived Intracellular Single-Molecule Fluorescence Using Electroporated Molecules”, *Biophysical Journal* **2013**, *105*, 2439–2450.
- [32] J. J. Sakon, K. R. Weninger, “Detecting the conformation of individual proteins in live cells”, *Nature Methods* **2010**, *7*, 203–205.
- [33] I. König, A. Zarrine-Afsar, M. Aznauryan, A. Soranno, B. Wunderlich, F. Dingfelder, J. C. Stüber, A. Plückthun, D. Nettels, B. Schuler, “Single-molecule spectroscopy of protein conformational dynamics in live eukaryotic cells”, *Nature Methods* **2015**, *12*, 773–779.
- [34] K. Okamoto, K. Hibino, Y. Sako, “In-cell single-molecule FRET measurements reveal three conformational state changes in RAF protein”, *Biochimica et Biophysica Acta (BBA) - General Subjects* **2020**, *1864*, 129358.
- [35] W. B. Asher, P. Geggier, M. D. Holsey, G. T. Gilmore, A. K. Pati, J. Meszaros, D. S. Terry, S. Mathiasen, M. J. Kaliszewski, M. D. McCauley, A. Govindaraju, Z. Zhou, K. G. Harikumar, K. Jaqaman, L. J. Miller, A. W. Smith, S. C. Blanchard, J. A. Javitch, “Single-molecule FRET imaging of GPCR dimers in living cells”, *Nature Methods* **2021**, *18*, 397–405.
- [36] R. Rosenzweig, N. B. Nillegoda, M. P. Mayer, B. Bukau, “The Hsp70 chaperone network”, *Nature Reviews Molecular Cell Biology* **2019**, *20*, 665–680.
- [37] Y. Hanazono, K. Takeda, M. Yohda, K. Miki, “Structural Studies on the Oligomeric Transition of a Small Heat Shock Protein, StHsp14.0”, *Journal of Molecular Biology* **2012**, *422*, 100–108.
- [38] T. R. M. Barends, R. W. W. Brosi, A. Steinmetz, A. Scherer, E. Hartmann, J. Eschenbach, T. Lorenz, R. Seidel, R. L. Shoeman, S. Zimmermann, R. Bittl, I. Schlichting, J. Reinstein, “Combining crystallography and EPR: crystal and solution structures of the multidomain cochaperone DnaJ”, *Acta Crystallographica Section D* **2013**, *69*, 1540–1552.
- [39] Y. Gomez-Llorente, F. Jebara, M. Patra, R. Malik, S. Nisemblat, O. Chomsky-Hecht, A. Parnas, A. Azem, J. A. Hirsch, I. Ubarretxena-Belandia, “Structural basis for active single and double ring complexes in human mitochondrial Hsp60-Hsp10 chaperonin”, *Nature Communications* **2020**, *11*, 1916.
- [40] M. M. U. Ali, S. M. Roe, C. K. Vaughan, P. Meyer, B. Panaretou, P. W. Piper, C. Prodromou, L. H. Pearl, “Crystal structure of an Hsp90–nucleotide–p23/Sba1 closed chaperone complex”, *Nature* **2006**, *440*, 1013–1017.
- [41] A. K. Shiau, S. F. Harris, D. R. Southworth, D. A. Agard, “Structural Analysis of E. coli Hsp90 Reveals Dramatic Nucleotide-Dependent Conformational Rearrangements”, *Cell* **2006**, *127*, 329–340.

- [42] C. Deville, M. Carroni, K. B. Franke, M. Topf, B. Bukau, A. Mogk, H. R. Saibil, “Structural pathway of regulated substrate transfer and threading through an Hsp100 disaggregase”, *Science Advances* **2017**, *3*, e1701726.
- [43] F. Hennessy, W. S. Nicoll, R. Zimmermann, M. E. Cheetham, G. L. Blatch, “Not all J domains are created equal: Implications for the specificity of Hsp40–Hsp70 interactions”, *Protein Science* **2005**, *14*, 1697–1709.
- [44] S. Alvira, J. Cuéllar, A. Röhl, S. Yamamoto, H. Itoh, C. Alfonso, G. Rivas, J. Buchner, J. M. Valpuesta, “Structural characterization of the substrate transfer mechanism in Hsp70/Hsp90 folding machinery mediated by Hop”, *Nature Communications* **2014**, *5*, 5484.
- [45] N. Morgner, C. Schmidt, V. Beilstein-Edmands, I.-o. Ebong, N. A. Patel, E. M. Clerico, E. Kirschke, S. Daturpalli, S. E. Jackson, D. Agard, C. V. Robinson, “Hsp70 Forms Antiparallel Dimers Stabilized by Post-translational Modifications to Position Clients for Transfer to Hsp90”, *Cell Reports* **2015**, *11*, 759–769.
- [46] B. Bukau, A. L. Horwich, “The Hsp70 and Hsp60 Chaperone Machines”, *Cell* **1998**, *92*, 351–366.
- [47] W. Voos, “Chaperone–protease networks in mitochondrial protein homeostasis”, *Biochimica et Biophysica Acta (BBA) - Molecular Cell Research* **2013**, *1833*, 388–399.
- [48] B. Roche, L. Aussel, B. Ezraty, P. Mandin, B. Py, F. Barras, “Iron/sulfur proteins biogenesis in prokaryotes: Formation, regulation and diversity”, *Biochimica et Biophysica Acta (BBA) - Bioenergetics* **2013**, *1827*, 455–469.
- [49] E. A. Craig, J. Marszalek, “How Do J-Proteins Get Hsp70 to Do So Many Different Things?”, *Trends in Biochemical Sciences* **2017**, *42*, 355–368.
- [50] F. H. Schopf, M. M. Biebl, J. Buchner, “The HSP90 chaperone machinery”, *Nature Reviews Molecular Cell Biology* **2017**, *18*, 345–360.
- [51] S. Walter, “Structure and function of the GroE chaperone”, *Cellular and Molecular Life Sciences CMLS* **2002**, *59*, 1589–1597.
- [52] E. Schleiff, T. Becker, “Common ground for protein translocation: access control for mitochondria and chloroplasts”, *Nature Reviews Molecular Cell Biology* **2011**, *12*, 48–59.
- [53] P. De Los Rios, A. Ben-Zvi, O. Slutsky, A. Azem, P. Goloubinoff, “Hsp70 chaperones accelerate protein translocation and the unfolding of stable protein aggregates by entropic pulling”, *Proceedings of the National Academy of Sciences* **2006**, *103*, 6166–6171.
- [54] R. Sousa, E. M. Lafer, “The Physics of Entropic Pulling: A Novel Model for the Hsp70 Motor Mechanism”, *International Journal of Molecular Sciences* **2019**, *20*, 2334.
- [55] J. L. Brodsky, J. Goekeler, R. Schekman, “BiP and Sec63p are required for both co- and posttranslational protein translocation into the yeast endoplasmic reticulum”, *Proceedings of the National Academy of Sciences* **1995**, *92*, 9643–9646.
- [56] P.-J. Kang, J. Ostermann, J. Shilling, W. Neupert, E. A. Craig, N. Pfanner, “Requirement for hsp70 in the mitochondrial matrix for translocation and folding of precursor proteins”, *Nature* **1990**, *348*, 137–143.
- [57] C. C. Deocaris, S. C. Kaul, R. Wadhwa, “On the brotherhood of the mitochondrial chaperones mortalin and heat shock protein 60”, *Cell Stress & Chaperones* **2006**, *11*, 116–128.

- [58] S. Ziętkiewicz, A. Lewandowska, P. Stocki, K. Liberek, “Hsp70 Chaperone Machine Remodels Protein Aggregates at the Initial Step of Hsp70-Hsp100-dependent Disaggregation”, *Journal of Biological Chemistry* **2006**, *281*, 7022–7029.
- [59] R. Dutkiewicz, M. Nowak, E. A. Craig, J. Marszalek in *Methods in Enzymology*, Vol. 595, (Ed.: S. S. David), Academic Press, **2017**, pp. 161–184.
- [60] T. Lutz, B. Westermann, W. Neupert, J. M. Herrmann, “The mitochondrial proteins Ssq1 and Jac1 are required for the assembly of iron sulfur clusters in mitochondria” Edited by B. Holland”, *Journal of Molecular Biology* **2001**, *307*, 815–825.
- [61] C. Voisine, B. Schilke, M. Ohlson, H. Beinert, J. Marszalek, E. A. Craig, “Role of the Mitochondrial Hsp70s, Ssc1 and Ssq1, in the Maturation of Yfh1”, *Molecular and Cellular Biology* **2000**, *20*, 3677–3684.
- [62] C. Voisine, Y. C. Cheng, M. Ohlson, B. Schilke, K. Hoff, H. Beinert, J. Marszalek, E. A. Craig, “Jac1, a mitochondrial J-type chaperone, is involved in the biogenesis of Fe/S clusters in *Saccharomyces cerevisiae*”, *Proceedings of the National Academy of Sciences of the United States of America* **2001**, *98*, 1483–1488.
- [63] F. Fontanesi, I. C. Soto, D. Horn, A. Barrientos, “Mss51 and Ssc1 Facilitate Translational Regulation of Cytochrome c Oxidase Biogenesis”, *Molecular and Cellular Biology* **2010**, *30*, 245–259.
- [64] L. Böttinger, B. Guiard, S. Oeljeklaus, B. Kulawiak, N. Zufall, N. Wiedemann, B. Warscheid, M. van der Laan, T. Becker, “A complex of Cox4 and mitochondrial Hsp70 plays an important role in the assembly of the cytochrome c oxidase”, *Molecular Biology of the Cell* **2013**, *24*, 2609–2619.
- [65] L. Böttinger, S. Oeljeklaus, B. Guiard, S. Rospert, B. Warscheid, T. Becker, “Mitochondrial Heat Shock Protein (Hsp) 70 and Hsp10 Cooperate in the Formation of Hsp60 Complexes”, *Journal of Biological Chemistry* **2015**, *290*, 11611–11622.
- [66] R. Sousa, H.-S. Liao, J. Cuéllar, S. Jin, J. M. Valpuesta, A. J. Jin, E. M. Lafer, “Clathrin-coat disassembly illuminates the mechanisms of Hsp70 force generation”, *Nature Structural & Molecular Biology* **2016**, *23*, 821–829.
- [67] S. Reeg, T. Jung, J. P. Castro, K. J. A. Davies, A. Henze, T. Grune, “The molecular chaperone Hsp70 promotes the proteolytic removal of oxidatively damaged proteins by the proteasome”, *Free Radical Biology and Medicine* **2016**, *99*, 153–166.
- [68] R. G. Smock, M. E. Blackburn, L. M. Gierasch, “Conserved, Disordered C Terminus of DnaK Enhances Cellular Survival upon Stress and DnaK in Vitro Chaperone Activity”, *Journal of Biological Chemistry* **2011**, *286*, 31821–31829.
- [69] Y.-W. Chang, Y.-J. Sun, C. Wang, C.-D. Hsiao, “Crystal Structures of the 70-kDa Heat Shock Proteins in Domain Disjoining Conformation”, *Journal of Biological Chemistry* **2008**, *283*, 15502–15511.
- [70] K. M. Flaherty, C. DeLuca-Flaherty, D. B. McKay, “Three-dimensional structure of the ATPase fragment of a 70K heat-shock cognate protein”, *Nature* **1990**, *346*, 623–628.
- [71] D. Bauer, D. R. Merz, B. Pelz, K. E. Theisen, G. Yacyshyn, D. Mokranjac, R. I. Dima, M. Rief, G. Žoldák, “Nucleotides regulate the mechanical hierarchy between subdomains of the nucleotide binding domain of the Hsp70 chaperone DnaK”, *Proceedings of the National Academy of Sciences* **2015**, *112*, 10389.

- [72] S. S. Mandal, D. R. Merz, M. Buchsteiner, R. I. Dima, M. Rief, G. Žoldák, “Nanomechanics of the substrate binding domain of Hsp70 determine its allosteric ATP-induced conformational change”, *Proceedings of the National Academy of Sciences* **2017**, *114*, 6040.
- [73] X. Zhu, X. Zhao, W. F. Burkholder, A. Gragerov, C. M. Ogata, M. E. Gottesman, W. A. Hendrickson, “Structural Analysis of Substrate Binding by the Molecular Chaperone DnaK”, *Science* **1996**, *272*, 1606–1614.
- [74] M. P. Mayer, H. Schröder, S. Rüdiger, K. Paal, T. Laufen, B. Bukau, “Multistep mechanism of substrate binding determines chaperone activity of Hsp70”, *Nature Structural Biology* **2000**, *7*, 586–593.
- [75] L. E. Horton, P. James, E. A. Craig, J. O. Hensold, “The Yeast hsp70 Homologue Ssa Is Required for Translation and Interacts with Sis1 and Pab1 on Translating Ribosomes *”, *Journal of Biological Chemistry* **2001**, *276*, 14426–14433.
- [76] S. Rüdiger, L. Germeroth, J. Schneider-Mergener, B. Bukau, “Substrate specificity of the DnaK chaperone determined by screening cellulose-bound peptide libraries”, *The EMBO Journal* **1997**, *16*, 1501–1507.
- [77] A. Sekhar, A. Velyvis, G. Zoltsman, R. Rosenzweig, G. Bouvignies, L. E. Kay, “Conserved conformational selection mechanism of Hsp70 chaperone-substrate interactions”, *eLife* **2018**, *7*, e32764.
- [78] A. Gragerov, M. E. Gottesman, “Different Peptide Binding Specificities of hsp70 Family Members”, *Journal of Molecular Biology* **1994**, *241*, 133–135.
- [79] M. Marcinowski, M. Höller, M. J. Feige, D. Baerend, D. C. Lamb, J. Buchner, “Substrate discrimination of the chaperone BiP by autonomous and cochaperone-regulated conformational transitions”, *Nature Structural & Molecular Biology* **2011**, *18*, 150–158.
- [80] A. Mashaghi, S. Bezrukavnikov, D. P. Minde, A. S. Wentink, R. Kityk, B. Zachmann-Brand, M. P. Mayer, G. Kramer, B. Bukau, S. J. Tans, “Alternative modes of client binding enable functional plasticity of Hsp70”, *Nature* **2016**, *539*, 448–451.
- [81] M. Vogel, B. Bukau, M. P. Mayer, “Allosteric Regulation of Hsp70 Chaperones by a Proline Switch”, *Molecular Cell* **2006**, *21*, 359–367.
- [82] R. Kityk, M. Vogel, R. Schlecht, B. Bukau, M. P. Mayer, “Pathways of allosteric regulation in Hsp70 chaperones”, *Nature Communications* **2015**, *6*, 8308.
- [83] M. P. Mayer, R. Kityk, “Insights into the molecular mechanism of allostery in Hsp70s”, *Frontiers in Molecular Biosciences* **2015**, *2*.
- [84] J. F. Swain, G. Dinler, R. Sivendran, D. L. Montgomery, M. Stotz, L. M. Gierasch, “Hsp70 Chaperone Ligands Control Domain Association via an Allosteric Mechanism Mediated by the Interdomain Linker”, *Molecular Cell* **2007**, *26*, 27–39.
- [85] R. Kityk, J. Kopp, M. P. Mayer, “Molecular Mechanism of J-Domain-Triggered ATP Hydrolysis by Hsp70 Chaperones”, *Molecular Cell* **2018**, *69*, 227–237.e4.
- [86] M. Samaddar, A. V. Goswami, J. Purushotham, P. Hegde, P. D’Silva, “Role of the loop L4,5 in allosteric regulation in mtHsp70s: in vivo significance of domain communication and its implications in protein translocation”, *Molecular Biology of the Cell* **2014**, *25*, 2129–2142.

- [87] A. Zhuravleva, L. M. Gierasch, “Substrate-binding domain conformational dynamics mediate Hsp70 allostery”, *Proceedings of the National Academy of Sciences* **2015**, *112*, E2865.
- [88] M. Rosam, D. Krader, C. Nickels, J. Hochmair, K. C. Back, G. Agam, A. Barth, C. Zeymer, J. Hendrix, M. Schneider, I. Antes, J. Reinstein, D. C. Lamb, J. Buchner, “Bap (Sil1) regulates the molecular chaperone BiP by coupling release of nucleotide and substrate”, *Nature Structural & Molecular Biology* **2018**, *25*, 90–100.
- [89] R. Schlecht, A. H. Erbse, B. Bukau, M. P. Mayer, “Mechanics of Hsp70 chaperones enables differential interaction with client proteins”, *Nature Structural & Molecular Biology* **2011**, *18*, 345–351.
- [90] E. A. Craig, J. Kramer, J. Kosic-Smithers, “SSC1, a member of the 70-kDa heat shock protein multigene family of *Saccharomyces cerevisiae*, is essential for growth”, *Proceedings of the National Academy of Sciences* **1987**, *84*, 4156–4160.
- [91] G. Pareek, M. Samaddar, P. D’Silva, “Primary Sequence That Determines the Functional Overlap between Mitochondrial Heat Shock Protein 70 Ssc1 and Ssc3 of *Saccharomyces cerevisiae*”, *Journal of Biological Chemistry* **2011**, *286*, 19001–19013.
- [92] Y. Kubo, T. Tsunehiro, S.-i. Nishikawa, M. Nakai, E. Ikeda, A. Toh-e, N. Morishima, T. Shibata, T. Endo, “Two distinct mechanisms operate in the reactivation of heat-denatured proteins by the mitochondrial Hsp70/Mdj1p/Yge1p chaperone system”, *Journal of Molecular Biology* **1999**, *286*, 447–464.
- [93] Q. Liu, J. Krzewska, K. Liberek, E. A. Craig, “Mitochondrial Hsp70 Ssc1: Role in Protein Folding”, *Journal of Biological Chemistry* **2001**, *276*, 6112–6118.
- [94] I. Wagner, H. Arlt, L. van Dyck, T. Langer, W. Neupert, “Molecular chaperones cooperate with PIM1 protease in the degradation of misfolded proteins in mitochondria”, *The EMBO Journal* **1994**, *13*, 5135–5145.
- [95] T. Bender, I. Lewrenz, S. Franken, C. Baitzel, W. Voos, “Mitochondrial enzymes are protected from stress-induced aggregation by mitochondrial chaperones and the Pim1/LON protease”, *Molecular Biology of the Cell* **2011**, *22*, 541–554.
- [96] C. Ungermann, W. Neupert, D. Cyr, “The role of Hsp70 in conferring unidirectionality on protein translocation into mitochondria”, *Science* **1994**, *266*, 1250–1253.
- [97] C. Ungermann, B. Guiard, W. Neupert, D. M. Cyr, “The delta psi- and Hsp70/MIM44-dependent reaction cycle driving early steps of protein import into mitochondria”, *The EMBO Journal* **1996**, *15*, 735–744.
- [98] M. Sichting, D. Mokranjac, A. Azem, W. Neupert, K. Hell, “Maintenance of structure and function of mitochondrial Hsp70 chaperones requires the chaperone Hep1”, *The EMBO Journal* **2005**, *24*, 1046–1056.
- [99] L. K. Sanjuán Szklarz, B. Guiard, M. Rissler, N. Wiedemann, V. Kozjak, M. van der Laan, C. Lohaus, K. Marcus, H. E. Meyer, A. Chacinska, N. Pfanner, C. Meisinger, “Inactivation of the Mitochondrial Heat Shock Protein Zim17 Leads to Aggregation of Matrix Hsp70s Followed by Pleiotropic Effects on Morphology and Protein Biogenesis”, *Journal of Molecular Biology* **2005**, *351*, 206–218.
- [100] T. Momose, C. Ohshima, M. Maeda, T. Endo, “Structural basis of functional cooperation of Tim15/Zim17 with yeast mitochondrial Hsp70”, *EMBO reports* **2007**, *8*, 664–670.

- [101] M. Blamowska, M. Sichting, K. Mapa, D. Mokranjac, W. Neupert, K. Hell, “ATPase Domain and Interdomain Linker Play a Key Role in Aggregation of Mitochondrial Hsp70 Chaperone Ssc1”, *Journal of Biological Chemistry* **2010**, *285*, 4423–4431.
- [102] M. Blamowska, W. Neupert, K. Hell, “Biogenesis of the mitochondrial Hsp70 chaperone”, *Journal of Cell Biology* **2012**, *199*, 125–135.
- [103] L. Burri, K. Vascotto, S. Fredersdorf, R. Tiedt, M. N. Hall, T. Lithgow, “Zim17, a Novel Zinc Finger Protein Essential for Protein Import into Mitochondria”, *Journal of Biological Chemistry* **2004**, *279*, 50243–50249.
- [104] P. Zhai, C. Stanworth, S. Liu, J. J. Silberg, “The Human Escort Protein Hep Binds to the ATPase Domain of Mitochondrial Hsp70 and Regulates ATP Hydrolysis”, *Journal of Biological Chemistry* **2008**, *283*, 26098–26106.
- [105] D. Bauer, S. Meinhold, R. P. Jakob, J. Stigler, U. Merkel, T. Maier, M. Rief, G. Žoldák, “A folding nucleus and minimal ATP binding domain of Hsp70 identified by single-molecule force spectroscopy”, *Proceedings of the National Academy of Sciences* **2018**, *115*, 4666.
- [106] A. V. Goswami, B. Chittoor, P. D’Silva, “Understanding the Functional Interplay between Mammalian Mitochondrial Hsp70 Chaperone Machine Components”, *Journal of Biological Chemistry* **2010**, *285*, 19472–19482.
- [107] A. Azem, W. Oppliger, A. Lustig, P. Jenö, B. Feifel, G. Schatz, M. Horst, “The Mitochondrial hsp70 Chaperone System: Effect of Adenine Nucleotides, Peptide Substrate, and mGrpE on the Oligomeric State of mHsp70”, *Journal of Biological Chemistry* **1997**, *272*, 20901–20906.
- [108] P. D. D’Silva, B. Schilke, W. Walter, A. Andrew, E. A. Craig, “J protein cochaperone of the mitochondrial inner membrane required for protein import into the mitochondrial matrix”, *Proceedings of the National Academy of Sciences* **2003**, *100*, 13839–13844.
- [109] F. Moro, A. Muga, “Thermal Adaptation of the Yeast Mitochondrial Hsp70 System is Regulated by the Reversible Unfolding of its Nucleotide Exchange Factor”, *Journal of Molecular Biology* **2006**, *358*, 1367–1377.
- [110] B. Miao, J. E. Davis, E. A. Craig, “Mge1 functions as a nucleotide release factor for Ssc1, a mitochondrial Hsp70 of *Saccharomyces cerevisiae*”, *Journal of Molecular Biology* **1997**, *265*, 541–552.
- [111] C. Prip-Buus, B. Westermann, M. Schmitt, T. Langer, W. Neupert, E. Schwarz, “Role of the mitochondrial DnaJ homologue, Mdj1p, in the prevention of heat-induced protein aggregation”, *FEBS Letters* **1996**, *380*, 142–146.
- [112] B. Westermann, B. Gaume, J. M. Herrmann, W. Neupert, E. Schwarz, “Role of the mitochondrial DnaJ homolog Mdj1p as a chaperone for mitochondrially synthesized and imported proteins”, *Molecular and Cellular Biology* **1996**, *16*, 7063–7071.
- [113] E. A. Craig, J. Marszalek, “A specialized mitochondrial molecular chaperone system: A role in formation of Fe/S centers”, *Cellular and Molecular Life Sciences CMLS* **2002**, *59*, 1658–1665.
- [114] D. Bursać, T. Lithgow, “Jid1 is a J-protein functioning in the mitochondrial matrix, unable to directly participate in endoplasmic reticulum associated protein degradation”, *FEBS Letters* **2009**, *583*, 2954–2958.

- [115] B. Westermann, C. Prip-Buus, W. Neupert, E. Schwarz, “The role of the GrpE homologue, Mge1p, in mediating protein import and protein folding in mitochondria”, *The EMBO Journal* **1995**, *14*, 3452–3460.
- [116] C. Weiss, A. Niv, A. Azem, “Two-Step Purification of Mitochondrial Hsp70, Ssc1p, Using Mge1(His)6 Immobilized on Ni-Agarose”, *Protein Expression and Purification* **2002**, *24*, 268–273.
- [117] A. Marada, P. K. Allu, A. Murari, B. PullaReddy, P. Tammineni, V. R. Thiriveedi, J. Danduprolu, N. B. V. Sepuri, “Mge1, a nucleotide exchange factor of Hsp70, acts as an oxidative sensor to regulate mitochondrial Hsp70 function”, *Molecular Biology of the Cell* **2013**, *24*, 692–703.
- [118] P. K. Allu, A. Marada, Y. Boggula, S. Karri, T. Krishnamoorthy, N. B. V. Sepuri, “Methionine sulfoxide reductase 2 reversibly regulates Mge1, a cochaperone of mitochondrial Hsp70, during oxidative stress”, *Molecular Biology of the Cell* **2014**, *26*, 406–419.
- [119] N. Rowley, C. Prip-Buus, B. Westermann, C. Brown, E. Schwarz, B. Barrell, W. Neupert, “Mdj1p, a novel chaperone of the DnaJ family, is involved in mitochondrial biogenesis and protein folding”, *Cell* **1994**, *77*, 249–259.
- [120] G. L. Ciesielski, M. Plotka, M. Manicki, B. A. Schilke, R. Dutkiewicz, C. Sahi, J. Marszalek, E. A. Craig, “Nucleoid localization of Hsp40 Mdj1 is important for its function in maintenance of mitochondrial DNA”, *Biochimica et Biophysica Acta (BBA) - Molecular Cell Research* **2013**, *1833*, 2233–2243.
- [121] M. van der Laan, D. P. Hutu, P. Rehling, “On the mechanism of preprotein import by the mitochondrial presequence translocase”, *Biochimica et Biophysica Acta (BBA) - Molecular Cell Research* **2010**, *1803*, 732–739.
- [122] D. Mokranjac, W. Neupert, “The many faces of the mitochondrial TIM23 complex”, *Biochimica et Biophysica Acta (BBA) - Bioenergetics* **2010**, *1797*, 1045–1054.
- [123] F. Moro, K. Okamoto, M. Donzeau, W. Neupert, M. Brunner, “Mitochondrial Protein Import: Molecular Basis of the ATP-dependent Interaction of MtHsp70 with Tim44”, *Journal of Biological Chemistry* **2002**, *277*, 6874–6880.
- [124] Q. Liu, P. D’Silva, W. Walter, J. Marszalek, E. A. Craig, “Regulated Cycling of Mitochondrial Hsp70 at the Protein Import Channel”, *Science* **2003**, *300*, 139–141.
- [125] K. N. Truscott, W. Voos, A. E. Frazier, M. Lind, Y. Li, A. Geissler, J. Dudek, H. Müller, A. Sickmann, H. E. Meyer, C. Meisinger, B. Guiard, P. Rehling, N. Pfanner, “A J-protein is an essential subunit of the presequence translocase-associated protein import motor of mitochondria”, *Journal of Cell Biology* **2003**, *163*, 707–713.
- [126] A. E. Frazier, J. Dudek, B. Guiard, W. Voos, Y. Li, M. Lind, C. Meisinger, A. Geissler, A. Sickmann, H. E. Meyer, V. Bilanchone, M. G. Cumsky, K. N. Truscott, N. Pfanner, P. Rehling, “Pam16 has an essential role in the mitochondrial protein import motor”, *Nature Structural & Molecular Biology* **2004**, *11*, 226–233.
- [127] D. Mokranjac, G. Bourenkov, K. Hell, W. Neupert, M. Groll, “Structure and function of Tim14 and Tim16, the J and J-like components of the mitochondrial protein import motor”, *The EMBO Journal* **2006**, *25*, 4675–4685.

- [128] B. Westermann, W. Neupert, “Mdj2p, a novel DnaJ homolog in the mitochondrial inner membrane of the yeast *Saccharomyces cerevisiae*”, *Journal of Molecular Biology* **1997**, 272, 477–483.
- [129] D. Mokranjac, M. Sichting, D. Popov-Čeleketič, A. Berg, K. Hell, W. Neupert, “The Import Motor of the Yeast Mitochondrial TIM23 Preprotein Translocase Contains Two Different J Proteins, Tim14 and Mdj2 *”, *Journal of Biological Chemistry* **2005**, 280, 31608–31614.
- [130] M. van der Laan, A. Chacinska, M. Lind, I. Perschil, A. Sickmann, H. E. Meyer, B. Guiard, C. Meisinger, N. Pfanner, P. Rehling, “Pam17 Is Required for Architecture and Translocation Activity of the Mitochondrial Protein Import Motor”, *Molecular and Cellular Biology* **2005**, 25, 7449–7458.
- [131] M. Horst, W. Oppliger, S. Rospert, H.-J. Schönfeld, G. Schatz, A. Azem, “Sequential action of two hsp70 complexes during protein import into mitochondria”, *The EMBO Journal* **1997**, 16, 1842–1849.
- [132] A. Strub, K. Röttgers, W. Voos, “The Hsp70 peptide-binding domain determines the interaction of the ATPase domain with Tim44 in mitochondria”, *The EMBO Journal* **2002**, 21, 2626–2635.
- [133] P. D’Silva, Q. Liu, W. Walter, E. A. Craig, “Regulated interactions of mtHsp70 with Tim44 at the translocon in the mitochondrial inner membrane”, *Nature Structural & Molecular Biology* **2004**, 11, 1084–1091.
- [134] H. C. Schneider, B. Westermann, W. Neupert, M. Brunner, “The nucleotide exchange factor MGE exerts a key function in the ATP-dependent cycle of mt-Hsp70-Tim44 interaction driving mitochondrial protein import”, *The EMBO Journal* **1996**, 15, 5796–5803.
- [135] J. E. Pais, B. Schilke, E. A. Craig, “Reevaluation of the role of the Pam18:Pam16 interaction in translocation of proteins by the mitochondrial Hsp70-based import motor”, *Molecular Biology of the Cell* **2011**, 22, 4740–4749.
- [136] P. Goloubinoff, P. D. L. Rios, “The mechanism of Hsp70 chaperones: (entropic) pulling the models together”, *Trends in Biochemical Sciences* **2007**, 32, 372–380.
- [137] K. A. T. Makepeace, Y. Mohammed, E. L. Rudashevskaya, E. V. Petrotchenko, F. N. Vögtle, C. Meisinger, A. Sickmann, C. H. Borchers, “Improving Identification of In-organello Protein-Protein Interactions Using an Affinity-enrichable, Isotopically Coded, and Mass Spectrometry-cleavable Chemical Crosslinker”, *Molecular & Cellular Proteomics* **2020**, 19, 624–639.
- [138] I. Lewrenz, N. Rietzschel, B. Guiard, R. Lill, M. van der Laan, W. Voos, “The Functional Interaction of Mitochondrial Hsp70s with the Escort Protein Zim17 Is Critical for Fe/S Biogenesis and Substrate Interaction at the Inner Membrane Preprotein Translocase”, *Journal of Biological Chemistry* **2013**, 288, 30931–30943.
- [139] G. Levy-Rimler, P. Viitanen, C. Weiss, R. Sharkia, A. Greenberg, A. Niv, A. Lustig, Y. Delarea, A. Azem, “The effect of nucleotides and mitochondrial chaperonin 10 on the structure and chaperone activity of mitochondrial chaperonin 60”, *European Journal of Biochemistry* **2001**, 268, 3465–3472.

- [140] M. Moczko, B. Schönfisch, W. Voos, N. Pfanner, J. Rassow, “The Mitochondrial ClpB Homolog Hsp78 Cooperates with Matrix Hsp70 in Maintenance of Mitochondrial Function”, *Journal of Molecular Biology* **1995**, 254, 538–543.
- [141] B. von Janowsky, T. Major, K. Knapp, W. Voos, “The Disaggregation Activity of the Mitochondrial ClpB Homolog Hsp78 Maintains Hsp70 Function during Heat Stress”, *Journal of Molecular Biology* **2006**, 357, 793–807.
- [142] J. Krzewska, T. Langer, K. Liberek, “Mitochondrial Hsp78, a member of the Clp/Hsp100 family in *Saccharomyces cerevisiae*, cooperates with Hsp70 in protein refolding”, *FEBS Letters* **2001**, 489, 92–96.
- [143] S. A. McKinney, C. Joo, T. Ha, “Analysis of Single-Molecule FRET Trajectories Using Hidden Markov Modeling”, *Biophysical Journal* **2006**, 91, 1941–1951.
- [144] L. C. Zanetti-Domingues, C. J. Tynan, D. J. Rolfe, D. T. Clarke, M. Martin-Fernandez, “Hydrophobic Fluorescent Probes Introduce Artifacts into Single Molecule Tracking Experiments Due to Non-Specific Binding”, *PLOS ONE* **2013**, 8, e74200.
- [145] A. A. Torrano, R. Herrmann, C. Strobel, M. Rennhak, H. Engelke, A. Reller, I. Hilger, A. Wixforth, C. Bräuchle, “Cell membrane penetration and mitochondrial targeting by platinum-decorated ceria nanoparticles”, *Nanoscale* **2016**, 8, 13352–13367.
- [146] C.-C. Wu, V. Naveen, C.-H. Chien, Y.-W. Chang, C.-D. Hsiao, “Crystal Structure of DnaK Protein Complexed with Nucleotide Exchange Factor GrpE in DnaK Chaperone System: Insight into Intramolecular Communication”, *Journal of Biological Chemistry* **2012**, 287, 21461–21470.
- [147] M. Dimura, T. O. Peulen, C. A. Hanke, A. Prakash, H. Gohlke, C. A. M. Seidel, “Quantitative FRET studies and integrative modeling unravel the structure and dynamics of biomolecular systems”, *Current Opinion in Structural Biology* **2016**, 40, 163–185.
- [148] B. Hellenkamp, P. Wortmann, F. Kandzia, M. Zacharias, T. Hugel, “Multidomain structure and correlated dynamics determined by self-consistent FRET networks”, *Nature Methods* **2017**, 14, 174–180.
- [149] R. Banerjee, Dissertation, LMU München, **2018**.
- [150] A. Plochowitz, R. Crawford, A. N. Kapanidis, “Characterization of organic fluorophores for in vivo FRET studies based on electroporated molecules”, *Physical Chemistry Chemical Physics* **2014**, 16, 12688–12694.
- [151] J. H. M. van der Velde, E. Ploetz, M. Hiermaier, J. Oelerich, J. W. de Vries, G. Roelfes, T. Cordes, “Mechanism of Intramolecular Photostabilization in Self-Healing Cyanine Fluorophores”, *ChemPhysChem* **2013**, 14, 4084–4093.
- [152] J. H. M. van der Velde, J. Oelerich, J. Huang, J. H. Smit, A. Aminian Jazi, S. Galiani, K. Kolmakov, G. Gouridis, C. Eggeling, A. Herrmann, G. Roelfes, T. Cordes, “A simple and versatile design concept for fluorophore derivatives with intramolecular photostabilization”, *Nature Communications* **2016**, 7, 10144.
- [153] Q. Zheng, S. Jockusch, G. G. Rodríguez-Calero, Z. Zhou, H. Zhao, R. B. Altman, H. D. Abruña, S. C. Blanchard, “Intra-molecular triplet energy transfer is a general approach to improve organic fluorophore photostability”, *Photochemical & Photobiological Sciences* **2016**, 15, 196–203.

- [154] P. K. Messer, A.-K. Henß, D. C. Lamb, J. Winterlin, “A Multiscale Wavelet Algorithm for Atom Tracking in STM Movies”, *submitted* **2021**.
- [155] G. J. Schütz, H. Schindler, T. Schmidt, “Single-molecule microscopy on model membranes reveals anomalous diffusion”, *Biophysical Journal* **1997**, *73*, 1073–1080.
- [156] W. Schrimpf, A. Barth, J. Hendrix, D. C. Lamb, “PAM: A Framework for Integrated Analysis of Imaging, Single-Molecule, and Ensemble Fluorescence Data”, *Biophysical Journal* **2018**, *114*, 1518–1528.
- [157] T. E. Tomov, R. Tsukanov, R. Masoud, M. Liber, N. Plavner, E. Nir, “Disentangling Subpopulations in Single-Molecule FRET and ALEX Experiments with Photon Distribution Analysis”, *Biophysical Journal* **2012**, *102*, 1163–1173.
- [158] A. Coullomb, C. M. Bidan, C. Qian, F. Wehnekamp, C. Oddou, C. Albigès-Rizo, D. C. Lamb, A. Dupont, “QuanTI-FRET: a framework for quantitative FRET measurements in living cells”, *Scientific Reports* **2020**, *10*, 6504.
- [159] A. N. Kapanidis, T. A. Laurence, N. K. Lee, E. Margeat, X. Kong, S. Weiss, “Alternating-Laser Excitation of Single Molecules”, *Accounts of Chemical Research* **2005**, *38*, 523–533.
- [160] A.-K. Henß, S. Sakong, P. K. Messer, J. Wiechers, R. Schuster, D. C. Lamb, A. Groß, J. Winterlin, “Density fluctuations as door-opener for diffusion on crowded surfaces”, *Science* **2019**, *363*, 715–718.

D. Acknowledgments

I want to thank my supervisor **Prof. Don C. Lamb**, for giving me the chance to do my PhD in your group. Thank you for believing in me and trusting me with interesting projects and collaborations. And for showing me that there is always another tricky analysis method I could apply to my data.

Thank you, **Dr. Dejana Mokranjac**, for our long and fruitful collaboration and for agreeing to be my second evaluator.

Many thanks to **Dr. Moritz Ehrl** and **Silke Steger** for supporting me with administrative stuff and helping me understand current rules and regulations.

I also want to thank **Prof. Philip Tinnefeld**, **Prof. Achim Hartschuh**, **Prof. Michael Sattler**, and **Prof. Karl-Peter Hopfner** for agreeing to be part of my committee. I also want to thank **Prof. Ralf Jungmann** for being part of my TAC committee.

I want to thank **Prof. Suzanne Blum** for encouraging me to believe in my scientific skills and for awakening in me my interest in scientific discussions. I also want to thank **Prof. Thorben Cordes**, as well as **Jasper** and **Jochem**, for teaching me a lot about single-molecule fluorescence microscopy and photostabilization, and Belgian beer.

I want to thank all the members of the **GRK1721**. It really was a special experience to be part of this amazing graduate program and I enjoyed it very much. A special thanks to **André**, **Katharina**, **David**, **Adrian**, **Max**, **Stephan**, **Marvin**, **Arpita**, **Matthias** and **Marijke** for all the fun times we had and for making me feel right at home.

Thank you **Rupa**, for a great collaboration, fun troubleshooting and making it a bit more enjoyable to sit in a dark room for hours.

I want to thank all members of the **FABlab**. Only as a team, supporting each other, it is possible to achieve great science. Thank you, **Evelyn** for slide prep skills and fluorophore expertise, **Anders** for pushing me outside my science comfortzone, **Kira** for fun times in the office and lab together. Thank you, **Bassem**, for maintaining the smTIRF (not an easy job), **Philipp** for the wavelet tracking algorithm and fun boulder sessions, **Sushi** for explaining the Mitra architecture to me. Thank you, **Lena**, for always taking the time to reply to my emails when I had questions regarding previous experiments on Ssc1 and for reading my thesis. Thank you, **Waldi**, for getting me started and always challenging me. Thank you, **Fabian**, for being a pleasant office mate and

for normalizing designated lunch spots. Thank you, **Pooyeh**, for taking over one of my projects, the smTIRF and my lab bench, take good care of them. Thank you, **Opa Ivo**, for announcing yourself from afar with your squeaky pedals and joining in on all the fun. Thank you, **Chen**, for your dry humor and comments. Thank you, **Adrian**, for calm vibes and valuable feedback and the occasional sarcastic comments. Thank you, **Dr. Oetker**, for getting me through countless lunch breaks. Thank you, **Ganesh**, for teaching me everything about Biochemistry, knowing more papers than google scholar and for our walks and talks together. Thank you, **Nader**, for fun office times and always sharing your Lab Snacks with me. Thank you, **Simon**, for deep and honest conversations, snack breaks and some sanity during crazy times and for all the boulder sessions. Thank you, **Frank**, for beer, memes and for letting me keep you from work. And special thanks for binding my thesis and saving the day. Since I leave soon, I guess we're officially leveling up from being colleagues to being friends. And finally, many thanks to the **Leberschuss Crew** for making the last year more memorable than one would expect from a pandemic.

I want to thank my family, for always supporting me and trusting me and my decisions. Danke, **Mama**, dass du deine Sorgen (die sicher da waren), nicht immer ausformuliert hast, und mich meinen Weg hast gehen lassen. Danke, dass du mich darin unterstützt, meine Ziele zu erreichen und ich mich immer für Ratschläge an dich wenden kann. Danke, **Papa**, dass du es mir ermöglicht hast, so sorgenfrei zu studieren. Danke, dass du mich immer unterstützt hast und für mich da bist. Danke, **Oma Gitte**, dass du so lange an mich geglaubt hast, wie du konntest. Ich wünschte, du könntest meinen Abschluss noch miterleben. Danke, **Oma Rösel**, dass du mir vertraust, dass ich den richtigen Weg gehe, und dass du immer da bist. Danke, **Patric** und **Pamela**, dass ihr mir immer die Daumen drückt und mitfiebert.

I further want to thank all the wonderful and strong women in my life for always believing in me. Thank you, **Carolyn**, for all the fun escapes from work, daydrinking and city trips and for being different together. Thank you, **Anna**, for Taco and Margarita nights, for being the calm voice outside my head and for always empowering me. Thank you, **Julia**, for active and challenging activities, and for great talks with wine or coffee. Thank you, **Sandra**, for countless walks together, delicious cooking sessions, enjoying the little things in life and making being friends so easy. Thank you, **Eva**, for being one of the most understanding people I know. Thank you, **Inés**, for being the best roommate in the world and for constantly reminding me of the life outside of science. Thank you, **Annie**, for fun girl nights and really interesting conversations. Thank you, **Jorong** and **Tanqueray**, for making all the stress disappear. Thank you, **Bine**, for countless knitting sessions and for being my first Munich friend outside of science. I also want to thank my honorary power woman **Peter**, for always backing me up and supporting me.